Pergamon Progress in Oceanography 41 (1998) 141–202

Progress in Oceanography

Twelve monthly experiments of 4D-variational assimilation in the tropical Atlantic during 1987: Part 1: Method and statistical results

Eric Greiner[a], Sabine Arnault[b,*], Alain Morlière[c]

[a]*CERFACS, 42 avenue Coriolis, 31057 Toulouse Cedex, France*
[b]*LODYC, T14-15 2ème boîte 100, 4 place Jussieu, 75252 Paris Cedex 05, France*
[c]*ORSTOM, 15 BP 917, Abidjan 15, Ivory Coast*

Abstract

GEOSAT sea level anomalies, XBT temperature profiles and Levitus (1982) climatologies are assimilated monthly during 1987 into a non-linear primitive equation model of the tropical Atlantic ocean. The model has a resolution of 1° longitude × 1/3° latitude × 20 vertical levels extending from 50°S to 50°N. The model physics are complex, including in particular an imbedded 1D-mixed layer model and a 3D-Richardson number dependent mixing under the mixed layer. The model is forced monthly by ship winds and Oberhüber (1988) climatologies of heat and fresh water fluxes. A 2° longitude × 1° latitude gridded optimal interpolation analysis of GEOSAT sea level anomalies is assimilated between 20°S and 20°N at each grid point of the model. Validated TOGA XBT profiles are also assimilated between 30°S and 30°N at their exact location. Decorrelation in space and time is assumed for the error structures. Data weights are taken to vary with data accuracy and with a proxy function of the model representativity.

The variational assimilation succeeds in determining initial conditions that reduce the model-data misfits and demonstrates that the temperature and the sea surface height of a general circulation model are sensitive to initial conditions. Despite the complex evolution of the present model over one month, the adjoint model is able to provide efficient descent directions for the minimization algorithm. Thus, 4D-variational assimilation can be used in the tropics with a general circulation model.

The assimilation of satellite altimetry helps to reduce the misfit between the model and the XBT profiles. The decay of the XBT misfit is faster and the corrections are not localized to the

* Corresponding author. Tel.: (33 1) 44 27 49 71; Fax: (33 1) 44 27 38 05; E-mail: arnault@lodyc.jussieu.fr

PII: S0079-6611(98)00016-0

XBT positions but influence the whole basin. The biggest impact appears where the GEOSAT variability is the highest, e.g. around the North Equatorial Counter Current and the North Equatorial Current (5°N–15°N). The assimilated sea level variability is close to the GEOSAT variability. On the other hand, the spatial variability of the modelled temperatures is less well defined in comparison with the XBT profiles; although the large scale is reproduced, details are missing in the vertical stratification at the surface and in the thermocline. The modelled equatorial upwelling is also too strong after assimilation with a 2°C cold bias at the surface in July.

The 11 one-month forecasts in 1987 following each month of assimilation show an improvement of the simulation with reference to XBT profiles below the mixed layer. Temperature profiles in the mixed layer are neither improved nor degraded. This could indicate the need of a better time resolution of the forcings, for example including the diurnal cycle and a prognostic model of the mixed layer. Compared to GEOSAT, the forecasts of 1987 show an improvement up until May. The equatorial upwelling of July is degraded by the assimilation, because of a combination of the heat flux correction and the surface cold bias which is increased by the assimilation. This demonstrates that the inadequacy between the heat fluxes and the mixed layer model is a critical issue with assimilation in thermodynamical models.

The pure forecast over the first 7 months of 1988 compares well to XBT profiles under the thermocline, showing that the initialization of the model has a positive impact for more than 7 months. The description of the warm anomaly of early 1988 relative to 1987 is globally improved by the assimilation. In particular, the variability of the north equatorial currents measured by altimetry is only reproduced after data assimilation. There is a benefit for the year-to-year signal in the Gulf of Guinea. This emphasizes the importance of the in situ observing network and satellite altimetric data.

Contents

1. Introduction 145
2. Equations and model 147
   2.1. The primitive equation system 147
   2.2. Vertical turbulent diffusion model 149
   2.3. The boundary conditions 151
   2.4. Grid and bathymetry 152
3. Reference run 153
   3.1. Climatological spin-up 153
   3.2. Monthly forcing 155
4. Data and errors 155
   4.1. Levitus's climatological data 156
   4.2. In situ XBT data 157
   4.3. Altimetric GEOSAT sea level data 158
   4.4. First guess data 159
5. Assimilation 160
   5.1. The control 160
   5.2. The cost function 161
   5.3. The assimilation window 161
   5.4. The strategy for assimilation and quality control 162

5.5. The optimization 163
6. Statistical results 164
6.1. The set of diagnostics and examples 164
6.2. XBT profiles 164
6.2.1. Statistics involving XBT over 25°C ("near surface zone") 164
6.2.2. Statistics involving XBT between 15 and 25°C ("thermocline zone") 167
6.2.3. Statistics involving XBT under 15°C ("deep ocean") 169
6.2.4. Vertical sections along XBT lines 174
6.2.5. Depth of the 20°C isotherm along XBT lines 177
6.2.6. Discussion on XBT statistics 178
6.3. GEOSAT sea level anomalies 182
6.3.1. Monthly statistics involving the reference level 182
6.3.2. Monthly statistics not involving the reference level 183
6.3.3. Time series 187
7. Conclusions 193
8. Acknowledgements 194
Appendix A Numerical peculiarities of the assimilation 195
9. References 201

NOMENCLATURE

α	parameter of the Richardson number dependent mixing = 5
α_ρ	coefficient of thermal expansion of the density
B_0	surface downward buoyancy flux $B_0 = \frac{\alpha_\rho g}{\rho_0 C_p}(Q_{np} + Q_{sr}) - 35.5\beta_\rho g E$
β_ρ	coefficient of haline expansion of the density
C	initial conditions of the control
C_p	ocean specific heat
c_{ML}	empirical parameters for the ML depth = 100m
δ^{η}_{GEO}	standard deviation for altimetric variations = 3cm
δ^{S}_{Lev}	standard deviation for salinity Levitus misfit = 0.2psu
δ^{S}_{g}	standard deviation for salinity guess misfit = 0.1psu
δ^{T}_{Lev}	standard deviation for temperature Levitus misfit = 3°C
δ^{T}_{XBT}	standard deviation for temperature XBT misfit = 1.5°C
δ^{T}_{g}	standard deviation for temperature guess misfit = 1.5°C
δ^{u}_{g}	standard deviation for velocity guess misfit = 0.05m/s
Δ_h	horizontal laplacian
Δt	time step = 1h30
Δx	zonal grid mesh $\geq 1°$
Δy	meridional grid mesh $\geq 1/3°$
Δz	vertical grid mesh $\geq$ 10m
E	fresh water flux
E	space of initial conditions allowed for the control
ϵ_{ML}	ML diffusive limitor while cooling = $2.10^{-8}m^2/s^3$
F	space of the states of the system
$f\,k$	Coriolis force
g	gravity
γ	intensity of the Asselin's filter = .1

γ_{Lev} dissipation drag coefficient towards climatology $\leq$ 1/20days
I solar irradiance
κ_h coefficient of horizontal diffusivity for temperature and salinity
κ_v coefficient of vertical diffusivity for temperature and salinity
κ_{v0} minimun for $\kappa_v = 1.10^{-7}\mathrm{m}^2/\mathrm{s}$
κ_{ML} diffusivity for temperature and salinity in the ML
κ_{RI} diffusivity for temperature and salinity under the ML
M projector from E onto F
N parametrer of the Richardson number dependent mixing = 2
ν_h coefficient of horizontal eddy viscosity
ν_v coefficient of vertical eddy viscosity
ν_{v0}, ν_{v1} extremes for ν_v with Richardson $= \begin{cases} 1.10^{-6} m^2 S^{-1} \\ 1.10^{-4} m^2 S^{-1} \end{cases}$
ν_{0ML} diffusivity at the surface $\nu_{0ML} = .014 \dfrac{u_*^2}{\sqrt{\mathrm{MAX}(\epsilon_{ML}, B_0)}}$.
ν_{ML} diffusivity for momentum in the ML
ν_{RI} diffusivity for momentum under the ML
P_{randtl} Prandtl number 1.
p_s surface pressure
Q_e latent heat part of the heat flux
Q_{lw} longwave radiative part of the heat flux
Q_{np} nonpenetrative part of the heat flux
Q_s sensible heat flux
Q_{sr} solar radiative part of the heat flux
R ratio of absorbtion of the irradiance
RI Richardson's number
ρ_0 reference density
ρ density relation depending on T, S and z
S salinity
σ proxy function of the model variance
T duration of the assimilation period = 1month
T temperature
τ wind stress
τ_{ML} limitor of the turbulent surface wind stress = 10^{-2}Pa
u horizontal velocity
u_* turbulent surface velocity $\rho_0 u_*^2 = max(|\tau|, \tau_{ML})$
w vertical velocity
X state of the system
ξ_1, ξ_2 lengths of absorbtion of the irradiance
ψ monthly mean estimated correction of GEOSAT altimeter
z depth
ζ relative error for GEOSAT data

SUPERSCRIPTS

u	velocity
T	temperature
S	salinity

SUBSCRIPTS

g	guess data
GEO	GEOSAT data
LEV	Levitus data
XBT	subscript for XBT data

ABBREVIATIONS

ass	assimilated run
for	forecast run
ref	reference run
COR	correlation
RMS	root-mean-square
VRB	variability
E	zone east of 60°W
H	water warmer than 25°C (Hot)
W	water between 15°C and 25°C (Warm)
C	water colder than 15°C (Cold)
ML	mixed layer
SSH	sea surface height
SST	sea surface temperature
EUC	Equatorial Under Current
NEC	North Equatorial Current
NECC	North Equatorial Counter Current
SEC	South Equatorial Current
SECC	South Equatorial Counter Current

1. Introduction

The last decade was characterized by the increase in oceanic observations, in particular from the improved satellite observations of sea surface height (SSH) and sea surface temperature (SST). Excellent spatial and temporal coverage of the SSH is available by altimetry (GEOSAT, TOPEX/POSEIDON, ERS1-2). In situ data networks such as TOGA-COARE and WOCE are widely used now by oceanographers.

Important progress has also been made in numerical simulations which are now able to reproduce quite reliable pictures of the ocean. As models become more

realistic and data coverage more synoptic, it is now possible to compare numerical simulation and data more objectively, and even to combine them through data assimilation techniques.

A basic goal of data assimilation is to provide realistic initializations for dynamical ocean models as an alternative to the many uncertainties in forcing fields and in model dynamics. Data assimilation can provide a more realistic description of the ocean as well as an evaluation of the model validity. These two results are of major importance for oceanographers, especially for short term climate studies. Indeed, the development of coupled models emphasizes the need for a realistic synoptic description of the ocean. During the first years of simulation, coupled models may present a fast drift of the seasonal cycle (such as a 2–3°C warming of the eastern part of the tropical basins after one year of coupling: Eric Guilyardi, personal communication, 1997). A precise oceanic reference would be useful to validate the results of the coupled models. The time validity of the oceanic model (e.g.: rms between model and in situ measurements) with assimilation will also provide an estimate of the time validity of the coupled model (if oceanic components of coupled models are worse than the forced oceanic models, this estimate would be a lower bound). Moreover, assimilation helps in providing additional information, such as quantifying the model errors and estimating forcing errors. Finally, while coupled models do not reproduce the full range of time variability because of the drift of their seasonal signal, assimilation is the best way to model both the seasonal signal and the interannual variability.

Data assimilation in oceanography has followed the progress in oceanographic modelling and a review of the recent techniques can be found in Ghil and Menalotte-Rizzoli (1991). The adjoint approach used here is described in Courtier and Talagrand (1990). The present work follows that of Greiner and Périgaud (1994) where GEOSAT altimetry was assimilated into a nonlinear shallow-water model of the Indian Ocean over 1987–88. In the present study, a similar technique of sea level anomaly assimilation is used, except that this new study is based on a 4D context: a 3D primitive equation model of the tropical Atlantic ocean is used to assimilate satellite altimetry and temperature profiles over 1987. This is the continuation of the OPERA project (Morlière et al., 1989a). The aim was then to nudge a numerical model with in situ XBT data in order to provide a synoptic and realistic description of the tropical Atlantic ocean. The behavior of this ocean is of primary importance for the rainfall in Brazil and Sahel (Hastenrath, 1985). Although the thermodynamics of the tropical Atlantic are now better documented (Merle, 1980; Arnault, 1987; Hénin and Hisard, 1987; Tang and Weisberg, 1993), there are still some gaps in the understanding of the oceanic circulation. In particular, the warming of the SST in the Gulf of Guinea has not been yet fully linked with subsurface thermodynamics. The present study extends the OPERA project by applying the more optimal variational method to assimilate data in the general circulation model. Our aim is to describe synopticly the 1987–88 warming event in the tropical Atlantic ocean. In particular, we want to evaluate how the ocean dynamics have contributed to the SST warming. The 1987–88 period was a fortunate choice since a warming of > 1°C in early 1988 was observed in the equatorial Atlantic and rare SSH observations were

provided by GEOSAT altimeter. Therefore, data assimilation could provide a synoptic and realistic description of the ocean. The variational method enabled us to take advantage of both in situ temperature data and satellite SSH in the tropics with a sophisticated general circulation model.

The principle of variational assimilation is to minimize the model-data misfit relative to the initial conditions with the use of the adjoint model. This is a particular case of the optimal control theory (Lions, 1968). The control is made from the initial conditions of the dynamical model and we search for an optimal control which minimizes a residual between the data and the model. Starting from a chosen control value, the forward model is run with the external forcings prescribed. The model state values (SST, SSH, velocity...) are then compared to the data. A cost function measuring the model-data misfit has to be defined, generally as a sum of the squares of the individual misfits. This cost function is then minimized by an algorithm of optimization. The particularity of the variational method is to use the backward adjoint model to compute the gradient of the cost function (Courtier and Talagrand, 1990). From the physical point of view, the variational method respects the modelled physics (no nudging dissipation, no successive corrections) and allows direct assimilation of any data that could be simulated by the model (in other techniques SSH is often transformed before assimilation). The limitations of this method concern the model physics (the cost function has to be smooth) and the spatial and temporal resolution (all the model time steps must be stored in computer memory).

This study will be divided in two parts. Part 1 is covered by this paper, and presents the method and a statistical analysis of the results of the assimilation over 1987 and the forecast over 1988. In Part 2, physical comparisons are made, in particular with the independent data set of satellite SST, and the benefits obtained through assimilation are analysed. The plan of the present paper now follows. In Chapter 2 we give the equations resolved by the model with a special attention to the mixed layer model. Boundary conditions are also discussed in the chapter. Chapter 3 gives the parameters (spin-up, forcings...) of the model as well as some qualitative comments on the run without assimilation. In Chapter 4, we introduce the data used in this study and explain how assimilation works through the variational method. We also comment on the various sources of errors and explain how we have accounted for these errors. Chapter 5 summarizes how assimilation combines model, data and errors and describes how the optimization is carried out. The results are presentated in Chapter 6 with an examination of the statistical results of the reference, forecast and assimilated runs compared with XBT profiles and GEOSAT data. In Chapter 7 we give our technical conclusions on the assimilation. Appendix A details the particular algorithms we used for this assimilation.

2. Equations and model

2.1. The primitive equation system

The set of model equations considered here are the "primitive equations". They describe the large scale motions of the ocean in a four dimensional domain:

$$\partial_t u + u\nabla u + fk \times u + \nabla p_s - \partial_z[\nu_v(u,T,S)\partial_z w]$$

$$- \nabla.[\nu_h \nabla.u] + \nabla \times [\nu_h \nabla \times u] = -\frac{g}{\rho_0} \nabla \int_0^z \rho(T,S,z)dz$$

$$\nabla.u + \partial_z w = 0$$

$$\partial_t T + u\nabla T - \kappa_h \Delta_h T - \partial_z[\kappa_v(u,T,S)\partial_z T] = -\frac{1}{\rho_0 C_p} \partial_z I$$

$$\partial_t S + u\nabla S - \kappa_h \Delta_h S - \partial_z[\kappa_v(u,T,S)\partial_z S] = 0$$

The state of the system X consists of the horizontal velocity u, the temperature T and the salinity S of the fluid. The vertical velocity w is deduced from the vertical integration of the nondivergence equation with the kinematic condition at the bottom. $f\,k$ is the Coriolis force, ν_h and ν_v are respectively the coefficients of horizontal and vertical viscosity, p_s is the surface pressure acting as a force coming from the rigid lid, ρ is the density relation depending on temperature and salinity and the depth z; κ_h and κ_v are respectively the coefficients of horizontal and vertical diffusivity for the temperature and the salinity. Details about the model formalism and discretization can be found in Morlière et al. (1989a, b); Reverdin et al. (1991); Blanke and Delecluse (1993).

An important factor in the exchange between atmosphere and ocean which strongly affects the SST and the mixed layer (ML hereinafter) is the fraction of the solar irradiance I that penetrates the ocean:

$$I = Q_{sr}[Re^{-z/\xi_1} + (1 - R)e^{-z/\xi_2}]$$

where ξ_1, ξ_2 and R are the characteristics of waters varying in space from Type 1A to Type III of Jerlov's classification (Simpson and Dickey, 1981). The most turbid type III is found along the Brazilian and African coasts, especially near river deltas. Intermediate type II can be found at the equator, in relation to the biological activity induced by the equatorial upwelling. The clearest type, IA, is found offshore at about 20°N or 20°S. It is important to use varying types in the Atlantic because the solar penetration is very low in coastal regions while it is high in the open sea. (In the Atlantic, river runoffs produce very turbid water. Biological activity is high along the coasts and at the equator. In the Pacific, the contrast between turbid coastal water and offshore clear water is not as strong.) For this purpose we have used an approximation inspired by Simonot and Le Treut (1987). The effects are especially evident in the Gulf of Guinea where the water is of Type III. The use of a Type IA for this region would have made the ML too deep. With the very turbid Type III, the ML remains shallow as expected. However, turbidities are poorly documented which results in another source of inaccuracy: Simpson and Dickey (1981) and Martin (1985) have shown that variations in turbidity of the sea water can lead to clear differences in the upper ocean structure. Ignoring such differences can lead to errors of the order of a degree Celsius, especially during heating when the ML shallows.

The horizontal coefficients of diffusion are taken to be constant all over the basin except near the artificial oceanic boundaries. Within twenty degrees of the northern and southern boundaries, these coefficients linearly increase poleward up to a factor 10 in order to damp the artificial curl of the wind stress which we have linearly decreased by a factor 10 at the boundary.

From 20°N or 20°S to the oceanic artificial northern and southern boundaries (see Fig. 1a), a dissipative term is added in order to relax the system towards the climatology:

$$\partial_t X \rightarrow \partial_t X + \gamma_{Lev}(X - X_{Lev})$$

for this purpose, we use the Levitus (1982) monthly climatology of temperature and the seasonal climatology of salinity. They are referenced by the subscript "*Lev*" hereinafter. These fields are linearly interpolated in time at each time step. At the artificial northern and southern boundaries, the Newtonian relaxation coefficient is maximum (1/20days). Between 20°N and 20°S the Newtonian relaxation coefficient is zero and the model interior is in free mode (there is a surface relaxation descibed in Section 2.3). Between 20°N (20°S) and 50°N (50°S), the relaxation coefficient increases as a cosine from 0 at 20° to 1 at 50°.

2.2. *Vertical turbulent diffusion model*

It is now known (Pacanowski and Philander, 1981, hereinafter PP81; Blanke and Delecluse, 1993, hereinafter BD93) that the previous equations are not sufficient to represent correctly the thermodynamics of the tropical oceans. A model of vertical turbulence is required in order to represent both the ML and the underlying turbulent activity. Since we want to produce realistic simulations of the tropics, we had to include such a model in our simulations. However, memory and computational limitations resulting from variational assimilation, led us to choose a rather simple model. In its formulation, we use a simple diagnostic 1D model in the ML, and a diagnostic 3D-Richardson number dependent mixing under the ML. More precisely, the coefficients of vertical viscosity and diffusivity are calculated differently within the mixed layer and under the ML.

Coefficients under the ML are linked as in PP81 to the Richardson's number, RI, following an empirical law (the relationship is estimated from in situ data by Jones, 1973):

$$\nu_{RI} = \nu_{v0} + \frac{\nu_{v1}}{(1 + \alpha RI)^N} \quad \text{and} \quad \kappa_{RI} = \kappa_{v0} + \frac{\nu_v}{1 + \alpha RI}$$

A major weakness of a pure Richardson number dependent mixing is its poor representation of the ML (PP81, BD93). In order to avoid the use of the complex turbulent kinetic energy closure of BD93, we simply replace the Richardson's parameterization in the ML by a one dimensional parameterization based on the Monin-Obukhov length. This parameterization was originally proposed by Kraus and Turner (1967) and revisited by Alexander and Kim (1976) and Simpson and Dickey (1981).

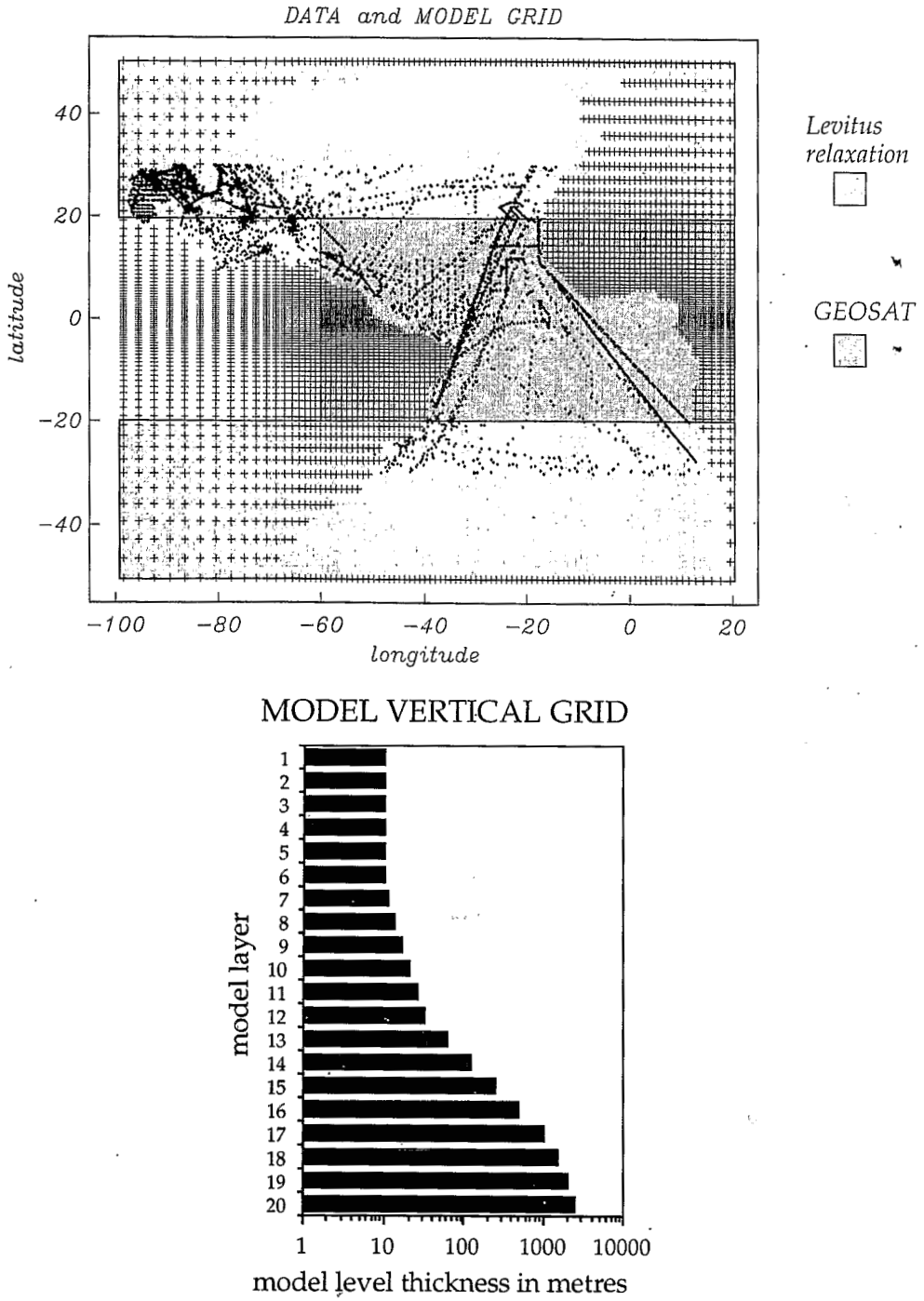

Fig. 1. (a) Model domain. Northern and southern boundaries are artificially closed. Levitus relaxation increases polewards from 20° latitude. GEOSAT is assimilated east of 60°W between 20°N and 20°S. XBT data are assimilated between 30°N and 30°S. " + " sign marks model land points. (b) Thickness of the model layers.

It is based on the balance between a positive surface downward buoyancy flux (B_0) and the energy input by the wind (u_*^2). It gives an estimate h_{ML} of the depth of the ML in the open sea (no advection) in a quasi-stationary case of heating:

$$h_{ML} = \mathrm{MIN}\left(c_{ML}, \frac{2u_*^3}{\mathrm{MAX}(\epsilon_{ML}, B_0)}\right)$$

The parameters ϵ_{ML} and c_{ML} limit the artificial winter deepening (Alexander and Kim, 1976).

We use the estimated depth of the ML in the calculation of the coefficients of vertical diffusion as follows:

$$\nu_{ML} = \nu_{0ML}\left[\frac{1}{2} + \frac{1}{2}\tanh\left(4\left(.35 - \frac{z}{h_{ML}}\right)\right)\right] \text{ and } \kappa_{ML} = \frac{1}{P_{randtl}}\nu_{ML}$$

where the hyperbolic tangent gives a fastly decreasing coefficient maximum at the top of the ML and null underneath the diagnostic depth. According to BD93 and Peters et al. (1988), we take the Prandtl number P_{randtl} equal to one in the ML. The diffusion at the surface is related to the forcings through a relationship inspired from BD93.

This simple closure has the advantage of being smooth with no discontinuities. This is important for the use with the adjoint (as evoked in Appendix A) but we must mention that it is probably the weakest point of this model. Fundamentally, the level of turbulent kinetic energy input by the forcing into the ML is poorly determined. It mainly affects the near surface variability (tests show the mean position of thermocline is more influenced by the windstress than by this ML parameterization). This closure also neglects the in situ state of the ocean and thus has a short predictability. For instance, it is not reliable in a non-stationary case like the winter deepening of the ML under cooling. Consequently we can expect reasonably good agreement during seasons of heating in regions where the horizontal effects of advection are neglectable. On the other hand, during seasons of cooling or in a region of strong advection like the Brazilian Coast, the estimated depth is incorrect, and, in fact, only bounded by the diffusive limitors ϵ_{ML} and c_{ML} . Moreover, as we do not use hourly forcings and the ML model is quasi-stationary, our model is unable to reproduce the diurnal signal which can be included as part of the XBT measurements.

2.3. The boundary conditions

The boundary conditions are of hybrid type for the velocity: at the bottom the velocity is set equal to zero (no slip) while at the surface (or rather at the rigid lid), a stress is imposed to the fluid by the wind stress τ:

$$\nu_v(u,T,S)\partial_z u = \tau/\rho_0 \text{ and } w = 0$$

For both temperature and salinity, the normal derivatives are prescribed every-

where. There are zero fluxes through the bottom and the artificial boundaries while at the surface, the nonzero fluxes give:

$$\kappa_v(u,T,S)\partial_z T = \frac{1}{\rho_0 C_p}\left(Q_{np} - \frac{20°\mathrm{W/m^2}}{1°\mathrm{C}}(T - T_{Lev})\right)$$

$$\kappa_v(u,T,S)\partial_z S = E\left(S - \frac{1\mathrm{mm/day}}{1\mathrm{psu}}(S - S_{Lev})\right)$$

Q_{np} is the nonpenetrative part of the heat flux, the penetrative part acting as a body force on the temperature (see system of the Section 2.1). E is the total flux of fresh water and consists of evaporation, precipitation and river runoffs. We use the usual interactive corrections for the nonpenetrative heat flux and the fresh water flux at the surface. They consist of a relaxation towards surface Levitus' temperature and salinity (as for the artificial boundary) with characteristic strengths of $20\mathrm{W/m^2}$ per °C (for the nonpenetrative part only) and 1mm/day per psu. This surface relaxation is necessary because of the inadequacy of the climatological thermohaline fluxes for the model. Without these terms, the model becomes unstable after several months of spin-up (the Gulf of Guinea becomes too hot). Hence, Levitus data is incorporated even in the reference run (the run without assimilation). In addition, the surface relaxation is used for the assimilated run and the forecast. In this paper, weekly satellite SST are used neither to determine the forcings nor as data for the assimilation. We will use the satellite SST as an independent dataset in the part 2. Thus, the thermohaline fluxes are purely climatological.

2.4. *Grid and bathymetry*

There are 95 × 77 points in the horizontal domain and the grid mesh varies with all directions. The resolution in longitude goes from 3° in the Gulf of Mexico, to 1° in the central basin to 2° at the southern tip of Africa. The resolution in latitude starts from 1/3° at the equator, is 1/2° at 4.5° and reaches 3.7° at the artificial oceanic boundaries.

There are 20 active levels in the vertical with 9 dedicated to the top 100m. The interval between two levels ranges from 10m at the surface to 2000m at the bottom (see Fig. 1b). The model time step is 1h30.

The bathymetry is obtained from the ETOPO5 5' × 5' grid (Smith, 1993) but we made some corrections in three cases. First, in the Gulf of Mexico where the grid mesh is about 3° × 1°, we have taken a rough estimate of the coastlines (Florida especially) and a unique Haïti-Cuba-Puerto Rico island. Secondly, we have set the continental shelf to a constant depth (50m) since the fine details of the shelf topography are missing (particularly in the northern Brazilian shelf and around the Caribbean islands). Thirdly, we removed some isolated points near the African coast near the bottom where we have poor vertical resolution.

3. Reference run

As we want to test the impact of the assimilation, we will define a classical run hereafter called the reference run. This run is obtained without assimilation. The forcings used for the reference run are also used for the assimilated and forecast runs.

3.1. Climatological spin-up

We start the integration on January 1, from a composite state made of the Levitus temperature and salinity and a velocity which is in geostrophic equilibrium outside of the equatorial band (5°N–5°S) and which follows a linear function depicting the mean equatorial currents. This function represents a surface westward current, an eastward current from 150m in the west to 50m in the east and a motionless ocean at depth, see figure below:

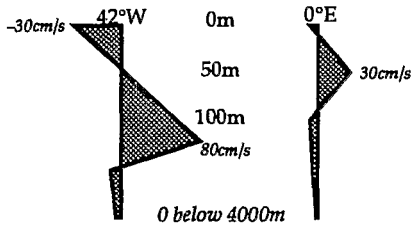

We force the model by the Hellerman and Rosenstein (1983) climatological winds until the end of December the second year. A previous experiment showed that a third year of climatological spin-up brings little change as can be deduced from the periodicity of Fig. 3. In fact, we scaled these winds by a factor 0.75 in order to have the correct equatorial slope of the thermocline. (Ji et al. (1995) use a factor 0.9 for both the Pacific and the Atlantic.) We also use the Oberhüber (1988) climatology of net heat flux, solar penetrative flux and freshwater flux. We add to the evaporation minus precipitation budget the fluvial contributions (taken as constant in time) of the Amazon, Orenoque, Congo, Uruguay-Paraña, Niger, Mississippi-Missouri and Rio Grande rivers (Larousse, 1968).

At this stage, there are clearly some differences between the climatology of the model and that of Levitus. Fig. 2 shows the mean difference at 65m between the model temperature and Levitus (the error is maximum at this depth, the seventh layer of the model). The modelled thermocline is generally too deep in the eastern part of the basin and in particular in the regions of the Angola dome (5°E–14°S) and Guinea dome (20°W–12°N). The same problem occurred with a pure Richardson number dependent mixing in Morlière et al. (1989b).

The surface and the deep ocean correspond well with Levitus, except during the equatorial upwelling in July when the model simulated SSTs are too cold by 2°C (the rising of the thermocline is visible on Fig. 2 near 15°W–0°N). The equatorial upwelling occurs in July. Equatorial easterly winds are particularly strong during

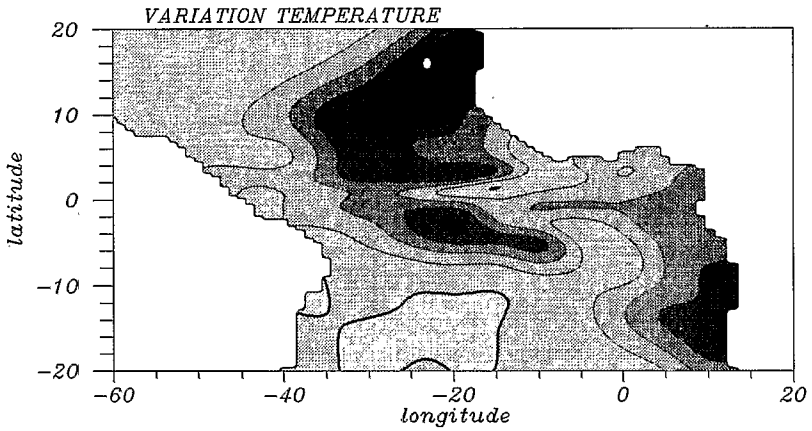

Fig. 2. Yearly difference between the model climatology and Levitus temperature at 65m. The contour interval is 1°C; the heavy black line corresponds to the 0°C isotherm. Darker shading corresponds to warm differences.

this period. It leads to an increased surface westward current and, due to the Coriolis force, an increased equatorial divergence. Underlying cooler waters surface and SST reaches its annual minimum (down to 24°C), even if the heat flux is maximum then. This upwelling is also visible in the rising thermocline and in the Equatorial Under Current which weakens in the East. This event will be illustrated in the context of assimilation in Section 6.2.6. Globally, the model follows the seasonal variations of the Levitus climatology but the absolute temperatures and salinities are biased.

To illustrate these effects, we plotted Fig. 3 the 20°C isotherm depth at 18°W–

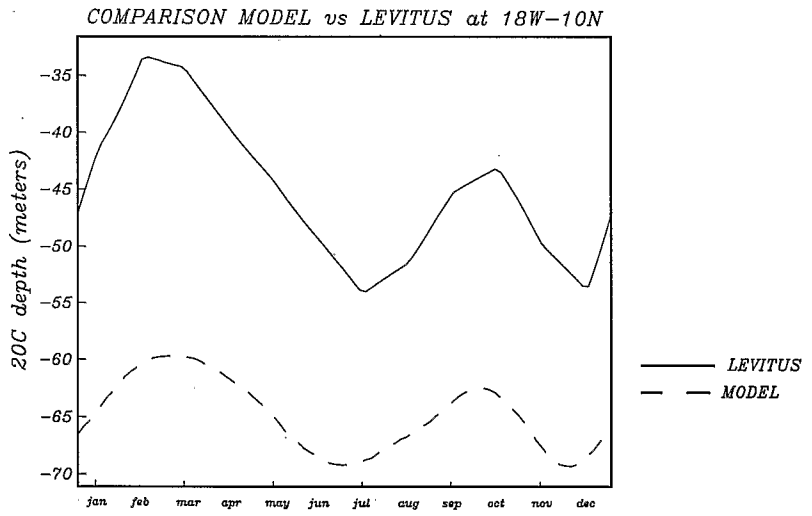

Fig. 3. Depth of the 20°C isotherm at 18°W–10°N during the second year of the climatological spin-up for the model and Levitus.

10°N during the second year for the model and compare it to the monthly Levitus climatology (the error of the model is maximum there in terms of thermocline depth and SST). Here, the seasonal signal is well reproduced (the time correlation is 0.95 and the standard deviation of the difference is 3m) but the root mean square difference is rather large (20m). In conclusion, there is often a bias between model and monthly Levitus climatologies which varies spatially but remains constant in time. It seemingly does not affect the quality of the seasonal cycle.

3.2. *Monthly forcing*

After these two years of climatological spin up, we start using on January 1985 the Servain and Lukas (1990) monthly wind stresses instead of climatological winds. These winds are limited to the band 20°S–30°N. The coverage of the ship reports used to produce these winds are rather homogeneous in time and space (J. Servain, personal communication). The gaps are generally located in the south-east but rarely exceed five degrees. The number of data is larger in the region of the equatorial currents (0°N–20°N). Outside the band 20°S–30°N, Hellerman and Rosenstein (1983) climatological wind stresses (still scaled by a factor 0.75) are used. We have checked that transitions are smooth in time and space between climatological and monthly forcings.

We continue using the Oberhüber's climatological heat and freshwater fluxes together with the interactive relaxation towards Levitus climatological surface temperature and salinity. These monthly forcings are also used for the assimilated and forecast runs so that the forcing configuration is the same for all runs.

4. Data and errors

The variational assimilation aims to minimize a user defined cost function which measures the model-data misfit. The state of the model consists of the velocity, the temperature and the salinity. Other quantities such as sea level and drifter trajectories can also be derived. The outputs of the model are combined with the data in order to form a sum of individual weighted model-data misfits. The expression of this sum is listed below relative to each specific data.

The different data sets used in the assimilation process include Levitus temperature and salinity climatologies, in situ XBT temperature profiles kindly provided by J.P. Rebert, GEOSAT altimetric sea level (Arnault et al., 1992) and a first guess obtained through a previous forecast.

About data weighting, we choosed the simplest statistics: decorrelation is assumed in space and time for the error structures. In doing so, we hope to evidence the difficulties related to the model, the data and the variational method, independently from complex error statistics. Nevertheless, the errors are varying in space (XBTs and Levitus) and time (GEOSAT).

4.1. Levitus's climatological data

The monthly temperatures and seasonal salinities are trilinearly interpolated onto the grid points of the model. These data are incorporated in the cost function by the criterion below. It compares the Levitus's climatology linearly interpolated in time and the temperature simulated at every time step t by the model at every gridpoint $x\ y\ z$ of the Atlantic without relaxation (where $\gamma_{Lev} = 0$):

$$J^T_{Lev} = \frac{\sum_{t}^{0\rightarrow T} \sum_{xyz}^{\text{Atl}\ \gamma_{Lev}=0} \left(\frac{(T - T_{Lev})^2}{\sigma(x,z)^2 \delta^{T\ 2}_{Lev}} \right) \Delta x \Delta y \Delta z \Delta t}{\sum_{t}^{0\rightarrow T} \sum_{xyz}^{\text{Atl}\ \gamma_{Lev}=0} \left(\frac{1}{\sigma(x,z)^2} \right) \Delta x \Delta y \Delta z \Delta t}$$

The grid mesh $\Delta x\ \Delta y\ \Delta z$ of the model is variable and thus included as weighting factors in the criterion, otherwise the criterion would be more sensitive to equatorial or surface deviations where the grid resolution is finer. The basic assumption of uncorrelated errors is made for the climatological observation. The weighting of each individual observation is given by its observational error and its model representativity. The error in the Levitus data set is known to increase with depth and distance to collected data. However, the spatial coverage in the equatorial Atlantic is rather homogeneous and the data error will be considered homogeneous in longitude and latitude. In the vertical, the data error is assumed to be proportional to the in situ variance. Moreover, for the sake of simplicity, we assume that the model representativity is proportional to the model variance. The in situ and model variance weighting function, σ, is modelled using a unique analytical estimate. This function (obtained from statistics of previous assimilation experiments and climatological spin-ups) depends mainly on the depth (the variance is maximum near the thermocline and higher at the surface than at depth) but also on the longitude (west of 60°W, the grid resolution is coarser and the model cannot represent the physics included in the climatology):

$$\sigma(x,z) = \begin{cases} 1 & \text{east of } 60°\text{W} \\ 2 & \text{west of } 60°\text{W} \end{cases} \times \begin{cases} 2/3 & \text{at } z = 0\text{m (surface)} \\ 1 & \text{at } z = 80\text{m (thermocline)} \\ 1/3 & \text{for } z \geq 200\text{m (deep ocean)} \end{cases}$$

Such a criterion favors the most accurate datum (which can be accurately representated by the model) and the largest amount of data. For instance, if the model cannot represent the climatological thermocline, the model-data difference is large, but the weight of this data is relatively small so that the criterion will not be dominated by this difference.

In any case, these climatological data are used only as a background state since it is the 1987–88 seasonal and interannual signals that are under examination in this study. The standard deviation δ^T_{Lev} is taken equal to 3°C. This value is taken from the quality control test of the XBTs (see Section 4.2). This criterion is like a quality control of the model. Following the weighting function, σ, it typically corresponds to a 2°C deviation at the surface, a 3°C deviation in the thermocline and a 1°C deviation at depth.

If the typical range of temperature in the equatorial Atlantic is 10°C–25°C, a standard deviation of 3°C corresponds to 20% of the signal. For the similar criterion J^S_{Lev} in salinity, if the typical range of salinity in the equatorial Atlantic is 35 to 36psu, the same percentage 20% leads to a standard deviation δ^S_{Lev} of 0.2psu:

$$J^S_{Lev} = \frac{\overset{\text{Atl}}{\overset{0\to T}{\sum_t}\ \overset{\gamma_{Lev}=0}{\sum_{xyz}}\left(\frac{(S-S_{Lev})^2}{\sigma(x,z)^2\delta^{S\ 2}_{Lev}}\right)\Delta x\Delta y\Delta z\Delta t}}{\overset{\text{Atl}}{\overset{0\to T}{\sum_t}\ \overset{\gamma_{Lev}=0}{\sum_{xyz}}\left(\frac{1}{\sigma(x,z)^2}\right)\Delta x\Delta y\Delta z\Delta t}}$$

These criteria are normalized by their expected errors (the weighting function, σ, is the same for temperature and salinity). By the way, several criterions of different natures (synoptic 3D climatologies, synoptic 2D sea level data and asynoptic XBT data) can be minimized together in the same cost function. The model is consistent with each dataset if the corresponding normalized criterion is less than one.

4.2. *In situ XBT data*

The XBT data used in this study came from ships of opportunity as well as oceanographic cruises. Data are validated by quality control test (Rebert, 1993). The position and the identification of the boats are controlled. Then, each measurement of a profile is compared to Levitus climatology. If the departure from the climatology exceeds 3 standard deviations, the profile is flagged. The profile is also flagged in case of temperature inversion. Finally, the profile is visually examined. In this study, we have kept only the profiles which passed all the checks without flag.

In space, the validated XBT data are assimilated at their precise sampling locations between 30°N and 30°S (see Fig. 1a): the model temperature is then interpolated in space to the data points. In time, we use the XBTs at the closest time step of the model which avoids interpolating the modelled temperature in time. The error involved is less than half an hour (the time step is 1h30), which is not very important since the diurnal signal is not included in our simulated temperatures. Thus the criterion of the cost function pertaining to XBT data is:

$$J^T_{XBT} = \frac{\sum_{XBT} \frac{(T - T_{XBT})^2}{\sigma(x,z)^2 \delta^{T\,2}_{XBT}}}{\sum_{XBT} \frac{1}{\sigma(x,z)^2}}$$

The standard deviation δ^T_{XBT} is taken equal to 1.5°C which corresponds to a surface error of 1°C, a thermocline error of 1.5°C and a deep ocean error of 0.5°C, following the error function σ introduced in Section 4.1. δ^T_{XBT} is higher than the accuracy of the XBT measurements but we overestimate the observational error in order to compensate model deficiencies (monthly windstress, climatological thermohaline fluxes, etc). This standard deviation is half the one corresponding to the climatology, which means that the weight of the XBT criterion is four times the climatological one.

4.3. Altimetric GEOSAT sea level data

GEOSAT sea level anomalies, η_{GEO}, are available everywhere between 60°W–20°E and 20°S–20°N (see Fig. 1a). The data processing included wet and dry tropospheric corrections, ionospheric corrections based on the Global Positioning System climatic ionospheric model, tidal corrections, along-track analysis and objective analysis (see Arnault et al., 1992, for further details). The resulting analysis has been mapped onto a 2° longitude × 1° latitude × 10 days grid. This is then interpolated at every time step and every gridpoint of the model together with the relative error ζ provided by the objective analysis.

In our rigid-lid model, the model sea level, η, is deduced from the surface pressure p_s by a rough vertical integration of the hydrostatic relation (the model surface pressure is determined up to a constant c (t) varying with time):

$$p_s = g\eta + c(t)$$

A problem arises because of the lack of an altimetric reference level (ARL) or absolute mean SSH for GEOSAT, which means that only time anomalies are accurate. To overcome this lack of an absolute oceanic mean SSH, a monthly mean correction ψ is used as a control variable (Greiner and Périgaud, 1994). ψ represents the oceanic mean SSH plus the model error in SSH. We saw in Section 3.1 that the model may have a bias in temperature of up to 3°C and this bias may vary in time (the simulated equatorial upwelling of July is too strong). This bias in temperature (similar bias exists in salinity) leads to a bias in heat content and thus in the model SSH. This varying bias in SSH (which may be caused for example by inadequate thermohaline fluxes) has to be corrected if one wants to use the GEOSAT variability to constrain the model dynamics. Consequently, ψ is optimized monthly as the initial conditions through the minimization of the following criterion:

$$J^{\eta}_{GEO} = \frac{\sum_{t}^{0\rightarrow T}\sum_{xy}^{Atl}\left[\frac{\zeta\overline{(\eta-(\eta_{GEO}+\psi))^2}}{\sigma(x,0)^2\delta^{\eta 2}_{GEO}}\right]\Delta x\Delta y\Delta t}{\sum_{t}^{0\rightarrow T}\sum_{xy}^{Atl}\left[\frac{\zeta}{\sigma(x,0)^2}\right]\Delta x\Delta y\Delta t}$$

The arc mark symbolizes the projection (the substraction of the spatial mean) used to filter out the constant $c(t)$ involved in the equation of the model-equivalent altimetry:

$$\overline{\eta} = \eta - \frac{\sum_{xy}^{Atl}\eta(x,y)\Delta x\Delta y}{\sum_{xy}^{Atl}\Delta x\Delta y}$$

For the weighting ζ of GEOSAT, we convert the relative error e_{GEO} calculated by the objective analysis (Arnault et al., 1992) as follows:

$$\zeta = (1 - e_{GEO})^2$$

This weight varies (within 0.6–1.) in space and time and reflects the satellite groundtrack pattern. A problem arising from the use of Servain and Lukas ship winds is that their analysis is relaxed towards Hellerman and Rosenstein winds south of 20°S. The model therefore cannot reproduce the interannual variability there and the agreement with GEOSAT altimetry will be poorer than north of 20°S. Consequently, we have deliberately increased the GEOSAT error in order to compensate for the modelling deficiencies (we linearly scale the error from 1 at 15°S to 2 at 20°S). The standard deviation δ^{η}_{GEO} is taken equal to 3cm which is an estimate of the error of the GEOSAT analysis over the basin.

4.4. First guess data

The first guess data are provided each month by the integration of the model over the previous month (the forecast) and this guess of the optimal initial condition contains the memory of the past for the velocity, temperature and salinity. For example, for the temperature, it is:

$$J^{T}_{g} = \frac{\sum_{xyz}^{Atl}\left[\frac{m(y)(T-T_g)^2}{\sigma(x,z)^2\delta^{T2}_{g}}\right]\Delta x\Delta y\Delta z}{\sum_{xyz}^{Atl}\left[\frac{m(y)}{\sigma(x,z)^2}\right]\Delta x\Delta y\Delta z}$$

We use similar criteria J_g^u and J_g^S for the velocity and the salinity with standard deviations δ_g^u and δ_g^S respectively equal to 0.05 m/s and 0.1 psu whereas J_g^T is 1.5°C. The deviations in temperature and salinity are taken as half the Levitus criteria. The factor two was chosen because it leads to the same weight in temperature first guess and XBT criterion. The chosen deviation in velocity corresponds to typical significant variations of current speed. For instance, if the mean speed of the North Equatorial Current is 0.1 m/s, a standard deviation of 0.01 m/s would have constrained the assimilation to stay very close to the first guess whereas a standard deviation of 0.1 m/s would have authorized a 100% change. This choice is an attempt to let the assimilation change the model currents reasonably from one month to the next. The weight, $m(y)$, is set equal to $1 + \frac{7}{40^\circ}|y|$ and varies with the latitude y. It describes the memory of the past: at the equator, where the oceanic temporal scales are fast (equatorial Kelvin waves cross the basin in 1–3 months), the memory is short and the control is mainly determined by the actual data; on the other hand, near the artificial boundary at 50°N/S, the memory is long and the absence of data means the control is entirely determined by the first guess (here it is not important because of the strong relaxation towards Levitus). In between, the impact of the first guess remains for a long time (1 year at 20°N, 2 years at 40°N) because the relaxation is weak or zero and the traveltime of the Rossby waves across the basin is longer than a year.

5. Assimilation

Once the model physics are chosen, the forcings imposed, the data and its weighting provided and the control defined, one still has to choose the assimilation window over which the optimization is done. This choice and the global parameters of the assimilations (optimizations) are summarized in this chapter. Monthly assimilations were made during 1987 and the model was run in forecast mode over 1988 starting from the optimal control, in order to test the impact in time of the assimilation and estimate the growth of the model error.

5.1. The control

The control consists of the initial conditions, C, and a mean correction for the SSH correction, ψ:

$$\text{control} = (C, \psi)$$

The control is estimated each month through the assimilation of the data for that month. There is no memory from the previous month for the SSH correction. The discretization of the initial conditions is detailed in Appendix A. In fact there are

additional controls which are the first guesses for the linear systems coming from the search for the barotropic streamfunction and the monthly spatial error of the model tendencies. The control of the linear systems is not fully coupled to the physical control so it will not be mentioned further (all the information about the control of these elliptic systems are in Greiner, 1993). The monthly error is not optimized (no descent is done is this direction) although we have collected the information provided by the gradient along this direction for a separate analysis.

5.2. *The cost function*

The cost function to be minimized for each month of 1987 is the sum of the criteria evoked in the previous sections. Its expression remains the same even if the data distribution varies in time (XBTs):

$$J(\text{control}) = \begin{cases} J^T_{Lev} + J^S_{Lev} & \text{Levitus climatologies} \\ + J^T_{XBT} & \text{in situ XBT} \\ + J^\eta_{GEO} & \text{GEOSAT altimeter} \\ + J^u_g + J^T_g + J^S_g & \text{first guesses} \end{cases}$$

5.3. *The assimilation window*

The assimilation window T still has to be chosen. It must be shorter than the physical limit of predictability. For the tropical Indian Ocean, Greiner and Périgaud (1996) showed that this limit ranges from 3 months north of the equator (subject to a strong monsoon) to more than 2 years in the region of the South Equatorial Counter Current (connected with the Southern Gyre and its Rossby waves). This could also apply to the tropical Atlantic: there is a monsoon in the Gulf of Guinea and the North Equatorial Counter Current is also affected by Rossby waves (their lifetime is 2 years at 20°N). However, the equatorial extension in the Atlantic is less than in the Indian and the interannual signal is weaker in the tropical Atlantic than in the tropical Indian. Hence, the limit is probably shorter in the Atlantic. Another restriction comes from the model representativity, which was about 9 months for the shallow water model in the tropical Indian. However, the climatological spinup showed that the current 3D model has difficulties in simulating the equatorial upwellings properly (January and especially July) which suggests that T should be less than 6 months and no more than a month in July. Also, one should remark that the ratio between the seasonal and interannual variability is around one in the tropical Atlantic (Arnault et al., 1992). Thus, both signals should be represented at once by the model with an accuracy comparable with GEOSAT. Since we use seasonal haline forcings, 3 months is the natural scale of model representivity. Another limit linked to the method of assimilation is the validity of the linear tangent model (and its adjoint). Our experience is that growth is linear near the equator (except some initial barotropic instabilities) and is bounded at high latitudes (the climatological relaxation acts like a damping term). But, some higher growth sometimes occurs with 10°–20°

latitude in a one month period. So, 1-3-6 months are natural candidates for a maximal assimilation window.

About a lower bound for T, one could consider the shortest time scale of the phenomena under interest. It might be of several days for a wind burst to a month for an equatorial Kelvin wave. Also important, is the minimum duration on which data can represent the large scale. Since it takes roughly 9 days for a boat to go from Rio to Europe (the main XBT line) and we have 3 different GEOSAT mappings per month, 10 days are a natural candidate for a minimal assimilation window.

Given all these arguments, we have chosen the assimilation window T to be one month (the arithmetic mean between 10 days and 3 months). This is convenient for the use of XBT data that are checked monthly. It also allowed us to realize the computations on today's computer. Nevertheless, if this set of experiences provides a first idea of the behavior of the 4D-variational data assimilation, it still has to be investigated further with other assimilation windows, in particular with improved covariance structures of the first guess.

5.4. *The strategy for assimilation and quality control*

For each month of assimilation we obtain three different trajectories of the model (see Fig. 4):

- the reference run (the trajectory without any assimilation),
- the assimilated run (containing all the data sets included in the cost function),
- the forecast run (the model allowed to run without assimilation for one month starting from the end of the assimilated run of the previous month).

Since we have a limited set of XBT profiles, we have not discarded any part of the original dataset in order to check the effect of the assimilation against an independent XBT dataset. On the other hand, each monthly assimilation is followed by

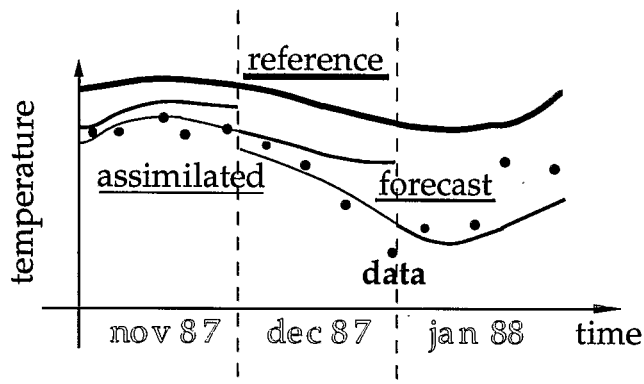

Fig. 4. Scheme of the data assimilation showing the reference (heavy thick line), forecast (thick line) and assimilated (thin line) runs. Forecasts are started from the last timestep of assimilation from the previous month. New assimilations are started monthly with changes to optimal control. Dots are symbols for data.

a forecast of one month. Hence, we use the dataset of the following month as an independent base for checking (i.e. forecast versus observations). One might find that one month forecasts are not very significant. However, the change over one month is of the order of a degree Celsius in the thermocline zone. Also, lag correlations computed from the satellite altimetry suggest a decorrelation timescale of less than 15 days in the equatorial Atlantic. Hence, given the small amount of data, two following months can be considered as independent so these one month forecasts are a reasonable check. Moreover, the positions of the XBTs vary strongly from one month to the next: the shipping lines Rio-Europe and Dakar-Cape of Good-Hope are regular on a monthly basis but for most of the data repetitivity is about 2–3 months. Thus, the forecast run is rarely compared to XBT observations at the same place that the XBTs were assimilated during the previous month. The strong spatial variations of temperature and the decorrelation radius (less than 10° from altimetry) in the equatorial Atlantic therefore suggest that this test is significant. This is also used by Bell (1994) and Ji et al. (1995).

In the second paper, we will further compare the assimilation results with weekly satellite SST. Although we have assimilated all the XBT profiles, we are more interested in the tropical Atlantic than the Caribbean Sea or the Gulf of Mexico. We are also interested in the impact of the assimilation on the the vertical structure. So, we have made a partition of the XBT in space:

- east of 60°W for the tropical Atlantic,
- west of 60°W for the Gulf of Mexico and the Carribean Sea,
- data warmer than 25°C for the near surface zone,
- data between 15°C and 25°C for the main thermocline zone,
- data colder than 15°C for the deep ocean.

In the following discussions, we will consider only the XBTs East of 60°W.

5.5. *The optimization*

The minimization of the cost function is done through a quasi-Newton BFGS (Broyton-Fletcher-Goldfarb-Shanno: see Fletcher, 1986) with limited memory and ten updates (Buckley and Lenir, 1983) with the preconditioning defined in Appendix A. The algorithm uses evaluations of the cost function J and its gradient. J is computed from the solver of the primitive equations, whereas its gradient is computed with the adjoint of the linear tangent of the solver. The linesearch of the quasi-Newton is of "coarse accuracy" type and the interpolation is at most cubic.

In order to run short jobs only, we divide the optimization into fractions: we make 5 iterations over one week, then 5 iterations over two weeks, 5 over three weeks and 10 over the whole month. The final reduction in the euclidian norm of the gradient is less than 0.1. Within this reduction, the initial decay of the cost function is mainly achieved at an affordable CPU time. (We checked that further minimization principally concerns small scales of the flow. Appendix A gives references on the controllability of the problem.)

6. Statistical results

6.1. The set of diagnostics and examples

In the following, we will make various comparisons between the three different runs of the model (reference, assimilated and forecast) and data (XBT and GEOSAT). These comparisons are dedicated to the misfits or related statistics coming immediately from the cost function. This gives an estimation of the "model error" used in the various configurations. However, the absolute values of the model can be far from the data whereas the time variations of the model can be close to observed. Thus, we will use the root mean square criterion to evaluate the absolute validity of the model, the relative validity of the model being evaluated by the correlation criterion and the standard deviation. The problem of evaluation is even more critical when one deals with the SSH signal: the altimetric reference level (ARL) is unknown and only optimized by the assimilation (see Section 4.3). So, reference run statistics based on the ARL simulated without assimilation would emphasize the error of the model whereas the fault could only come from an inadequate ARL. Hence, one must not use statistics that favor the assimilated run, and, we will make little use of spatial rms and correlation and use more time variability and time series (only time anomalies are unambiguous because the ARL is eliminated).

6.2. XBT profiles

Here we discuss the XBT profiles but the reader must keep in mind that all the data sets (Levitus climatologies, GEOSAT and XBTs) have been included at once in the assimilated runs and as initial conditions for forecast runs.

6.2.1. Statistics involving XBT over 25°C ("near surface zone")

There are about 1500 individual measures per month over 25°C, corresponding mostly to SST and near surface temperature. Monthly mean values of the root mean square (rms hereinafter) differences between XBT observations above 25°C and the model values during 1987 are given in Fig. 5. Surprisingly, the assimilated run is seldom better than the reference one (3 months out of 12). Rms differences are 1.7°C in mean for the reference run, 1.9°C for the forecast one and 1.8°C for the assimilated one. Though, the variation of the seasonal signal in the equatorial SST deduced from Levitus, is typically 3°C between the warmest month, March, and the coldest, August. Relative to this typical variation, the runs are not significantly different. Therefore the near surface is little changed by the assimilation.

The main reason for this slight degradation is that observations above 25°C are few (10% of the XBTs east of 60°W) so their relative weight in our cost function is of least importance for the minimization. The second reason is that the surface temperature of the model is relaxed towards the Levitus climatology (see Section 2.3) and thus is not at all free. This can be checked by looking at the rms differences between XBT observations and Levitus or the reference run (Fig. 6): the reference run follows Levitus in 1987. The reference run is not much better than the clima-

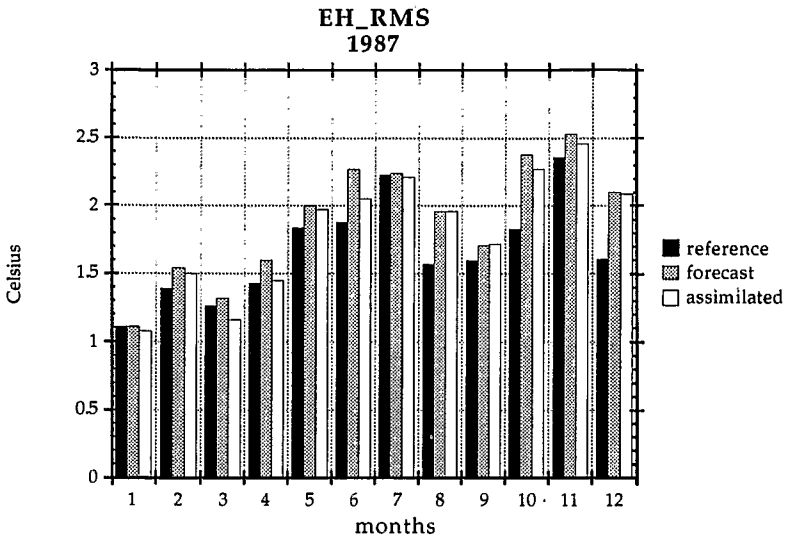

Fig. 5. Rms between XBTs east of 60°W above 25°C (EH) and model runs during 1987.

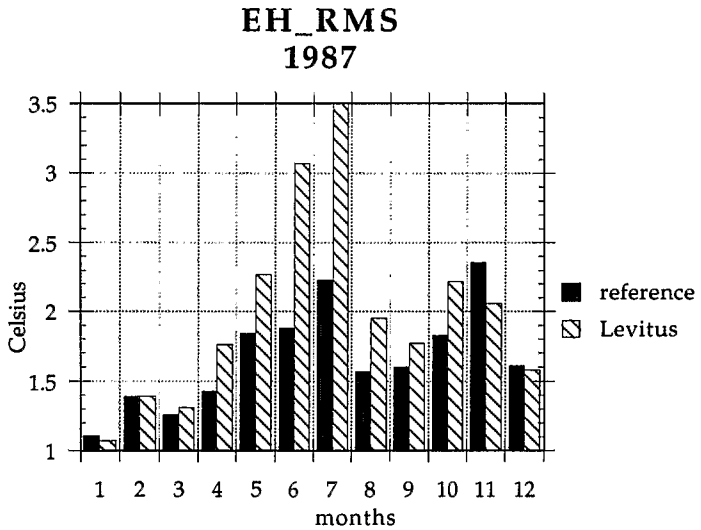

Fig. 6. Rms between XBTs east of 60°W above 25°C (EH) and Levitus during 1987.

tology except in June–July during the equatorial upwelling (an event possibly not well represented in the monthly climatology). The third reason is that the near surface temperature is strongly determined by the external forcings and the ability of the ML model to reproduce its thermodynamical response. As we use monthly winds and climatological thermohaline fluxes, the model logically looks like the climatology. The determination of the initial conditions cannot correct for the deficiencies

of the basic ML model which quickly modifies the initial near surface structure. Consequently, the response of the modelled SST is modulated by the weak model variability and by the error in the physics.

The spatial correlations (not shown) reproduce a different behavior than the rms values. Correlations between Levitus and the XBTs are between 0.5 and 0.7 whereas correlations between the model runs and the XBTs are generally higher and almost reaches 0.8 in March 1987. These better correlations suggests that the model may have a bias. This can be checked with the mean difference between the model runs and the XBTs (not shown). For instance, during May–December 1987, the model without assimilation is 0.7°C too cold compared to this particular set of XBTs. It is even colder with assimilation since the bias reaches 1.2°C. This bias is not negligible and penalizes the rms statistics even if the variability can be correct (see a striking example in section:3.1).

Fig. 7 compares the reference run and the forecast run during the first seven months of 1988. Again, the forecast is seldom better than the reference run and for the same reasons (model SST partly follows the climatology). However, the rms of the forecasts over April, June and July of 1988 are slightly better than the reference run (it is not legitimate to compare 1988 with the statistics of 1987 because the data sets of XBTs are different). Correlations from March to May are around 0.7 (the model still exhibits a cold bias during this period).

These surface statistics point out that, despite the sophistication of the method, this present data assimilation is not yet adequate to provide a significant improvement and the prediction skill is low for the near surface water. This shows that important progress is still required to produce a better forecast of the near surface water. It can come from the forcings, the model or the assimilation itself. However, it raises

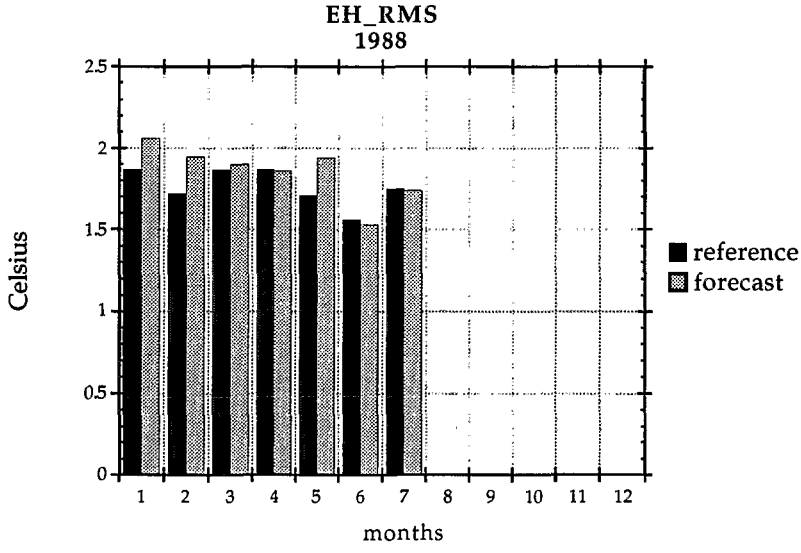

Fig. 7. Rms between XBTs east of 60°W above 25°C (EH) and model runs during 1988.

the question of the utility of the initialization to determine the thermodynamics of the top meters. This could suggest that a large improvement of the simulation of the near surface water by coupled models may not come from oceanic initialization.

6.2.2. Statistics involving XBT between 15 and 25°C ("thermocline zone")

There are about 3600 individual measures per month in the range 15°C–25°C, corresponding to the thermocline zone. Monthly mean values of the rms between these XBTs and the model corresponding values during 1987 are shown in Fig. 8. As expected and contrary to the surface layers, the statistics of the assimilated run (2.7°C in mean) are better than the reference one (3°C in mean). The variation of the seasonal signal in the equatorial thermocline (between 50m and 100m) deduced from Levitus, is typicallly 2°C. Relative to this typical variation, the improvement represents 15% of the seasonal signal. The rms differences can also be compared to the local variability of the XBT measurements at 100m which is within 1.2 ± 0.2°C during 1987 (Fig. 13 gives an example of data dispersion). The improvement is especially important during the first 7 months and reaches a maximum of 0.5°C. After the equatorial upwelling in July, the improvement is no longer so large. In December, the model-data misfit was particularly high and the assimilated run is worse than the reference run. December is a quiet month in the Equatorial Atlantic and the natural altimetric variability is low. Moreover, the processing may have filtered some oceanic signal (see Arnault et al., 1992, about this problem). So, little information was available from GEOSAT analysis, and XBTs below 15°C produced the leading criterion of the cost function. This criterion has been decreased by the assimilation.

Eight of the 12 one month forecasts of 1987 are better than the reference run (Fig.

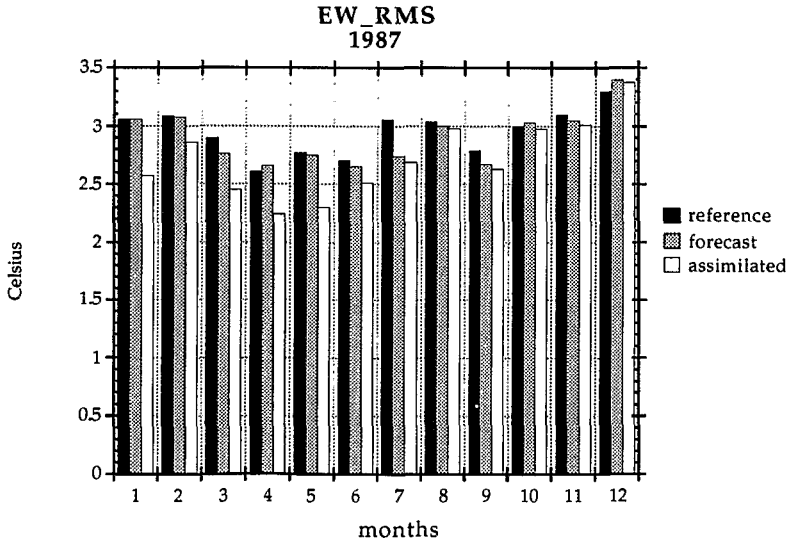

Fig. 8. Rms between XBTs east of 60°W within 15°C–25°C (EW) and model runs during 1987.

8). The 8 forecast improvements indicate that the variational assimilation does not create shocks in the forecast within the two months following the optimized initial conditions. We recall that the 2–3 months XBT repetitivity joined to the strong spatial variations of temperature and the decorrelation scales suggest that this test has some significance. The rms values for the assimilated run are between 2.2°C and 3.4°C (correlation between 0.5 and 0.8). This can be compared (not shown) with the rms obtained with Levitus climatology. Levitus rms are less than 2°C (correlation around 0.8) except between June and October (rms around 2.2°C and correlation around 0.75) when they are poorer. So, considering only spatial snapshot statistics, the climatology still performs better than the model with assimilation.

Thermal profile data has also been assimilated in the Atlantic ocean using the nudging method during the test period July–September 1993 (Bell, 1994). He also used a similar primitive equation model but with a Richardson number dependent mixing throughout the column. Unlike the current study, this model was forced by the 6 hourly winds from the United Kingdom Meteorological Office analysis. For the region east of 30°W and south of 30°N and the data between 35m and 67m, it obtained a rms of 1.5°C without assimilation and only 2.3°C with. As in our case, the climatology is slightly better than the reference run. Also interesting, the run forced by the French Meteorological Office analysis (Roquet, 1994) over 1992–94 (no data assimilation) gives rms below 1.5°C. Given all the restrictions for the different period and data, this shows how far we are from a fully realistic numerical simulation of the ocean variability as given by the XBTs. However, the statistics of our assimilated run underestimate the ability of the model to simulate the spatial and time variability of the large-scale ocean. This is explained in detail through the examination of one XBT line in the Section 6.2.4.

The mean difference between the model runs and the XBTs during 1987 in the "thermocline zone" generally fluctuates between − 0.3°C and + 0.3°C (not shown). It is therefore not very significant and sometimes the assimilation has reduced the bias, sometimes increased it. This suggests that the thermocline is well located in the mean. If the thermocline is correct but the ML is not, this suggests that the poor simulation of the ML may not be a result of the mean forcing. The effects of a lack of high frequency variability in the forcing (monthly wind and climatological thermohaline fluxes) will be examined later using one XBT line and several SSH time series.

The rms for the first 7 months of 1988 (Fig. 9) shows an improvement of the forecast from February to May, but a subsequent degradation during the equatorial upwelling in June–July. Springtime heating favors the ML model and thus leads to some predictive skill for the model in the thermocline zone for the subannual signal. On the other hand, the equatorial upwelling appears to inhibit the prediction skill. We will show in Section 6.2.6 how the ML model can be responsible for this. Consequently, it is hard to appreciate globally the prediction skill of the model in the thermocline zone. Though, the improved forecast of spring 1988 and of most of the one month forecasts of 1987 suggest that this basic data assimilation system has already had a positive impact on the thermocline.

One may wonder which dataset (GEOSAT, XBTs or Levitus) has the greatest

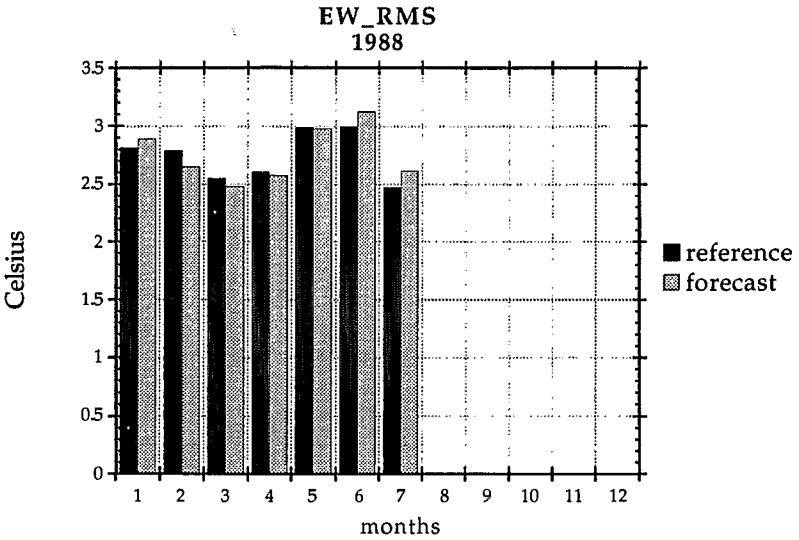

Fig. 9. Rms between XBTs east of 60°W within 15°C–25°C (EW) and model runs during 1988.

effect on the simulated thermocline. For instance, we tried the same assimilation experiment without GEOSAT data. Then, the minimization of the XBT criterion (the leading term) is slow, even if still steady. Corrections provided by the assimilation are restricted to the neighborhood of the XBT data (up to several degrees if it is in a region of equatorial waves or strong currents). On the other hand, assimilating GEOSAT at the same time (this experiment) speeds up the minimization of the XBT criterion and provides a correction of all the large-scale variables (velocity, temperature and salinity). In summary, sea level variations give the thermodynamical variations relative to the thermocline depth and the XBTs provide absolute information of this depth. The positive results of the experiment encourage us to analyze the impact of each individual data on the assimilation (covariance structures) in a more favorable situation (better data coverage and computing resources) like in Carton et al. (1996).

6.2.3. Statistics involving XBT under 15°C ("deep ocean")

Finally, there are about 11,000 individual measures per month below 15°C, corresponding to temperature between 100m and 1000m (8 model levels). The monthly mean values of the rms between these XBTs and the model values during 1987 are given in Fig. 10. The reference run is about 1.2°C in mean while the Levitus climatology is steady around 0.75°C (not shown, space-time correlations are above 0.98 for all runs and climatology). The forecast run (1.1°C in mean) is between the reference run and the assimilated run. The assimilation improves the simulation (1.0°C in mean) except in March and August (the warmest and coldest months). As a comparison, the variation of the seasonal signal in the equatorial Atlantic between 200m and 500m deduced from Levitus, is typicallly 1°C. Residuals can also be compared

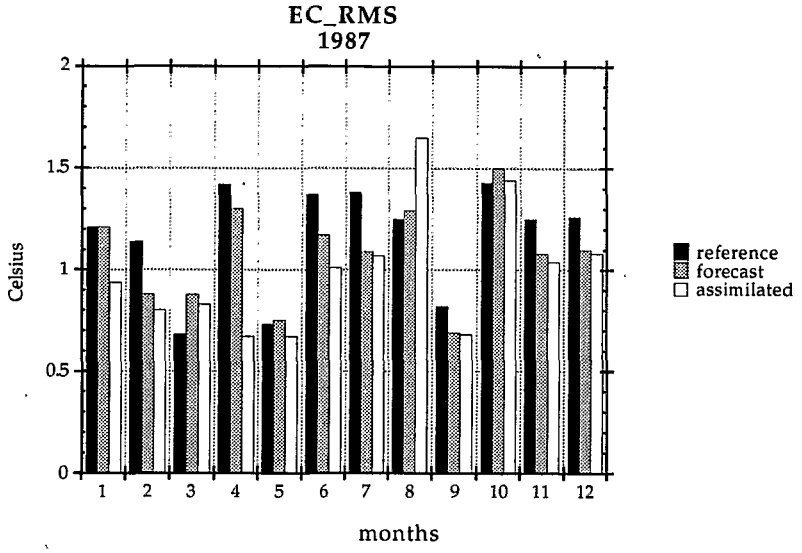

Fig. 10. Rms between XBTs east of 60°W below 15°C (EC) and model runs during 1987.

to the local variability of the XBT measurements at 500m which is within 0.4 ± 0.2°C during 1987.

The assimilated run is nearly as good as the climatology during the first months. This shows that the Richardson number dependent mixing can produce a good climatology under the thermocline with variational data assimilation. The run forced by the French Meteorological Office analysis (Roquet, 1994) over 1992–94 gives rms around 1.25°C.

Fig. 11 depicts the mean difference between the model run and the XBTs during 1987 for the "deep ocean". The reference run presents a warm bias generally higher than 0.5°C. The assimilation greatly reduced this bias by a rise of the isotherms below the thermocline. We noted in previous sections that the model presents a cold bias in the near surface layer, which was increased by the assimilation. This is not systematically linked to the cooling of the deep ocean since the mean position of the thermocline was not changed by the assimilation. Indeed, these statistics regroup different behaviors, in particular the ones of the region of both the equatorial upwelling and the north equatorial currents. In the latter case for instance, the increased surface cold bias in spring compared to XBT data is the result of a westward migration of a cold correction provided by the assimilation (Part 2) across the Rio-Europe line. Thus, this cannot be interpreted in terms of a homogeneous increasing bias: the lack of good data coverage (100 to 200 XBT profiles per month) prevents us from making a synoptic analysis of the model bias.

The rms for 1988 (Fig. 12) shows an improvement of the forecast for 5 out of 7 months (we have not pushed the forecast beyond the model limit—July and its upwelling) and all the spatial correlations are improved (not shown). Despite the

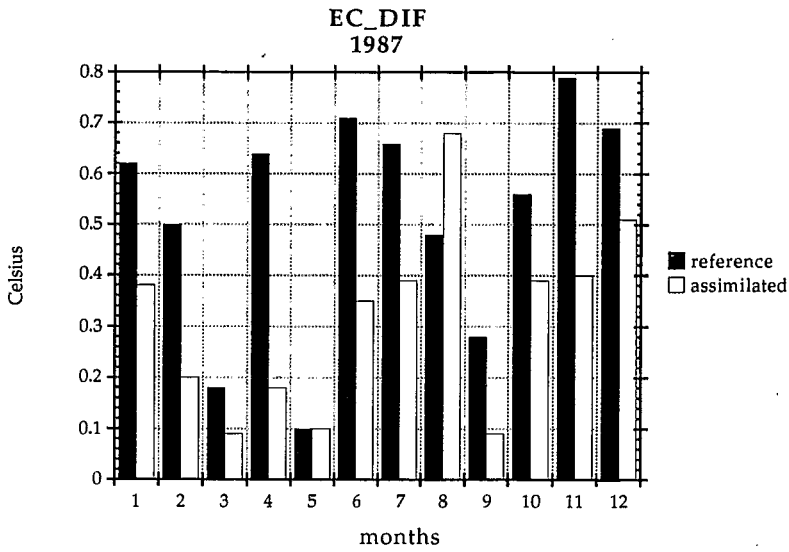

Fig. 11. Mean difference between XBTs east of 60°W below 15°C (EC) and model runs during 1987.

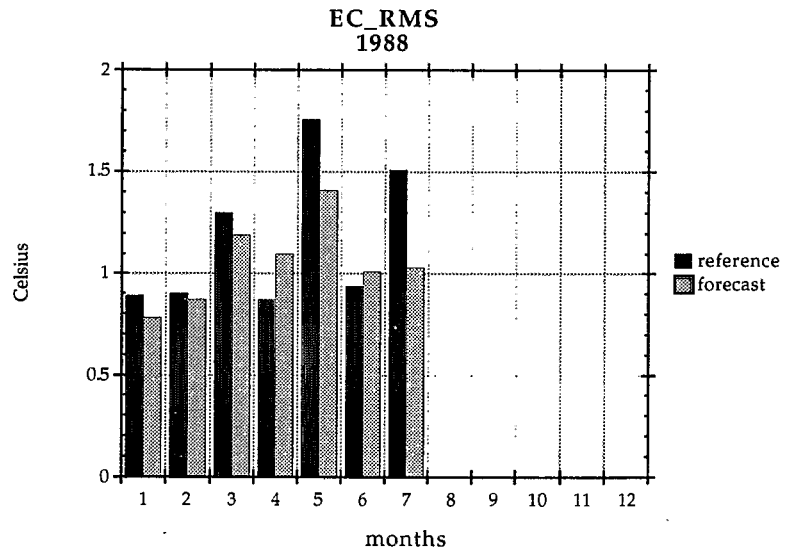

Fig. 12. Rms between XBTs east of 60°W below 15°C (EC) and model runs during 1988.

deficiencies of our simulations, the variational assimilation has been able to take benefit of all the data sets in order to improve our short forecast.

However, the significance of this improvement is questionable. XBTs do not go below 1000m so direct measures of the deep ocean are few. Since most of the variability in sea level is restricted at or above the level of the thermocline, it is likely

that GEOSAT provides little information on the deep ocean. Thus, one may wonder if the improvement of the forecast results principally from the Levitus data. Indeed, this dataset has been used by the assimilation to correct the model bias at depth which is rather consistant in time. If the climatology is really the main source of information at depth, little or no information on the interannual signal would be input at depth by the assimilation. In order to document this hypothesis, we have examined the temperature at depth along the main shipping lines. Unfortunately, the year-to-year signal was not clear in 1988 below 200m. Moreover, if the signal captured by assimilation principally concerns the north equatorial currents in 1987, the impact of the assimilation is stronger in the Gulf of Guinea in 1988, and especially south of the Equator (this point is analysed in the Part 2). From this point of view, the XBT lines are not much helpful to validate the year to year change at depth from 1987 to 1988. The most significant signal in the north west was obtained at 120m (near the base of the thermocline) near 31°W–1°N (this crossing of 3 shipping lines produced the best sampling at this location). The XBT casts (Fig. 13, top) present temperatures warmer by 2°C in July 1987 compared to the climatology (second from top). An anomalous warming is also visible in July 1988. The climatology presents a maximum in November which is not clearly defined on the XBT plot. The reference run (second from bottom) simulates some warming in July 1987 and July 1988 and rather cold temperatures in November 1987. The assimilated run (bottom) is closer to the XBTs than the reference run or the climatology. This shows that the assimilation provides information at depth which does not come from the climatology. The forecast run is closer to the XBTs than the reference run in spring 1988 but presents a 5°C warming in July 1988 relative to January 1988 (3°C for the XBTs, 0°C for the climatology, 4°C for the reference run).

There is only one shipping line to study the impact of the assimilation at depth in 1988 in the Gulf of Guinea. Fig. 14 shows this line between 9°W–13°S and 13°W–3°N in April 1988. It is a representative month of the warm event (see Part 2 for the context), the main feature being the eastward Equatorial Under Current (EUC) and its considerably deep extension at 2°S (300m and below). The subsurface core of the EUC can be diagnosed from the increased thickness of the warm waters within 15°C–25°C, and the deep extension is clear on the meridional gradient between 3°S and 5°S. It is also possible to identifiy the westward South Equatorial Current (SEC) thanks to the rising of the isotherms at about 4°S above 150m and at 1°N. The eastward South Equatorial Counter Current (SECC, Molinari, 1982) can be deduced as well from the deepening at 5°S above 140m. The zonal velocity showed by the reference run along the XBT line (Fig. 15) includes a weak SECC South of 5°S. However, a deep westward equatorial current is strongly developed below 90m. The deep extension of the EUC is thus broken by an opposite current. The zonal velocity showed by the forecast run (Fig. 16) presents a continuous deep extension of the EUC at about 2°S. Velocities are weak, but the shearing between 7°S and 12°S, concerning the south equatorial gyre is strengthened in the forecast and affects considerable water masses. The importance of the southern gyre and its offshore cooling are discussed in the Part 2.

Globally, these two examples suggest that the assimilation can be useful for the

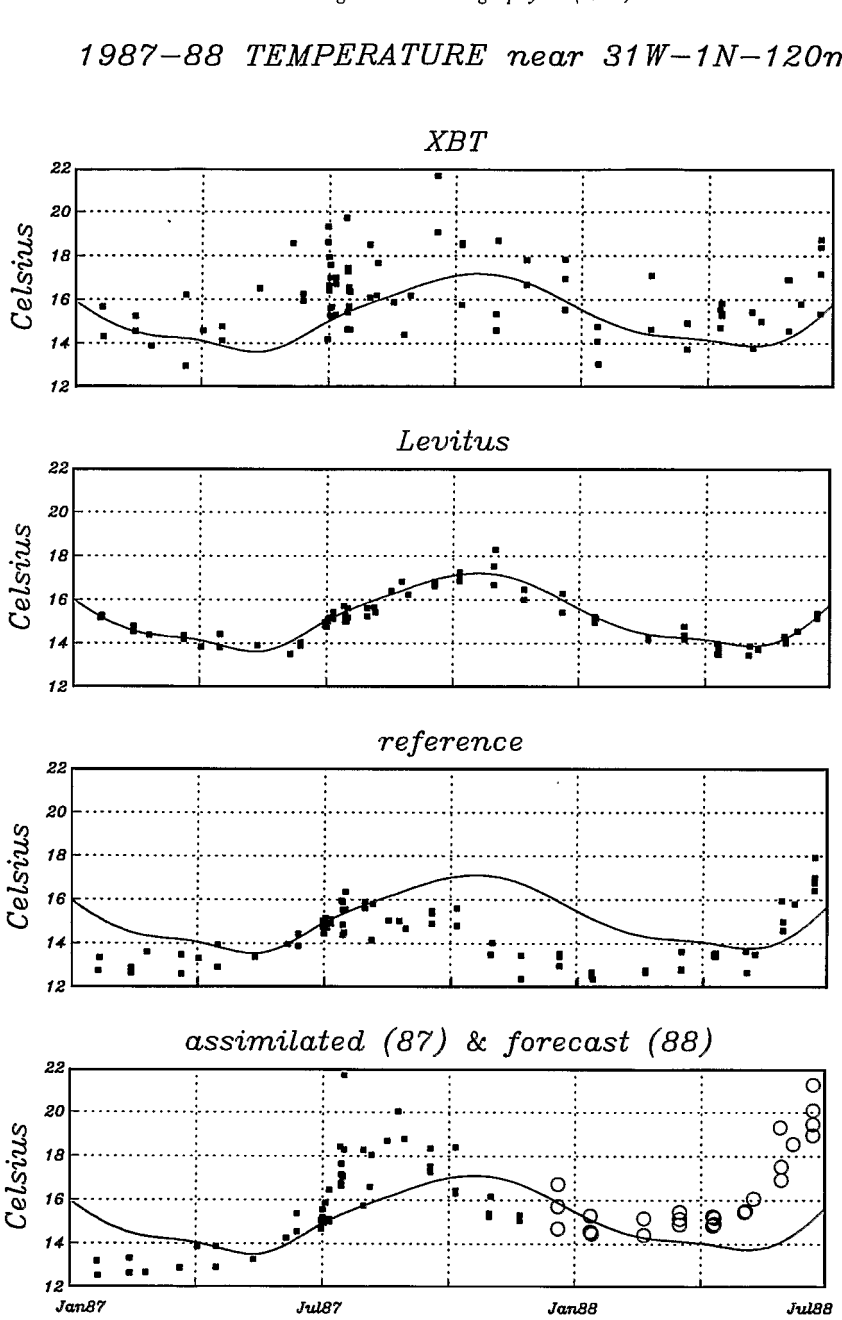

Fig. 13. Temperature time series from January 1987 to July 1988 near 31°W–1°N (distance less than 2°) near 120m (distance less than 5m). XBT casts are displayed in the top pannel, Levitus climatology in the second pannel, the reference run in the third pannel, the 1987 assimilated run in the bottom pannel (boxes) and the 1988 forecast run in the bottom pannel (circles).

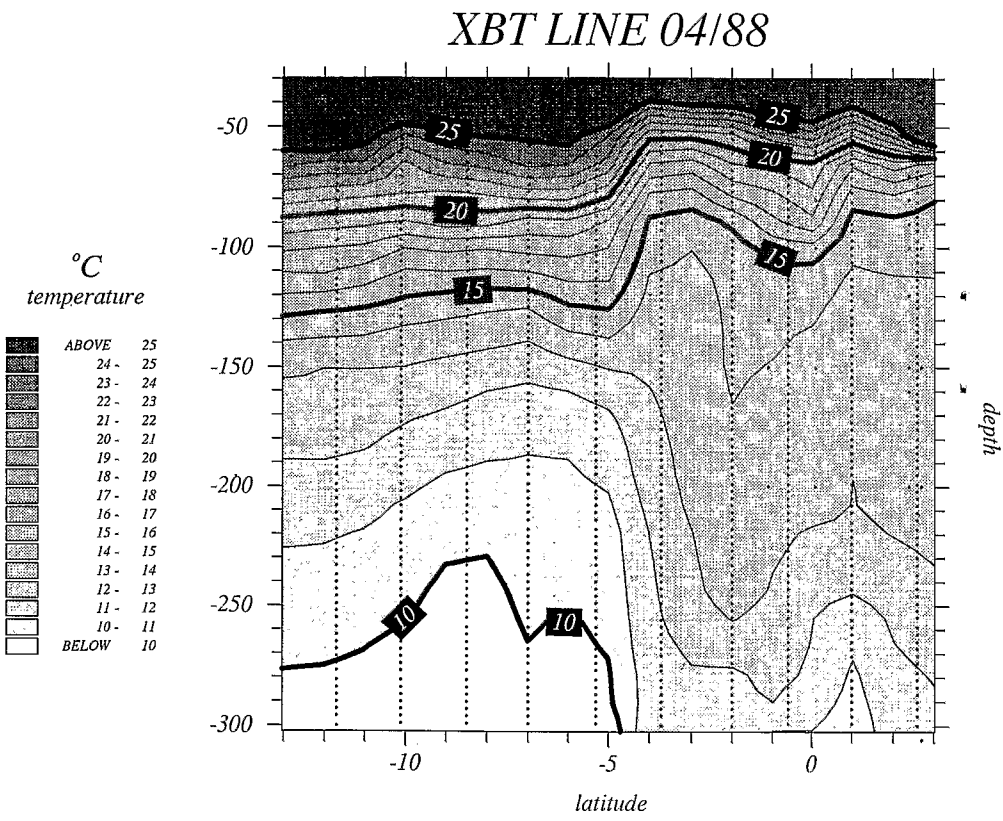

Fig. 14. Vertical section of XBT temperature observations within 30–300m along a ship track from 9°W–13°S to 13°W–3°N during April 1988. The black dots indicate the position of each mesurement.

predictability of the low variability of the large scale motions of the ocean. But, because of a weak signature of the year-to-year signal on the deep XBTs, further investigations in more favorable situations (stronger signal, better data coverage and improved data assimilation) are still needed to confirm this possibility (such a contribution can be found in Carton et al., 1996). In summary, the important result is that the assimilation has provided a better structure of the "deep ocean" without sacrificing the dynamics. This is important for a short term climate forecast. This also recalls the importance and adequacy of all observations (even climatologies) for short term climate studies.

6.2.4. Vertical sections along XBT lines

We illustratred here the previous statistics by a characteristic example. This example consists in a vertical section of temperatures along one XBT line from Rio to Europe during January 1987. Fig. 17 shows the in situ measurements as used. The thermocline is well defined and presents the normal north-south slope of January. This can be compared to Levitus climatology (Fig. 18). The slope is correct in the

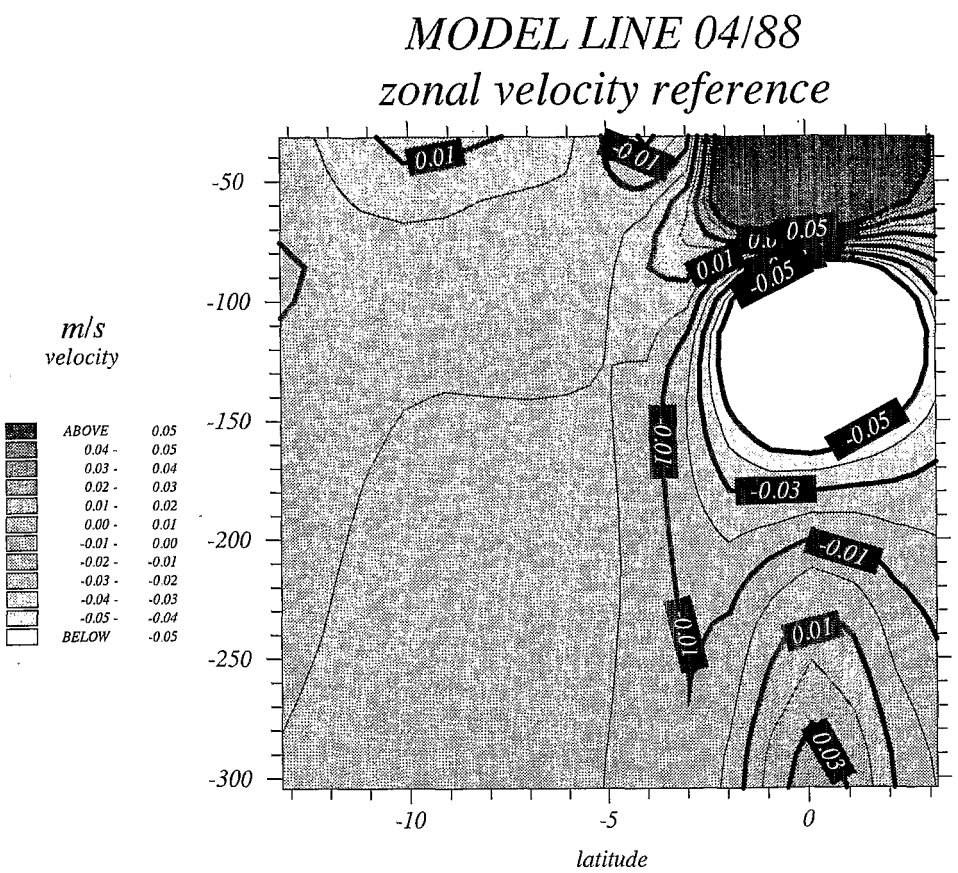

Fig. 15. Same section for the model zonal velocity of the reference run. Darker shading corresponds to eastward velocities. Labels are in m/s.

climatology but the shoaling of the thermocline near the equator is weak. This can be explained by the gridding procedure used by Levitus (it does not have the same resolution at the equator in the Atlantic as the example XBT line). On the other hand, Levitus and the XBT data match closely away from the equator. These two points hold true for all the XBT lines of 1987–1988. In other words, Levitus climatology has good quality information away from the equator, which is why we used it as a background data constraint. The climatological data was also accurate enough to diagnose the bias of our model.

The reference run performs (Fig. 19) a little bit better than the climatology in two ways. First, the equatorial shelf is more visible in the simulation, for instance on the 15°C isotherm. Second, the equatorial thermocline thickness is closer to the XBT than the climatology, which is too broad. However, the faults of the model compared to the XBT line are also clear. The thermocline slope is too flat and its depth too deep. The shelf is also much less pronounced in the reference run than on the XBT

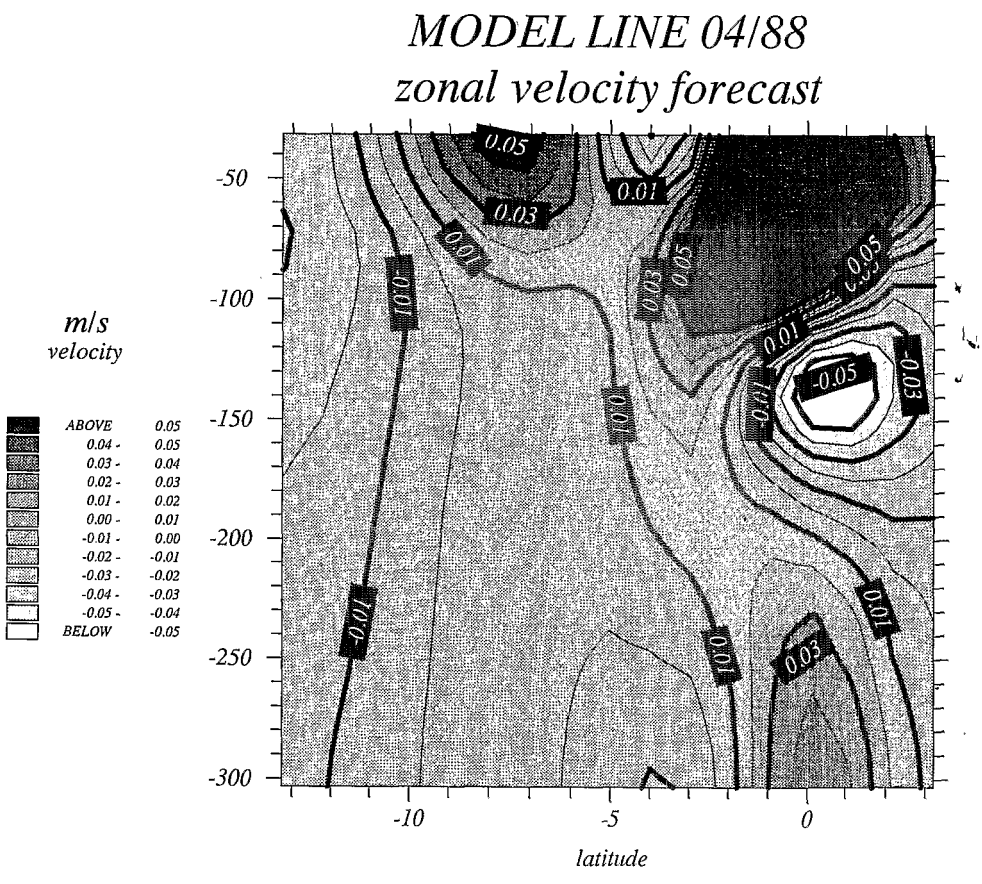

Fig. 16. Same as Fig. 15 for the forecast run.

line. Finally, the simulation presents an unrealistic upwelling with an equatorial surfacing of water within 26–27°C, structure which is absent from the XBT line. The thermocline is also too narrow in the north. The flatter than observed slope could be a consequence of a weak meridional wind stress, which balances the pressure (density) gradient force across the basin. The inability of the ML model to simulate the winter deepening probably accounts for this too. The smoothness in space of the slope could come from the smoothness in space of the forcings. The stronger upwelling and the narrower thermocline in the north could come from the vertical diffusivity given by the ML model.

The assimilation corrects part of these deficiencies (Fig. 20). The weakest improvement concerns the upwelling. This is not surprising since the vertical diffusivity in the ML is an external forcing with our basic ML model. The cold bias of the "near surface" has been increased. We can see in the example (all the lines reveal this fault) that the assimilation did not bring any particular correction in the vertical structure of the top layers. Other faults were corrected. In particular the thermocline

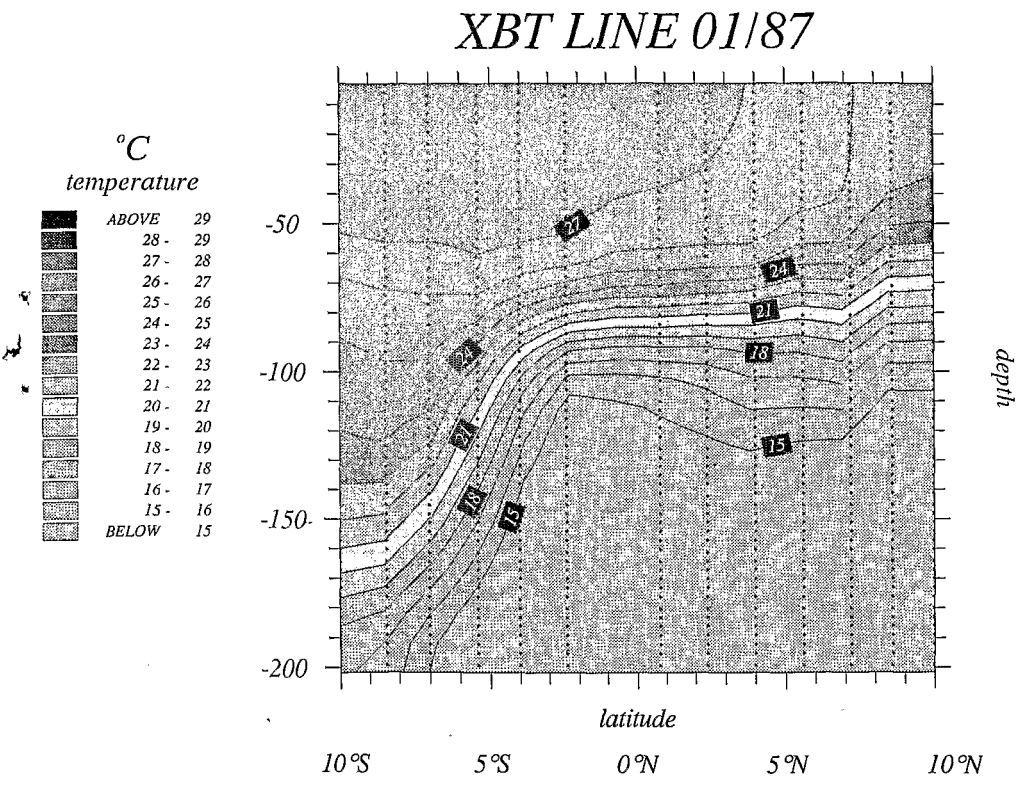

Fig. 17. Vertical section of XBT temperature observations within 0–200m along a ship track from 36°W–11°S to 28°W–11°N during January 1987. The black dots indicate the position of each measurement.

has been pushed upwards and the warm bias of the "deep ocean" (see Section 6.2.3) is removed. The thermocline is well placed and now reproduces all the large scale features of the data. The small-scale details are still missing but they depend less on the initialization than on the forcings or on the resolution of the model.

6.2.5. Depth of the 20°C isotherm along XBT lines

In this section we consider the depth of the 20°C isotherm along one XBT line from Rio to Europe during 1987 and 1988 (Fig. 21). This line shows a meridional slope and an annual signal. In Fig. 22, the reference run simulates an annual signal which is well in phase but the intensity of the signal is too weak. The meridional slope is much less steep than in the XBT data. The assimilation (Fig. 23) provides very little improvement. The difference between the assimilation and the XBT (not shown) is less than 10m from 4°N to 4°S but there is a constant bias in the north-south slope. Errors obtained by Ji et al. (1995) are of order of 6–15m by optimal interpolation with a slightly simpler model of both the Pacific and the Atlantic. Both results can be compared to the 5m accuracy in the thermocline depth obtained from the XBT profiles.

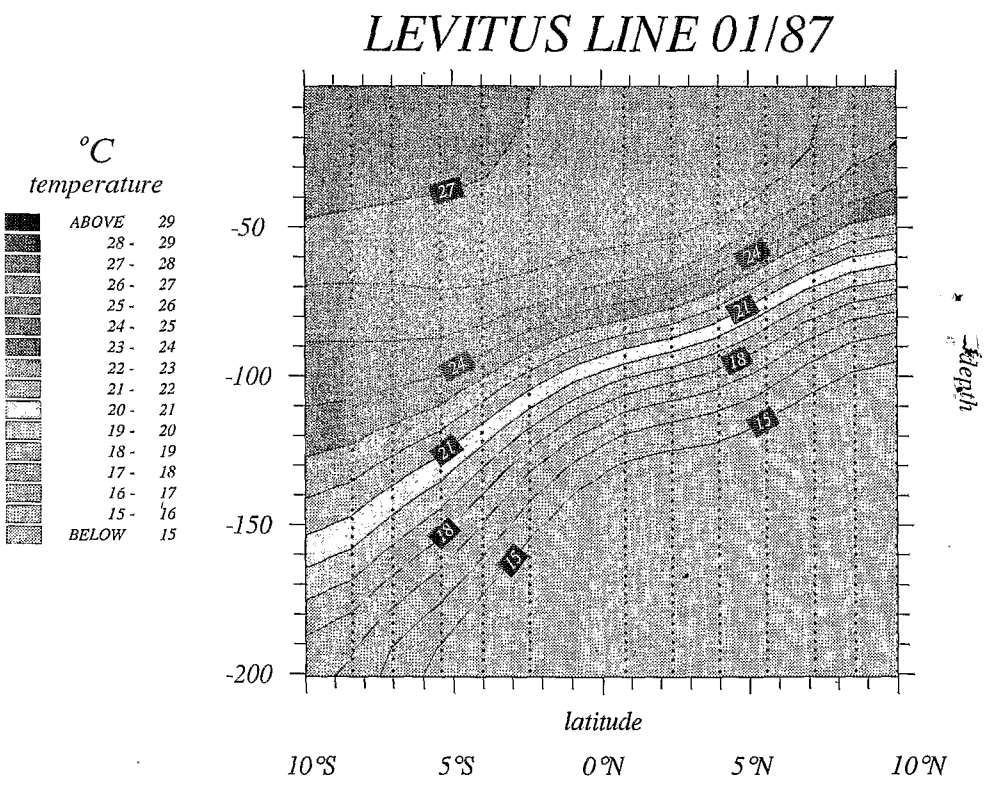

Fig. 18. Levitus section. Same conventions as Fig. 17.

6.2.6. *Discussion on XBT statistics*

The model without or with assimilation (Figs. 24 and 25 respectively) performs poorly during the equatorial upwelling, as revealed by the statistics. This can be explained as follows. During May–June, the equatorial Atlantic is cooled by the atmosphere. The basic diagnostic 1D imbedded ML model is unable to prescribe accurately to the 3D model the deepening of the ML resulting from this cooling (see Section 2.2). The ML depth of the 3D model is overestimated, which is purely a numerical problem of limitation of the ML depth. There is an increased vertical diffusion at depth which slows down the EUC. But, the kinetic energy is the main cause of the penetration of the EUC in the eastern half of the basin where the zonal density gradient is weaker (BD93). Since the impact of the equatorial divergence is no longer balanced by the kinetic energy, the upwelling develops too strongly (Fig. 24). The EUC slope, which is normaly constant (BD93) from America to Africa, is increased in the west and decreased in the east. It reinforces the zonal density gradient in the west and diminishes it in the east (deep western cold water no longer reaches the Gulf of Guinea). Consequently, the mechanism of the penetration of the EUC in the Gulf of Guinea is partly broken during the set up of the equatorial

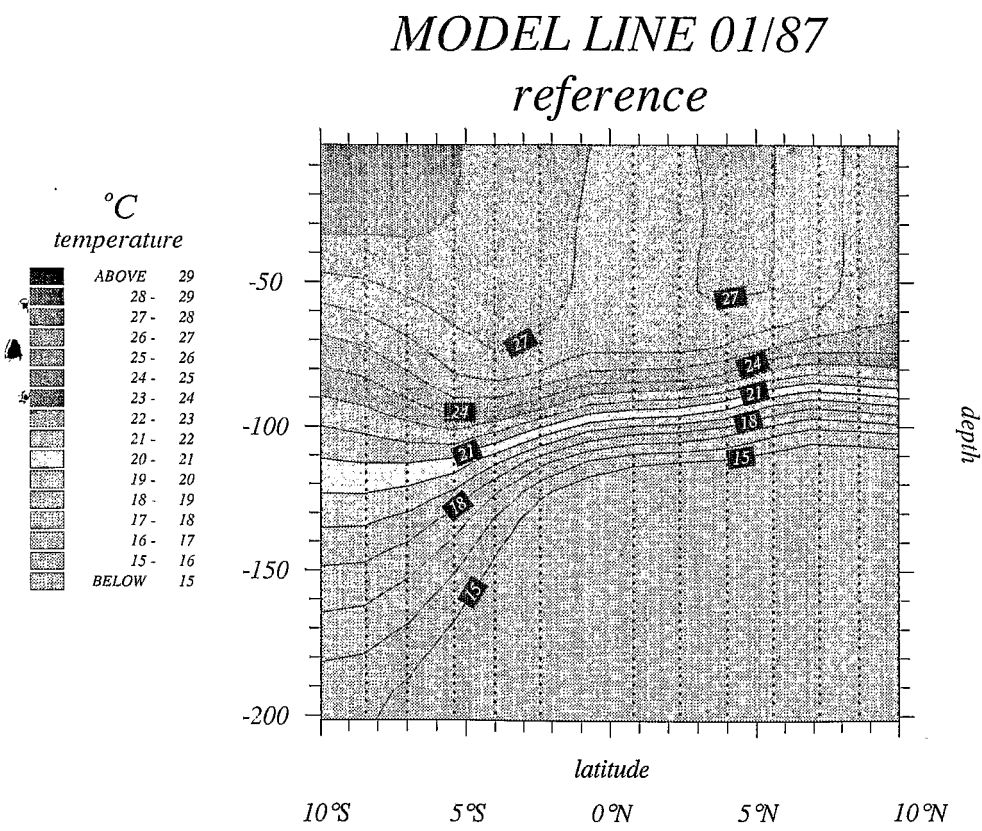

Fig. 19. Model section of the reference run. Same conventions as Fig. 17.

upwelling because of the ML model. Such failure of the ML model, already identified without assimilation in BD93, is not corrected by the assimilation (Fig. 25). During the equatorial upwelling, the heating of the ocean is reestablished but the adverse effects of the ML model have already been introduced in the equatorial strip. The propagation of this error can quickly affect the whole tropical basin because of mass and momentum conservation (the system of the equatorial currents is interconnected).

We saw that the same vertical structure of the ML holds for the reference and the assimilated run, the isotherms being pushed toward the surface if necessary. In fact, the top layers are homogeneous in the model with or without assimilation. The XBT profiles tend to prove that this lack of stratification near the surface is wrong. However, the ML model may not be solely responsible. It may also come from this particular data set: it was found (Roquet, 1994) that some XBTs present a warm bias (0.25°C) in the top meters because the thermographs are stored on the deck when not in use. Another problem is the use of a climatological heat flux which is constant daily. Hence, the diurnal signal is not reproduced by the model. This signal can create variations in the first 10 meters of up to 0.5°C (Peters et al., 1988).

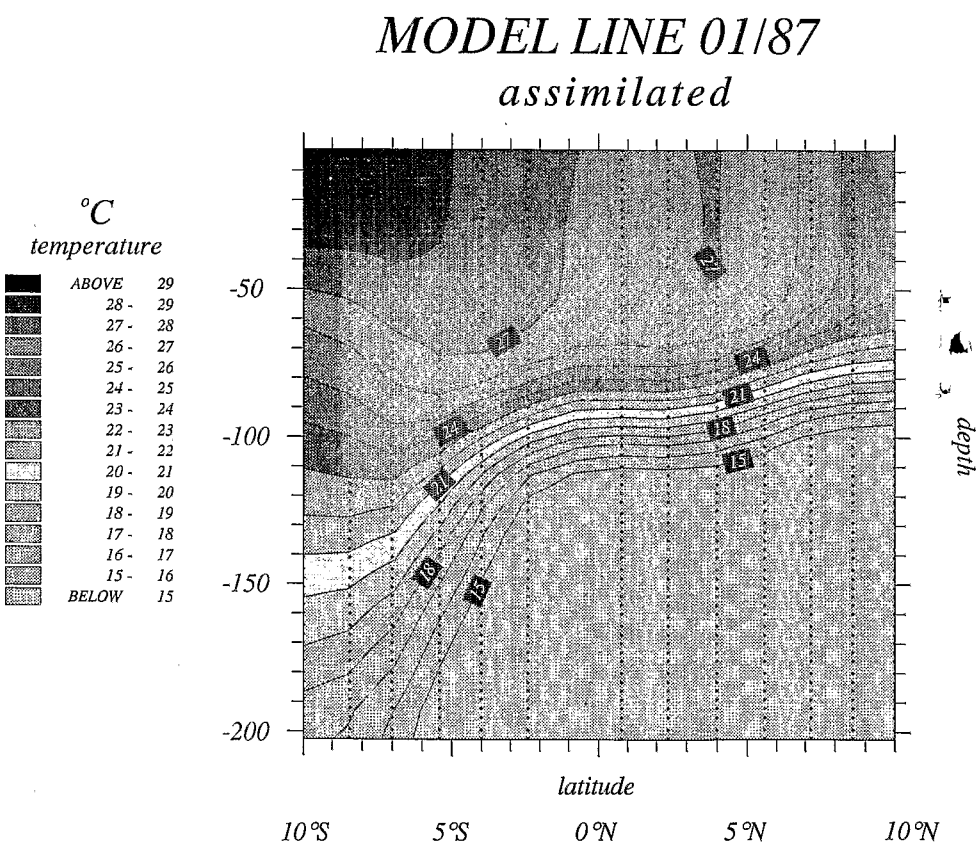

Fig. 20. Model section of the assimilated run. Same conventions as Fig. 17.

Unfortunately, fewer XBT casts are made at night than during the day (J.P. Rebert, personal communication, 1995) and thus the data set itself presents a warm bias which is not compatible with a daily heat flux. Consequently, a model assimilating pure XBT data should reproduce the diurnal signal in order to produce a reliable result. This means that we will need at least 6 hourly forcings. If we eliminate the use of an artificial diurnal signal, this leads us to use the products of the weather centers.

Nudging assimilation of thermal profiles in the Atlantic ocean during the test period July–September 1993 (Bell, 1994) gives an insight of the impact of the forcings. His model is forced by the 6 hourly United Kingdom Meteorological Office analysed winds. For the region east of 30°W and south of 30°N, he obtains a rms of 1.0°C for the surface layer with assimilation, 1.1°C without assimilation, the climatology being near 0.8°C. Firstly, it emphasizes that data sets can be very different from one to another (the mean score for the climatology during 1987 is 1.7°C). A repeat network of in situ measurements such as the proposed PIRATA Mooring Array (Servain, 1996) would facilitate such inter-comparisons. Secondly, even if this example is different, the weak impact of the assimilation on the near surface is also

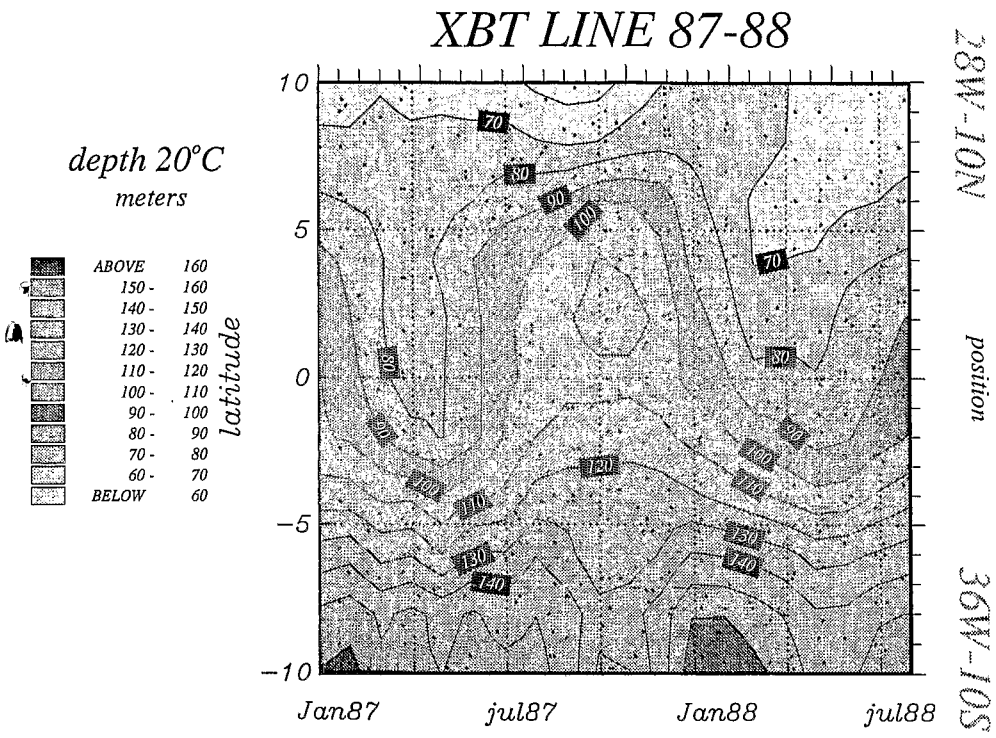

Fig. 21. Depth of the 20°C isotherm extracted from the XBT line 28°W–10°N to 36°W–10°S. The back dots indicate the position of measurements. The labels are in meters.

pointed out. Another comparison is the run forced by the French Meteorological Office operational analysis over 1992–94 (Roquet, 1994). The discretization is nearly the same as ours but they use a turbulent kinetic energy closure of the vertical diffusion. The 6 hourly wind-stress and heat fluxes from the operational analysis forced the model. A relaxation to an analysed SST and to Levitus salinity hold too. In these conditions, they obtain a rms difference around 0.75°C for the near surface. So, the operational analysis seems to provide good results, even without assimilation. Of course, it is neither the same year nor the same datasets. However, the impact of 6 hourly analysed winds could be thought of as a way to improve oceanic simulations. United Kingdom and French Meteorological Office experiments are encouraging for the oceanographers.

6.3. GEOSAT sea level anomalies

In the following, we make a statistical analysis of the results of the model compared to GEOSAT. The main difficulty comes from the lack of an altimetric reference level (ARL) for GEOSAT. This major difficulty is explained in Section 6.1. The

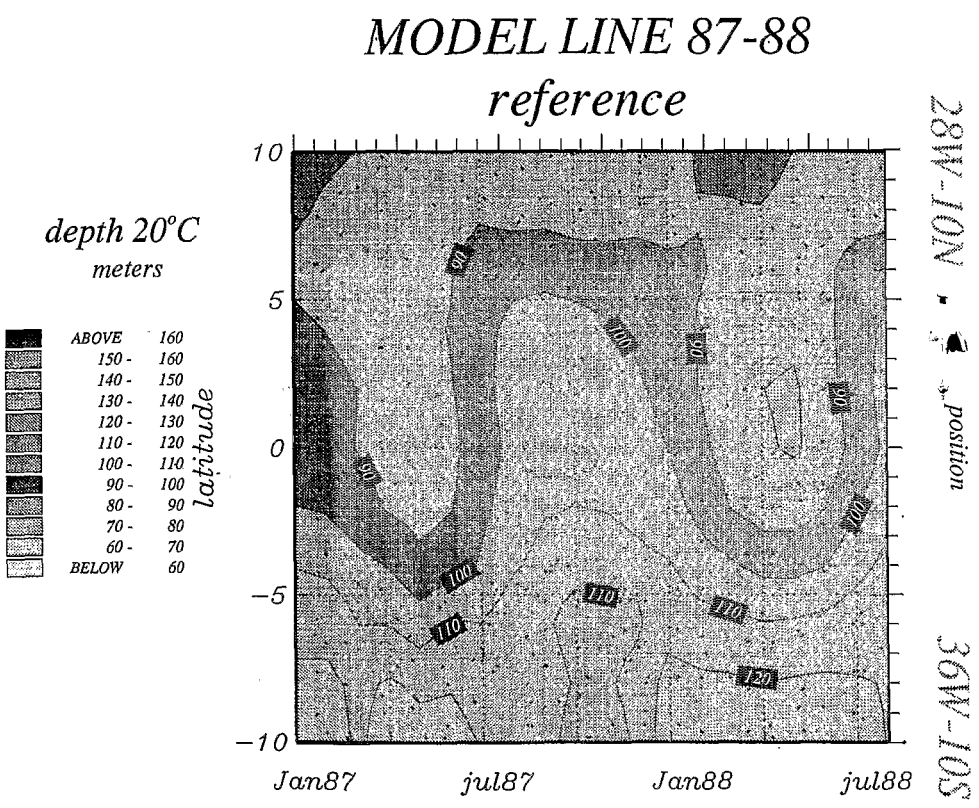

Fig. 22. Same as Fig. 21 for the reference run.

ARL is estimated only through the variational assimilation. Consequently, the ARL is not data and we will identify the statistics which involve the ARL.

6.3.1. Monthly statistics involving the reference level

The rms difference between the SSH of the assimilated run and GEOSAT is near 1.5cm except from July to October when it is closer to 2cm. In either case, this is satisfying, given the level of error of GEOSAT which is around 3cm. Also, the spatial correlation reaches 0.8 with assimilation whereas it is close to 0.1 without. So, the assimilated run reproduces the spatial variability of GEOSAT. The forecast run is rarely below 4cm rms and exceeds 5cm during June–August. Thus, part of the information put into the model by the assimilation seems to be lost very quickly after each month of assimilation. The next sections will provide information on this mechanism.

6.3.2. Monthly statistics not involving the reference level

In order to compare model runs and data independantly of the ARL, one has to consider only anomalies over a given month. GEOSAT repetitivity being 17 days,

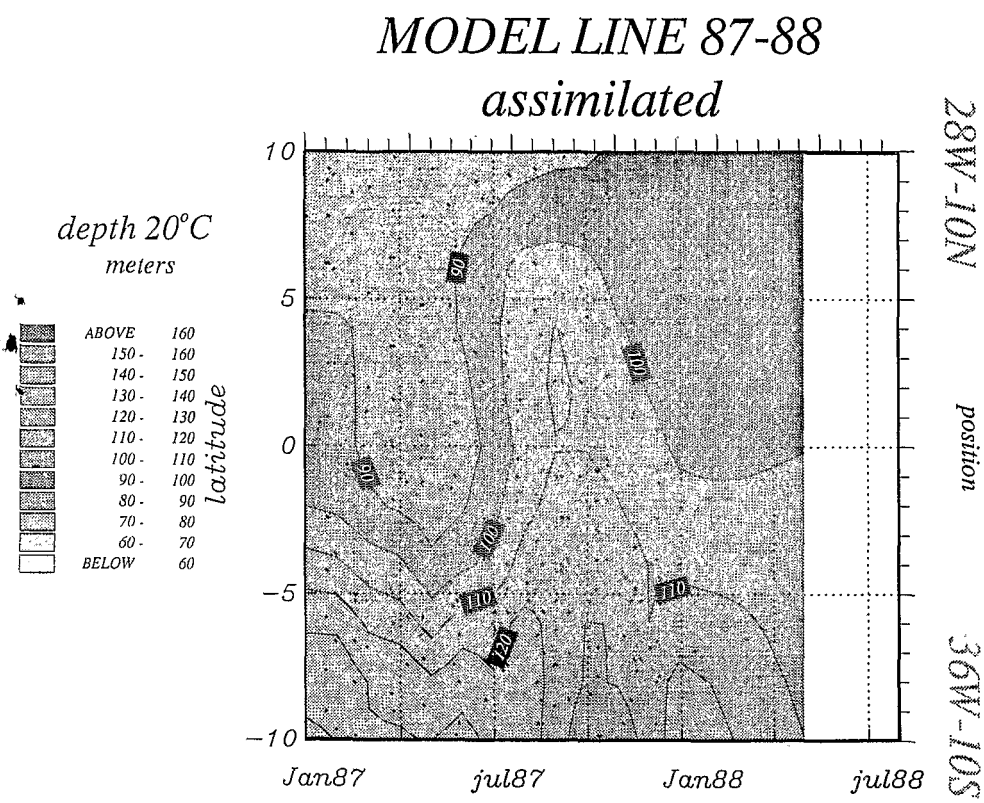

Fig. 23. Same as Fig. 21 for the assimilated run.

ascending and descending tracks allowed us to derive analysed SSH maps each 10 days (Arnault et al., 1992). In other words, we have 4 degrees of liberty of the SSH data per month. Given the short decorrelation timescale in the equatorial Atlantic ($\leq$ 15 days), this allows us to document the variability of the equatorial currents. This is the purpose of this section, the following being dedicated to the examination of longer time series.

The monthly time correlations between GEOSAT SSH and model equivalent SSH do not involve the reference level. The score of the reference and assimilated runs are low and do not exceed 0.2 (not shown). This poor result compared to the good spatial agreement may appear like a weakness of the data assimilation.

If one compares the time variability during one month for GEOSAT SSH (Fig. 26) and the reference run (Fig. 27), the weakness of this run is striking. In the northern part of the basin, the model shows a weak variability (generally less than 1cm) associated with the North Equatorial Current (NEC) and North Equatorial Counter Current (NECC) without assimilation. Thus, the dynamics of the reference run are far from reality. With assimilation (Fig. 28), the model performs well. This points out that the variability of the model forcing is too low and fails to produce the

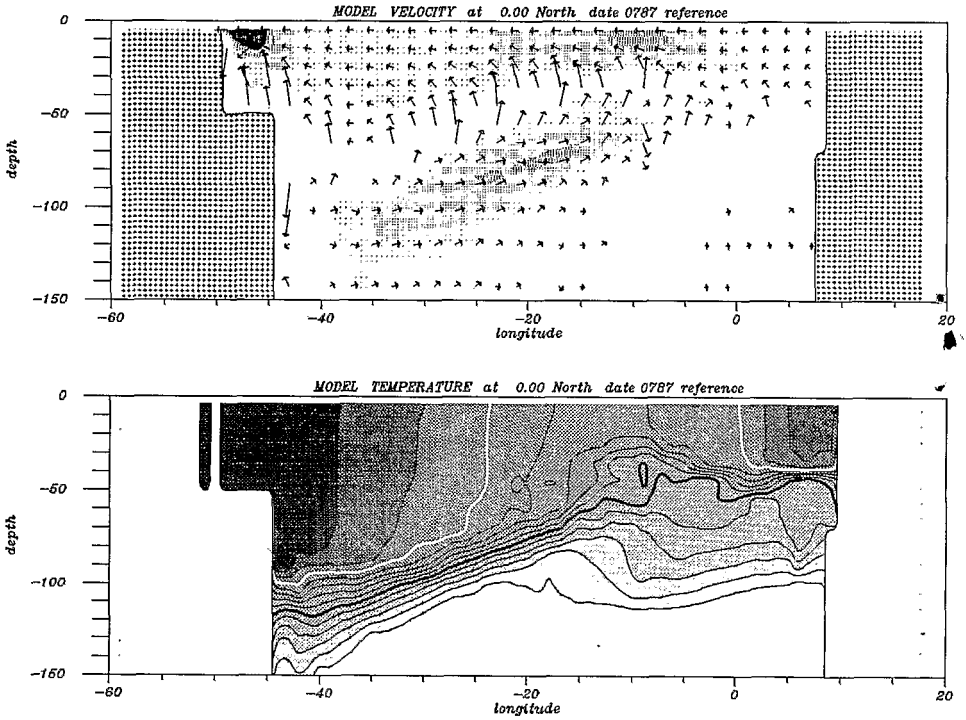

Fig. 24. Monthly mean values of the reference run during July 1987. Velocity and temperature are plotted at the equator. Arrows are drawn at each second node of the model in longitude and at each node in depth. The flow motion gives the direction of the arrows. The axis units (degrees vs meters) imply a scaling by 10^5 of the vertical velocity. The length of the arrows is proportional to the square root of the rescaled velocity. Arrows are not visible under 10cm/s. Darker shading corresponds to higher velocity. Temperature contouring starts from 15°C and ends at 29°C; the contour interval is 1°C; the heavy black line corresponds to the 20°C isotherm and the heavy white line corresponds to the 25°C isotherm.

variability of the northern currents. The altimetric assimilation has partly compensated for this low input of energy: a kick in the initial conditions gives kinetic energy to the currents. For instance, in spring 1987, the north equatorial currents were often strengthened by the assimilation by 20cm/s (this is examined in greater details in Part 2). The combination of this kick, the monthly wind and the inertia of the currents, produces better rms and variability. The exact location of the fronts are not as precise which explains why the time correlations are so low. Note also that the kick of the assimilation is not enough to ensure a good forecast (not shown). Thus, the lack of variability partly explains our results in SSH.

6.3.3. Time series

Global statistics do not reveal the different behavior of some regions of the tropical Atlantic. In this section, we examine SSH time series in the region of the NEC-NECC (40°W–10°N), in the region of the Guinea Dome (18°W–10°N) and in the

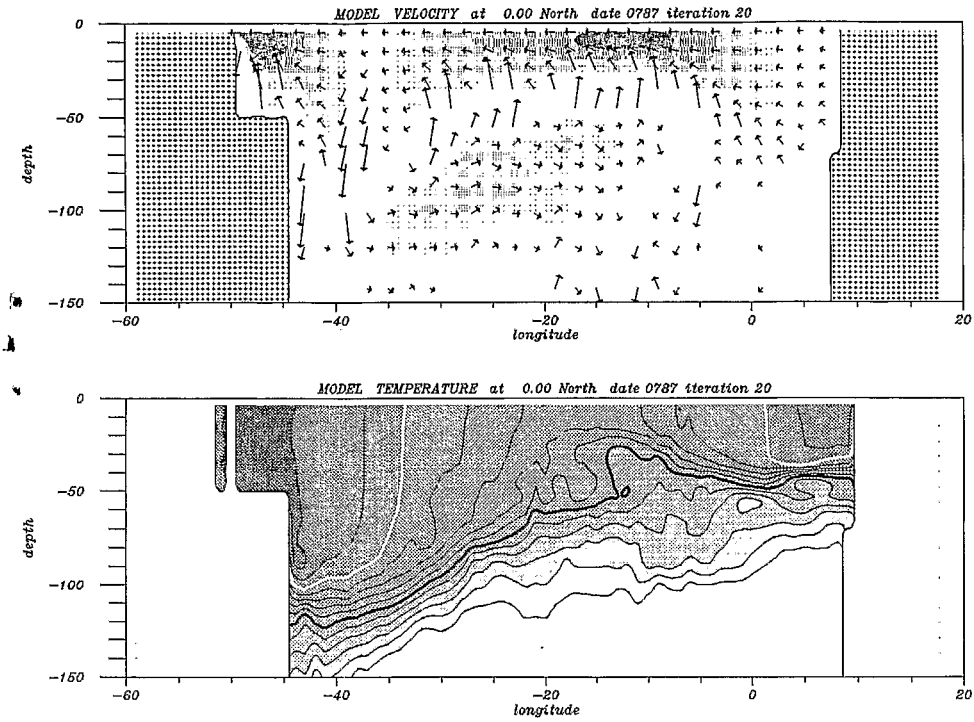

Fig. 25. Same as Fig. 24 for the assimilated run.

Gulf of Guinea (5°E–0°N). As in Section 4.3, the altimetric reference level (ARL) ψ is either simulated by the model without assimilation, or estimated monthly by the assimilation. This monthly estimation of the ARL explains the discontinuities at each first of the month for the assimilated run or the forecast run. The model time series (η is the model equivalent SSH) and its data counterpart are respectively

$$\overline{\eta - \psi} \text{ and } \overline{\eta_{GEO}}$$

The framework of the cost fuction is conserved (the ark mark means that a basin homogeneous rising or deepening is filtered out): the difference between model and data is the one (with weights included) which was minimized by the optimization.

At 40°W–10°N (Fig. 29), the sea level variations from GEOSAT reach 15cm and principally shows the meridional migration of the NEC-NECC system. 30–60 day oscillations are also captured by GEOSAT. In comparison, the SSH simulated without assimilation (top) shows a very weak monthly variability. (All the runs are ran monthly, hence there is a restart each first of the month. The forward Euler scheme used for the first time step generates the small discontinuity and the oscillations at the begining of each month.) The variability over several months is more satisfying: the standard deviation (not involving the altimetric reference level) is 2.3cm, the time correlation is 0.93. The ARL is not correct with a mean difference of 4.7cm.

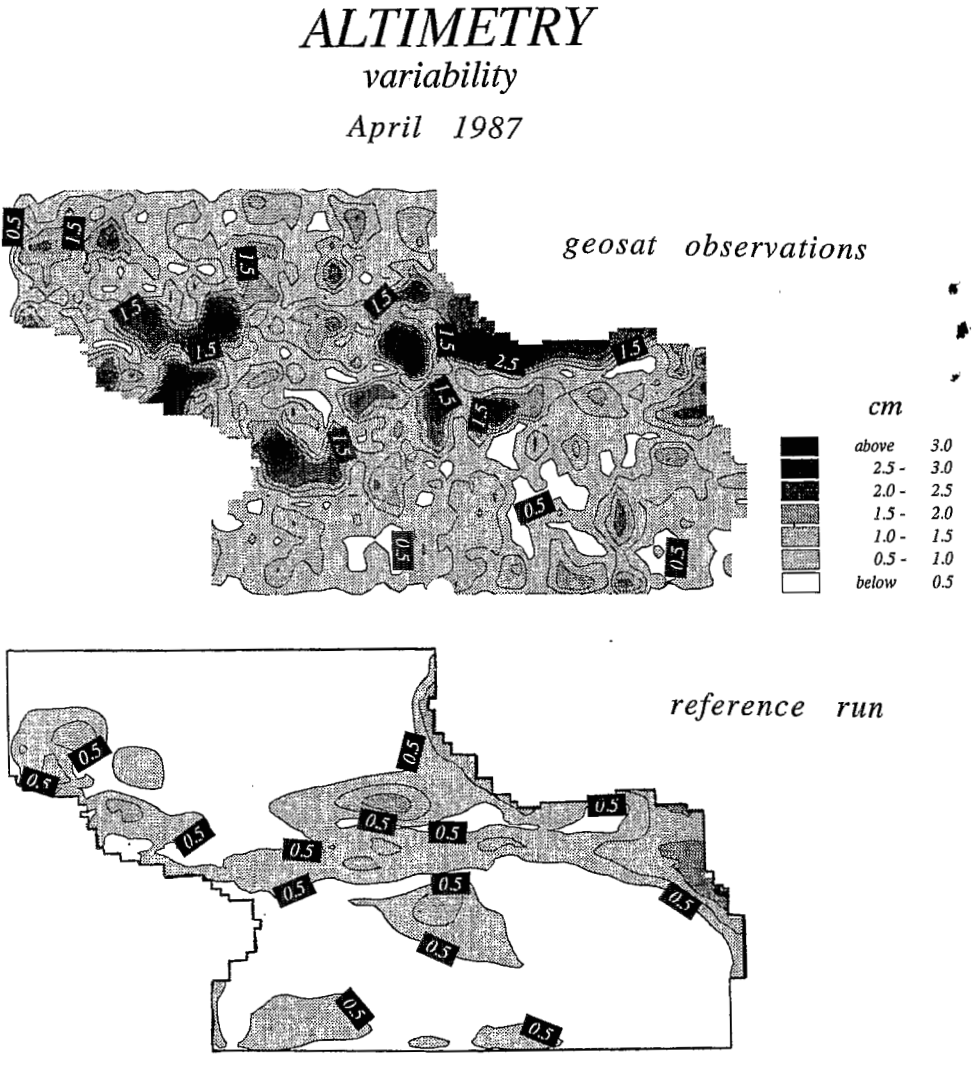

Fig. 26. Monthly mean sea level variability during April 1987 for GEOSAT.

Fig. 27. Same as Fig. 26 for the reference run.

With assimilation (middle), the time variability of the model is comparable to the GEOSAT one. Statistics are also improved (standard deviation = 1.7cm, correlation = 0.95, mean difference = 0.3cm). The monthly variations are rather consistent with the data except in February and July–August. The increase in February and decrease in July are overestimated by the model. It leads to consequent (5cm) changes in the estimated ARL, whereas, for six months of the year, the changes do not exceed 3cm. The forecast (bottom) has poorer statistics (standard deviation = 6cm, correlation =

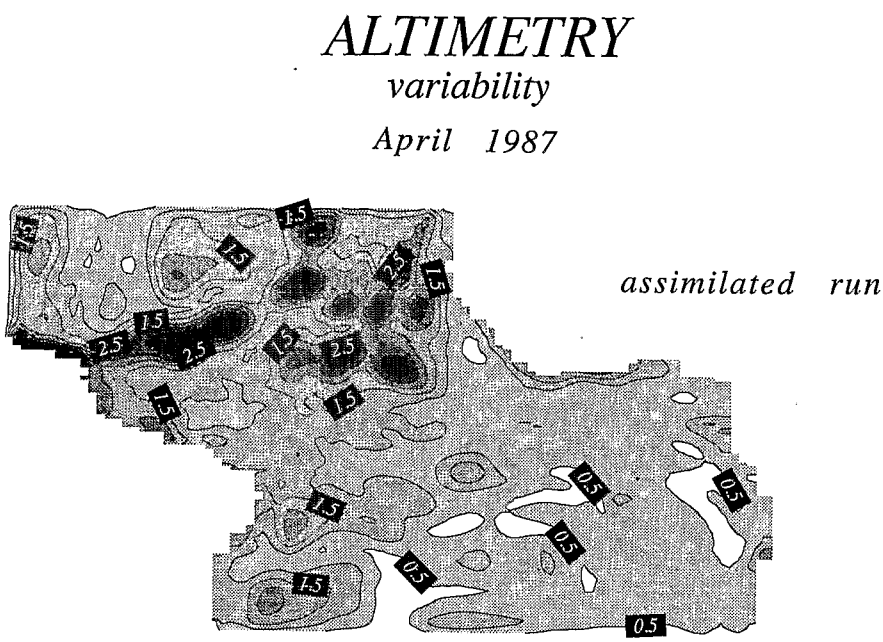

Fig. 28. Same as Fig. 26 for the assimilated run.

0.63) even if the mean remains correct (mean difference = 0cm). The time evolution of the forecast are comparable to GEOSAT in April and September–December. The bad forecast statistics are principally caused by a systematic lowering of the sea level between May and July, corresponding to the northern migration of the NEC at this position. This was corrected by the assimilation in May–June slowing down the NECC (not shown). In November, the forecast overestimates the sea level rise produced by the northern migration of the NECC. The assimilation has corrected for this by providing more dense water (not shown). Hence, in both cases, the forecast tends to accelerate the northern migration of the NEC and then of the NECC (exaggerating sea sevel lowering then rising). This increased northward transport was corrected by the assimilation through different mechanisms. Since the reference run did not include such an acceleration, inaccurate winds (too strong easterly winds) are not a candidate for this fault of the forecast. The examination of the SST (part 2), shows that this region is cooled (– 0.5°C in mean, – 1.4°C in May–June) by the assimilation. This leads to a positive correction of the heat flux (+ 10W/m^2) because of the relaxation to climatological SSTs (Section 2.3). Together with the easterly winds, this causes a shallowing of the modelled ML depth (Section 2.2) and therefore an increase in the northward transport of the near surface water (simulated NEC and NECC are maximum in the ML, e.g. in the upper 40 m). This shows a possible example of a negative feedback of the concurrent use of the surface SST relaxation and the variational assimilation.

The time series at 18°W–10°N (Fig. 30), in the region of the Guinea Dome, is

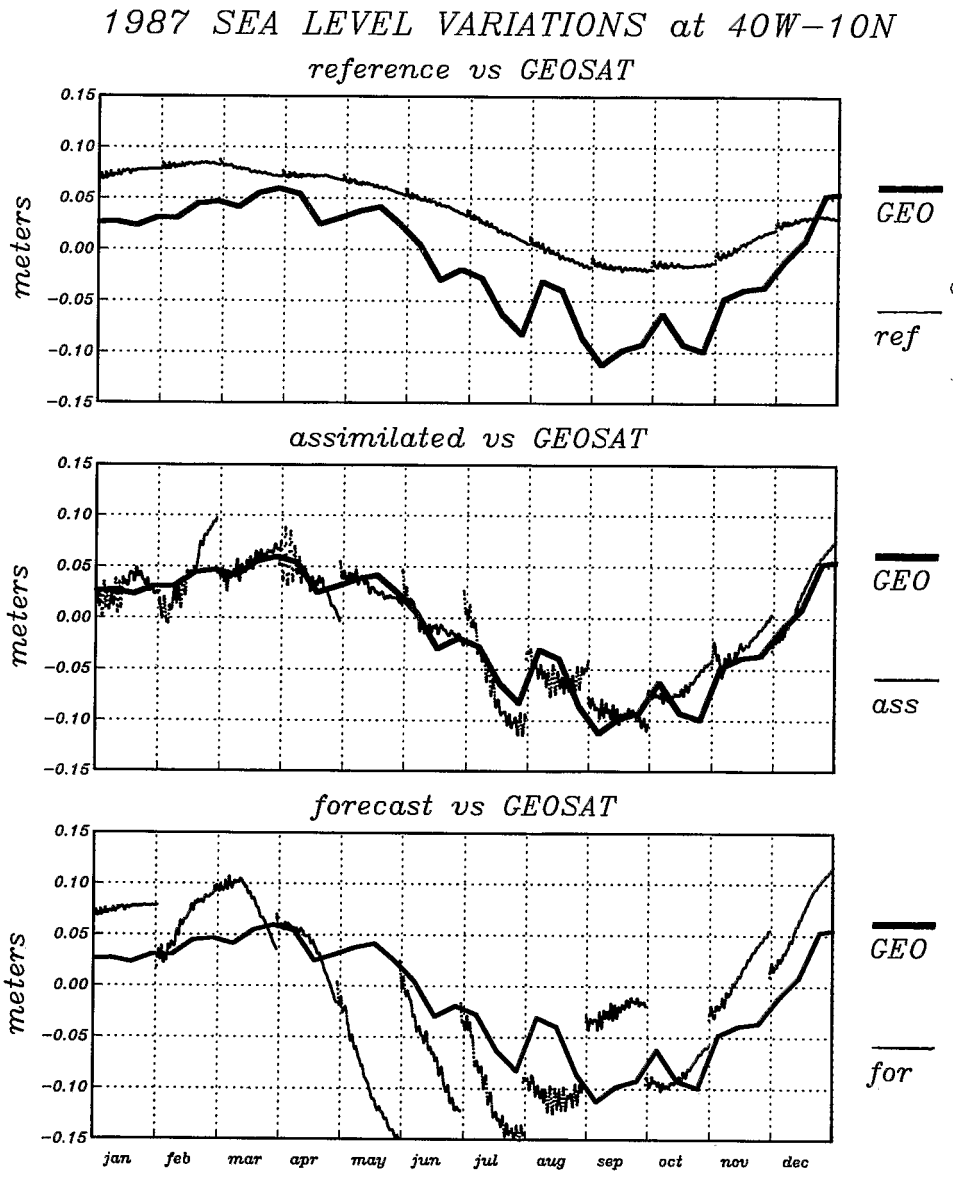

Fig. 29. Sea level variations at 40°W–10°N (northern part of the NECC) for GEOSAT and model runs in 1987.

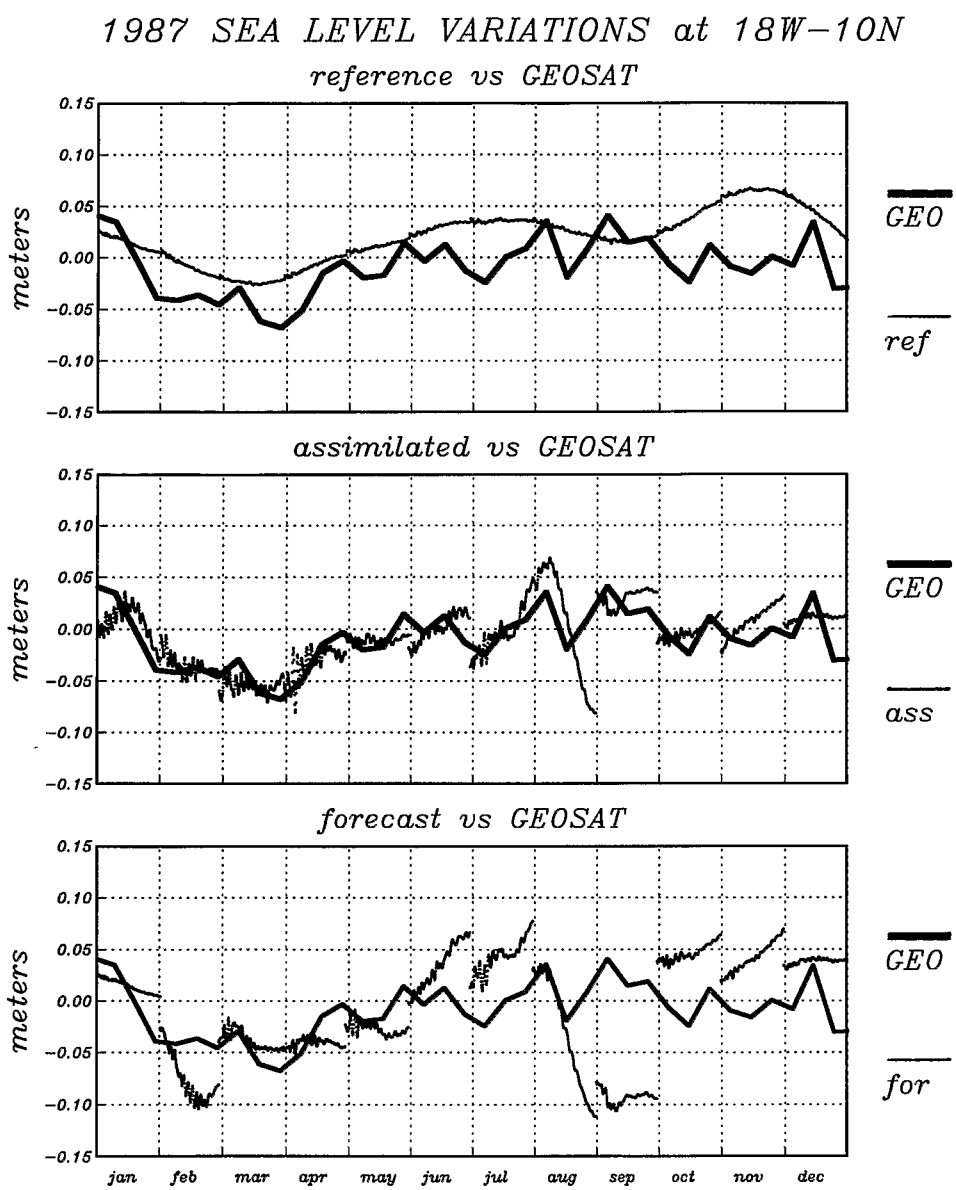

Fig. 30. Sea level variations at 18°W – 10°N (near the area known as the Guinea Dome) for GEOSAT and model runs in 1987.

interesting because the dynamics were unusual in this region in 1987. It also highlights the worse case scenario for data assimilation. Indeed, the correlation between the SSH of the reference run and the depth (counted negatively: heating produces both a surface rising and a thermocline deepening) of the 20°C isotherm deduced from Levitus (see Fig. 3) is 0.94 during the first part of 1987. It shows how much the reference run is subject to the climatological forcing in this region. In contrast, the correlation between GEOSAT and the Levitus 20°C depth during the second half of the year is 0.11. This suggests that the climatological forcing could have a negative impact on the model simulation over the second half of 1987. Another difficulty for the data assimilation is the data itself: this region is 1° off the continental shelf and tidal corrections may be inaccurate. The main signal showed by GEOSAT is sea level falling from January to March and then rising from April to September. As mentioned above, the model without assimilation (top) reproduced the lowering in sea level but its rise appeared in the fall and so is rather out of phase. Over the year, the standard deviation is 2.3cm, the correlation is 0.58 and the mean difference is 2.9cm (the warm bias of the model is maximun there). The assimilation (middle) reproduces well the subannual signal during the first five months (yearly standard deviation = 2.1cm, correlation = 0.7, mean difference = – 0.3cm). During this period, the change in estimated ARL is small from one month to another and the assimilation has principally corrected the initial conditions. The examination of the estimated fields (Part 2) reveals that the lowering corresponds to the western migration of the Guinea Dome. The assimilated run suggests that the boreal summer rising is caused by successive intrusions of warm water provided by the NECC. During boreal fall, the model fails to simulate the periods of lowering observed by GEOSAT and in all runs simulates a rise instead. The forecast run (bottom: yearly standard deviation = 5.4cm, correlation = 0.19, mean difference = 0.2cm) emphasizes the lowering observed by GEOSAT in late August. It also shows that the failure in reproducing the autumnal drop in lower sea level holds for all simulations. Thus, these deficiencies may not be caused by the initialization being inadequate. Indeed, the assimilation did not modify the initial conditions but only changed the reference level. The problem here could be caused by inadequate forcings (shared by all runs): the modelled SSH at 18°W–10°N is principally determined by the climatological forcings (relaxation to monthly SST and seasonal sea surface salinity) and the assimilation could not correct for this. The assimilation could only account for the deficiencies of the first half of the year.

The last comparison with GEOSAT deals with the sea level variation in the Gulf of Guinea at 5°E–0°N (Fig. 31). The signal included in GEOSAT is weak and may be contaminated by GEOSAT corrections (Arnault et al., 1992). The signal is similar at 20°W–0°N in the core of the modelled equatorial upwelling. During the TOPEX/POSEIDON period, the standard deviation in the Gulf of Guinea is around 4–5cm. However, the continuous rise from April 1987 to February 1988 is above the noise level. In addition this is consistent with the warm event of early 1988 in the Gulf of Guinea (see part 2). The SSH given by the tide gauge at Principe Island (7°E–1°N) also shows this rise. The comparison with GEOSAT illustrates the uncertainty in the measure (see also Arnault and Cheney, 1994, for further details). The

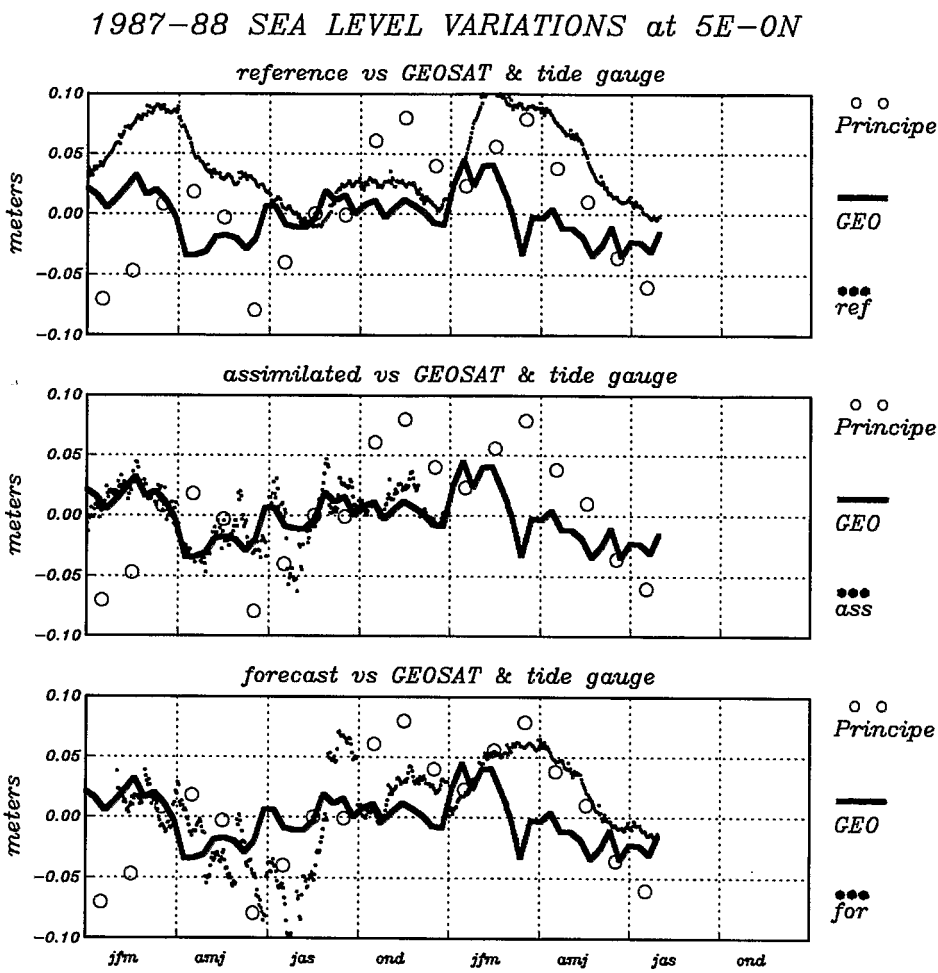

Fig. 31. Sea level variations at 5°E–0°N (near Sao Tome) for GEOSAT and model runs in 1987.

signal without assimilation (top, 1987 yearly standard deviation = 2.8cm, correlation = 0.22, mean difference = 3.3cm) presents a weak variability at 10 days, except some two day oscillations. The early rise in 1988 is not very different than in 1987. The assimilated run (middle, 1987 yearly standard deviation = 1.4cm, correlation = 0.77, mean difference = 0.2cm) closely follows the GEOSAT variations up until June. In June–July, the model tends to lower the SSH 5cm more than GEOSAT. This is consistent with the anomalously strong upwelling analysed in Section 6.2.6 and in BD93: the turbulent kinetic energy of the EUC is underestimated and the simulated current comes too close to the surface creating an increase in upwelling. The assimilation could not correct for this deficiency. On the contrary, the assimi-

lation cooled the surface in order to correct a warm bias at depth. This increased cooling has generated a positive correction of the heat flux (20W/m^2 per °C) since the SST is relaxed toward the climatology (Section 2.3). The increased heating leads to shallow the mixed layer by 10m to 20m. The corresponding change in SSH is negligible (0.2cm if the water below the ML is cooler by 1°C and raised by 10m), but, the shallower ML gives smaller coefficient of vertical viscosity (see Section 2.2) and thus increased surface currents. The consequences at the equator are an increased divergence and upwelling (Fig. 25). So, the stronger lowering of the SSH is an increase of model error produced by the concurrent use of surface flux correction and assimilation. As a fix, the assimilation modified the reference level in order to avoid drifting too far from GEOSAT. So, during the upwelling, the reference level is more a correction of the error in the model than an estimate of a time invariant level. It is also the case during the rest of the year except that the model trends are in agreement with GEOSAT. This becomes particularly obvious on the forecast runs of 1987 (bottom, standard deviation = 3.6cm, correlation = 0.48, mean difference = − 0.1cm). In 1988, the forecast compares badly with GEOSAT, whereas agreement with the tide gauge is more satisfying.

7. Conclusions

We developed a basic 4D-variational assimilation with a primitive equation model in the tropical Atlantic ocean during 1987 and a forecast up until July 1988. We used a resolution close to the one of the "high resolution" nudging assimilation of 1989 (Morlière et al., 1989b) and improved physics. We used climatological temperature and salinity data, XBT temperature data and analysed GEOSAT sea level data associated with basic error structures. The variational assimilation is able to reduce the model data misfit as the cost function significantly decreased. It shows that the dataset provides information that can be used by the variational assimilation to produce a statistically improved simulation. It shows that the linear tangent model and its adjoint are valid over one month for such a complex oceanic model (4D-variational assimilation is currently carried out with atmospheric models over 24h).

The benefit of the GEOSAT altimetric data is particularly valuable for the northern equatorial currents. The simulated variability after assimiliation is close to the one shown by GEOSAT. The level of energy is much higher after assimilation than before. Moreover, this input of energy has been transfered from the altimetry without shocks.

However, the assimilated run is not perfect. The assimilation of GEOSAT data revealed that the simulation is unable to reproduce the full range of space-time variability included in the data. This is mostly because of the use of monthly forcings.

GEOSAT revealed the weakness of our basic ML model in the central equatorial Atlantic. During June-July, the ML model overestimates the ML depth and thus simulates an erroneously strong upwelling. The model without assimilation presents a warm bias with a thermocline which is too deep. This error hides the anomalously strong upwelling. The assimilation has corrected the warm bias of the model and

emphasized the equatorial upwelling. However, the SST presents a cold bias after assimilation. This characteristic error of the model has been highlighted by the variational assimilation as part of the estimation of the reference level. Therefore, the assimilated reference level may be too contaminated by modelling shortcomings to be considered as the mean ocean topography. Model and forcings must be improved if one wants to consider the assimilated reference level as a physical invariant.

The GEOSAT comparisons pointed out the danger of the use of surface relaxation for thermohaline fluxes in a context of assimilation. This relaxation prevents the model from drifting away from the observed surface because of inadequate ocean-atmosphere exchanges. In the case of the north equatorial currents, the assimilation emphasized a cold bias of the modelled SST. It led to an increased heating because of the surface relaxation. The consequence was a shallower ML and a northward deflection of the currents. At the equator, the relaxation similarly increased the divergence of the surface westward SEC which reinforced the equatorial upwelling and affected the penetration of the deep eastward EUC in the Gulf of Guinea. This fault of the surface relaxation questions the use of thermohaline fluxes in a context of assimilation. This problem is open since thermohaline flux estimates will not be significantly improved in the near future (Gleckler and Weare, 1995).

XBTs revealed that the assimilation did not change the vertical structure of the simulated temperature profiles. Thus, the diagnostic vertical diffusion that we used is unsuitable for good representation of either the deep ocean or the near surface. A prognostic turbulent vertical diffusion (BD93) and better heat flux (Roquet et al., 1993) will help us progress towards an accurate description of the large scale ocean.

Given these difficulties in modeling, the forecast made over the first 7 months of 1988 showed an improvement below the ML. This proves that the variational assimilation of climatologies, XBTs and GEOSAT successfully transformed these data into useful information about the long term variability of the deep ocean. Despite the weaknesses of this current data assimilation, this is an encouraging result for the initialization of coupled ocean-atmosphere models. This also emphasizes the importance of these datasets, in particular of accurate satellite altimetric measurements and *in situ* observational network.

8. Acknowledgements

The authors thank J.P. Rebert (ORSTOM) who provided the XBT data and the staff at the TOGA Center of Brest who validated the data. They also thank R. Morrow for her fruitful comments on the manuscript.

E. Greiner's research was funded by CNES, La Société de Secours des Amis des Sciences and CERFACS. S. Arnault and A. Morlière were supported by ORSTOM, PNTS and PNEDC. Assistance and CPU time on C98 was provided by IDRIS. Experiments were carried out from January 1995 to March 1995. Analysis of the results were carried out at the LODYC, at the GRGS and at CERFACS.

Appendix A

Numerical peculiarities of the assimilation

The major difficulties of the optimal control in this problem are:

- the nonsmoothness of the cost function,
- the amount of memory storage needed for the trajectory,
- the under determination of the least–squares problem,
- the conditionning of the well-posed problem.

Now we will examine what are our choices to overcome these difficulties. This chapter is rather technical but gives the necessary information on a large scale ocean variational assimilation.

Regularity of the cost function

The cost function is a measure of the model-data misfit and we want to minimize this function with an algorithm of optimization. However, one evaluation of the function is as expensive in CPU as a forward integration of the system (the price of a backward integration of the adjoint model is twice that of a forward integration). This is too expensive for the use of a random method like Monte-Carlo. We have to employ a method requiring fewer function evaluations. Fortunately, the physics of the large scale phenomena is rather smooth in oceanography so we can expect to take benefit of the regularity of the cost function. Thus we can use a descent method based on the calculation of the gradient. This assumes that the gradient is defined everywhere. However, the numerical models may contain some threshold mechanisms and the gradient could not exist in some situations. It is especially true with turbulent energy closures, which is why we did not use the calculation of the vertical viscosity based on the kinetic turbulent energy model developed in BD93 (the meteorologists' point of view is similar as exposed in Courtier et al., 1994).

Instead, we have employed a simpler hybrid parameterization which has the nice property of being smooth and rather realistic. Our diffusive coefficients are made of two different parts. First, we do not link the processes in the ML to the local RI number (the fitting slope in RI^{-8} after Peters et al. (1988) is highly non differentiable). On the contrary, these values are imposed by the external forcings. Thus, they are model independent. By the way, this non differentiable part is absent in the gradient as it is done in meteorological context (Courtier et al., 1994). Second, the other part addresses diffusion below the ML which is linked as usual to the local model value RI. This relationship has reasonably bounded derivatives and causes no trouble (the problem is we do not use any convective adjustment algorithm and static stability is only provided by vertical diffusion: coefficients have to be high in case of instability).

On the other hand, the depth of the ML is an external factor independent of the *in situ* state, and any error in the given forcing will contaminate the internal structure

of the model; this is true even after assimilation (it would be the same problem with a turbulent kinetic energy closure).

Memory storage of the trajectory

One disadvantage of the nonlinear variational method is the need to store the trajectory of the forward model. This trajectory is not only used to compute the cost function but also the gradient of this cost function with the adjoint. Any nonlinarity of the forward model appears in the adjoint one and thus has to be set to the correct value if one wants a correct gradient of the cost function. It is impossible to recalculate the trajectory backward in time as it can be done with some hyperbolic systems.

A practical limitation on the most powerful machines is not the CPU time but still the amount of memory required in order to store the trajectory of the model. To save memory, we can firstly store only the state of the system and, eventually, recompute the nonlinearities as in the forward model. The second saving is to store only the sea points of the domain. This is really valuable in the case of the Atlantic where there is only 60% of real sea points in a rectangular model domain. A third saving is to reduce the accuracy of the binary representation of the storage. In fact, any way to reduce storage requirements can be used, although bit operations are vectorized and can be parallelized. This efficiency explains our choice (a similar procedure is used at the European Center for Medium Weather Forecasting). Here we take advantage of the fact that the variations of the physical values are not large from a coding point of view. For instance, a relative precision of 10^{-4} for a horizontal velocity measurements has a high accuracy in oceanographic terms. Thus, we do not need to save 13 digits when 4 are sufficient to describe the physical phenomena in a reasonable way. Consequently, we save only 16 over the 64 bits of the binary representation of the reals on CRAY systems ((example: X before storage (.3087,.1026, 22.762, 35.9046) and after (.3086,.1026, 22.761, 35.9044)) this somewhat complex operation costs 10% of the forward CPU time integration). This accuracy is good enough for the minimization process and no failures were encountered But, to reach this accuracy, we had to neglect in the adjoint the variation of the coefficients of diffusion resulting from the Richardson number dependent mixing (saving 16 bits over 64 is good enough for temperature and salinity but *RI* depends on their vertical gradients and thus may be completely wrong, leading to a poor gradient. Saving 32 bits provides the good *RI* and the gradient has then 5 good digits but the amount of memory is almost doubled...). This was only possible because the variations of the *RI* number are small below the ML. In these ways we deliberately used a good approximation of the gradient in order to use the smallest amount of memory storage.

In our case of a $95 \times 77 \times 21$ grid, we can summarize (in term of number of reals) the saving attained for 31 days as:

saving of $X = (u, T, S)$: 4 fields	$\times 4$
only sea points	$\times .6$
compacting: 16/64 bits	$\times .25$

trajectory: 496 time steps of 1h30 $\times$ 496

The total is close to 46 megawords of 64 bits.

We also used a filtered leap-frog scheme for the temporal integration and its two levels must both be saved. Fortunately, the filtered stage X_f^{n+1} can be deduced by the recurrence:

$$X_f^{n+1} = X^n + \gamma(X^{n+1} - 2X^n + X_f^n)$$

With this formulation it is possible to recalculate the filtered levels with only one filtered field and all the time steps of the state. In practice, because of the truncation to the 16 most important bits, we store one filtered field over three. Finally the amount of memory needed for the storage of the trajectory is nearly 60 megawords (the total memory is less than 110 megawords).

Under determination of the least square problem

As usual for physical problems, we defined the cost function as a sum of squares of the model-data misfits. The least square problems regroup this category of parameter estimation. This theory covers several situations. When there is not enough data to determine in a unique way the parameter to estimate, the least square problem is under determined.

A major problem in oceanography is the lack of *in situ* data: a month with 20000 single temperature measures (or 200 XBT profiles) can be considered as a good month. It is far from the number of degrees of freedom of an unsteady numerical model and the problem of initialization is under determined, even with the information coming from SST, altimetry and drifting buoys. Of course there are climatological data but they are not useful if we are interested in the interannual signal. We can naturally include the information from a previous analysis. However, this achieves the determination of the problem more with data from the past than future data. Consequently, the under determination is still hidden behind the first guesses. Generally one adds a penalty function. It is a physical way to impose smoothness of the solution and a mathematical skill to insure convergence. But this is not very satisfying either numerically or physically. Moreover, the lack of balance between time dependant data and degrees of freedom is not solved in this way.

Obviously, it would be easy to decrease the spatial discretization of the model but we do not want to loose the resolution required to describe correctly the tropical ocean dynamics. The possibility is to keep the high resolution for the model but use a coarser resolution or sampling for the control. This can be referred to as a multigrid method but here the cycle is reduced: the control, C, always lies in the same subspace, E, of the space, F, of the states of the system. If the size of E is comparable to the amount of time dependent data, the problem is well determined. Mathematically, this method of compaction is a classical way to insure convergence (see Greiner, 1993, for further notes in this context). Physically, it can be linked to the assumption of smoothness of the attractor or to a hypothetical slow manifold

(Temam, 1989). Practically with our finite differences model, we can take one point for E every two points of F which is equivalent to a restriction to the low frequencies for a spectral model. The projector M from the control space onto the space of the states of the system is a simple bilinear interpolation.

It is possible to have an idea of the efficiency of the sampling by considering the following 1D problem:

$$J(c) = |\Delta u - data|^2 \text{ where } u = c \text{ or } u = Mc$$

The control c is either in E or in F. In this example, F is the discretization $\{(i/(N+1), i = 0, N+1\}$ of the interval [0, 1] with homogeneous Dirichlet conditions. A base of this space is made of the eigenvectors of the Laplacian Δ with Dirichlet conditions: $\{\sin(ip\pi/(N+1), p = 1, N\}$. If we use the centered differences for the Laplacian and if the minimum is searched over E, the conditioning of the Hessian $\Delta^*\Delta$ where eigenvalues are $(2(N+1)\sin(p\pi/2(N+1)))^4$ is close to the ratio $((2N/\pi))^4$. (The lower the conditioning is, the easier the inversion is: 1 for the identity.) If N is even, we take one point over two for E and we take for the projector M the simple linear interpolation given by:

$$Mc = \begin{cases} c_i & \text{if } i \text{ is even} \\ \dfrac{1}{2}(c_{i-1} + c_{i+1}) & \text{if } i \text{ is odd} \end{cases}$$

then the eigenvalues are $4((N+1)\sin(p\pi/(N+1)))^4$ and the conditioning $((N/\pi))^4$. The gain is thus 2^4 (and 2^2 for a gradient instead of the laplacian) and it is very valuable for the speed of convergence.

We have taken the sampling of C to be not very different from this sketch. Our aim is to reduce as much as possible the degrees of freedom compared to the amount of time dependent data. Thus for E we take one point over two in longitude and latitude but all the points in the vertical. Moreover, because of nonlinearities, we can not rely on the smoothness of E near the boundaries; we consequently take all the points within 2° of the coastlines. A possible explanation is to say that otherwise the projector M would create large errors on the initial conditions and generate (without an additional initialization filtering) fast travelling waves, which is not consistent with the regularity of a slow manifold. The same subspace E is used for velocity, temperature and salinity even if we can take a larger space for the temperature.

Preconditioning of the least square problem

Even if the cost function is smooth and the least square problem well determined, it still does not imply that the convergence of the optimizer will be fast. The same problem occurs with a linear system when the conditioning of the matrix is not good. In such case, one uses an estimate of the inverse of the matrix as a preconditioner for the linear system in order to speed up the convergence. The same technique applies within the present context of nonlinear least square problem.

In this section we describe the preconditioner used to accelerate the convergence of the minimization. In fact, as we do not reach the asymptotic convergence speed, this favors the subspaces on which we prefer to make the optimization. The objective of a preconditioner is to approach the inverse of the hessian $\partial^2_{X_0}J$ of the cost function. First, we suppose that the hessian is block diagonal and we are going to examine each block separately. For the sake of simplicity, we will not mention the Hessian of the first guess criterions since they are simply weighted identities. We suppose in the following sketch that all the weights involved in the criteria are unity.

The block $\partial^2_{T_0}J$ is close to diagonal because we have many temperature data (Levitus climatology and XBTs) that we assumed uncorrelated (see Chapter 4). Nevertheless, it does not mean that its conditioning is good if, despite the relatively small amount of XBTs, you give the same importance to the whole XBT dataset as to the climatology. (If, for instance you have N model points and take errors equal to unity, the relative weight of one climatological observation is $1/N$; if you have P XBT data, the weight of each XBT observation is $1/P$. Then, the corresponding block of the hessian is diagonal but the coefficient is either $1/N$ if it is a point without XBT, or $1/N + 1/P$ with XBT. The conditionning is then $1 + N/P$ and, in our situation with 90,000 sea points and 40 XBT observations per time step, that leads to the high number 2250.) It is thus important to approximate the inverse of $\partial^2_{T_0}J$. The part $\partial^2_{T_0}J^T_{Lev}$ coming from the climatological data can be taken as identity, neglecting the time evolution because of the spreading of the observations. The part $\partial^2_{T_0}J^T_{XBT}$ coming from the XBT data has to be evaluated and we do it simply by searching the zone of the initial temperature which influences the XBT criterion. We start the approximation by keeping only the quadratic term of the hessian:

$$\partial^2_{T_0}J^T_{XBT} \sim \sum_{XBT}\left(\frac{\partial T}{\partial T_0}\right)^*\left(\frac{\partial T}{\partial T_0}\right)$$

Here we replace the time evolution of the forward integration by the linear growth of a small perturbation over the assimilation period T:

$$\frac{\partial T}{\partial T_0} \sim T$$

and this gives us the following diagonal approximation:

$$\partial^2_{T_0}\tilde{J}^T_{XBT} \sim T\sum_{XBT}\left(\frac{\partial T}{\partial T_0}\right)^*$$

We compute it once at the begining of the minimization through the homogeneous backward adjoint integration of

$$\partial_t T + u_g \nabla T + \kappa_h \Delta_h T + \partial_z[\kappa_g \partial_z T] = 0$$

where u_g is the first guess and κ_g the vertical diffusivity of the guess.

We now have an estimate of $\partial^2_{T_0}J^T_{XBT}$ but we still have to deal with the two other blocks of the hessian. For salinity, $\partial^2_{S_0}J$, we have only climatological data so as a

first approximation we could consider this block equivalent to identity. Obviously, this is not the best choice because salinity variations are often linked with those of temperature. Indeed, XBTs provide information on salinity (and velocity) at the same places because advection and diffusion are close for temperature, salinity and velocity. So we make the crude assumption that density is a constant within the Hessian approximation. Then, using its thermohaline expansion, we have the relationship between temperature and salinity variations:

$$\frac{\partial T}{\partial S} = \frac{\beta_\rho}{\alpha_\rho}$$

Consequently, the double derivative in salinity of the XBT criterion is approximated by

$$\partial^2_{S_0} J^T_{XBT} \sim \left(\frac{\partial T}{\partial S}\right)^2 \partial^2_{T_0} J^T_{XBT} = \left(\frac{\beta_\rho}{\alpha_\rho}\right)^2 \partial^2_{T_0} J^T_{XBT}$$

The last block $\partial^2_{u_0} J$ is the hardest to estimate. For the XBT criterion, we can as previously reach formally the approximation

$$\partial^2_{u_0} J^T_{XBT} \sim \left(\frac{\partial T_0}{\partial u_0}\right)^* \partial^2_{T_0} \tilde{J}^T_{XBT} \left(\frac{\partial T_0}{\partial u_0}\right)$$

where we only have to estimate $\frac{\partial T_0}{\partial u_0}$. This static relationship could be obtained using the geostrophic equilibrium but this would lead to an elliptic non local inverse problem. This problem, that is the same problem for altimetry and velocity, could not be inverted easily. An explicit relation giving velocity from altimetry can be derived from geostrophy but its inverse is neither explicit nor local. Moreover, the result would not even be useful at the equator. Thus, we take simply $\frac{\partial T_0}{\partial u_0} = \frac{1°\mathrm{C}}{0.3\mathrm{ms}^{-1}}$, hoping that local processes like advection give sense to this approximation. (This is a rule of thumb: a local variation of 1°C leads to a local variation of 30cm/s.)

The preconditioning of the GEOSAT criterion is built with the same method. We start again by keeping only the quadratic term of the hessian

$$\partial^2_{T_0} J^\eta_{GEO} \sim \sum_t \sum_{z=0} \zeta \left(\frac{\partial \eta}{\partial T_0}\right)^* \left(\frac{\partial \eta}{\partial T_0}\right) = \sum_t \sum_{z=0} \zeta \left(\frac{\partial T}{\partial T_0}\right)^* \left(\frac{\partial \eta}{\partial T}\right)^* \left(\frac{\partial \eta}{\partial T}\right) \left(\frac{\partial T}{\partial T_0}\right)$$

Then we suppose that the geostrophic relation is satisfied and thus

$$fk \times u + \nabla\left(\eta g + \frac{g}{\rho_0} \int_0^z \rho \mathrm{dz}\right) = 0$$

We deduce from this relation (at a given depth z in a discrete form):

$$\frac{\partial \eta}{\partial T(z)} \sim -\alpha_\rho \Delta z$$

Under the same assumption that the time evolution for the forward integration is neglectable, we finally obtain

$$\partial^2_{T_0} J^\eta_{GEO} \sim T \sum_t^u \zeta (\alpha_\rho \Delta z)^2 \left(\frac{\partial T}{\partial T_0}\right)^*$$

As previously we compute this backward integration once at the begining of the minimization. The two other terms of the hessian of this criterion are given again by:

$$\partial^2_{S_0} J^\eta_{GEO} \sim \left(\frac{\partial T_0}{\partial S_0}\right)^2 \partial^2_{T_0} J^\eta_{GEO} \text{ and } \partial^2_{u_0} J^\eta_{GEO} \sim \left(\frac{\partial T_0}{\partial u_0}\right)^2 \partial^2_{T_0} J^\eta_{GEO}$$

This preconditioning is very valuable because the analysed GEOSAT data are provided only over a resticted area and this strongly affects the conditioning number.

Practically, we still have to invert the whole approximation of the hessian of J within the context of the quasi-newton algorithm: the approximated inverse must be symetrical and positive definite. This is achieved by a cubic least square polynomial preconditioner (Johnson et al., 1983).

9. References

Alexander, R.C., & Kim, J.W. (1976). Diagnostic model study of mixed-layer depths in the summer north Pacific. *Journal of Physical Oceanography, 6*, 293–298.

Arnault, S. (1987). Tropical Atlantic geostrophic currents and ship drifts. *Journal of Geophysical Research, 92*(C5), 5076–5088.

Arnault, S., & Cheney, R.E. (1994). Tropical Atlantic sea level variability from Geosat (1985-1989). *Journal of Geophysical Research, 99*(C9), 18207–18223.

Arnault, S., Morlière, A., Merle, J., & Ménard, Y. (1992). Low-frequency variability of the tropical atlantic surface topography: altimetry and model comparison. *Journal of Geophysical Research, 97*(C9), 14259–14288.

Bell, M.J., 1994. Experiments with the assimilation of thermal profile data into a dynamical model of the Atlantic Ocean, Forecasting Research Division, Technical report, 134, UKMO, London Rd, Bracknell, RG12 2SZ, UK, 22pp.

Blanke, B., & Delecluse, P. (1993). Variability of the tropical Atlantic ocean simulated by a general circulation model with two mixed layer physics. *Journal of Physical Oceanography, 23*, 1363–1388.

Buckley, A., & Lenir, A. (1983). Q-N like variable storage conjugate gradients. *Mathematical Programming, 27*(1), 155–175.

Carton, J.A., Giese, B.S., Cao, X., & Miller, L. (1996). Impact of altimeter, thermistor, and expendable bathythermograph data on retrospective analyses of the tropical Pacific Ocean. *Journal of Geophysical Research, 101*(C9), 14147–14159.

Courtier, P., & Talagrand, O. (1990). Variational assimilation of meteorological observations with the direct and adjoint shallow-water equations. *Tellus, 42A*, 531–549.

Courtier, P., Thépaut, J.-N., & Hollingsworth, A. (1994). A strategy for operational implementation of 4D-VAR using an incremental approach. *Quarter Journal Royal Meteorological Society, 120*, 1367–1388.

Fletcher, R., 1986. Practical methods of optimization, 1, Wiley-Interscience, New York, 431pp.

Ghil, M., Menalotte-Rizzoli, P., 1991. Data assimilation in meteorology and oceanography, Advances in Geophysics, 33, Academic Press, 141–266.

Gleckler, P.J., Weare, B.C., 1995. Uncertainties in global ocean surface heat flux climatologies derived from ship observations, Program for Climate Diagnosis and Intercomparison, report n°26, University of California, Lawrence Livermore National Laboratory, Livermore, CA 94550, USA, 39pp.

Greiner, E., 1993. Mise en oeuvre de méthodes de contrôle optimal pour l'assimilation de données *in situ* et satellitaires dans les modèles océaniques, Thesis of University P. and M. Curie, Paris, France, 211pp.

Greiner, E., & Périgaud, C. (1994). Assimilation of Geosat altimetric data in a nonlinear reduced-gravity model of the Indian Ocean by adjoint approach, part 1: methods ans statistical results. *Journal of Physical Oceanography, 24*(8), 1783–1804.

Greiner, E., & Périgaud, C. (1996). Assimilation of Geosat altimetric data in a nonlinear reduced-gravity model of the Indian Ocean by adjoint approach, part 2: physical results. *Journal of Physical Oceanography, 26*, 1735–1746.

Hastenrath, S., 1985. Climate and circulation of the tropics, Reidel, Dordrecht, Holland, 455pp.

Hellerman, S., & Rosenstein, M. (1983). Normal monthly wind stress over the world ocean with error estimates. *Journal of Physical Oceanography, 13*, 1093–1104.

Hénin, C., & Hisard, P. (1987). The NECC observed during the Programme Français Océan Climat dans l'Atlantique equatorial experiment in the Atlantic ocean, July 1982 to August 1984. *Journal of Geophysical Research, 92*(C4), 3751–3758.

Ji, M., Leetma, A., & Derber, J. (1995). An ocean analysis system for seasonal to interannual climate studies. *Monthly weather review, 123*, 460–481.

Johnson, O.G., Miccheli, C.A., & Paul, G. (1983). Polynomial preconditioners for conjugate gradient calculations. *Siam Journal Numerical Analysis, 20*(2), 362–376.

Jones, J.H. (1973). Vertical mixing in the equatorial undercurrent. *Journal of Physical Oceanography, 3*, 287–296.

Kraus, E.B., & Turner, J.S. (1967). A one dimensional model of the seasonal thermocline, part II. *Tellus, 19*, 98–105.

Levitus, S., 1982. Climatological atlas of the world ocean, NOAA professional paper, 13, US department of commerce, Rockville, MD, 174p.

Larousse, 1968. Encyclopédie, Editions Larousse, Paris, 24 volumes.

Lions, J.L., 1968. Contrôle optimal de systèmes gouvernés par des équations aux dérivées partielles, Dunod, Paris.

Martin, P.J. (1985). Simulation of the ML at OWS November and Papa with several models. *Journal of Geophysical Research, 90*(C1), 903–916.

Merle, J. (1980). Seasonal heat budget in the equatorial Atlantic ocean. *Journal of Physical Oceanography, 10*, 464–469.

Molinari, R.L. (1982). Observations of eastward currents in the tropical South Atlantic Ocean: 1978-1979. *Journal of Geophysical Research, 87*, 9707–9714.

Morlière, A., Reverdin, G., & Merle, J. (1989). Assimilation of temperature profiles in a general circulation model of tropical Atlantic. *Journal of Physical Oceanography, 19*(12), 1892–1899.

Morlière, A., Delécluse, P., Andrich, P., & Camusat, B. (1989). Evaluation des champs thermiques simulés par un modèle de circulation générale de l'Atlantique tropical. *Oceanologica Acta, 12*(1), 9–22.

Oberhüber, J.M., 1988. An atlas based on the "coads" data set: the budgets of heat, buoyancy and turbulent kinetic energy at the surface of the global ocean, Max Planck institut für meteorologie, 15, Germany, 202pp.

Pacanowski, R.C., & Philander, S.G.H. (1981). Parameterization of vertical mixing in numerical models of tropical oceans. *Journal of Physical Oceanography, 11*, 1443–1451.

Peters, H., Gregg, M.C., & Toole, J.M. (1988). On the parameterization of equatorial turbulence. *Journal of Geophysical Research, 93*, 1199–1218.

Rebert, J.P., 1993. Data quality control at the TOGA subsurface data Centre, Manual of quality control procedures for validation of Oceanographic data, Manual and guides, 26, UNESCO, 13pp.

Reverdin, G., Delecluse, P., Levy, C., Andrich, P., Morliere, A., & Verstraete, J.M. (1991). The near surface tropical Atlantic in 1982-1984: results from a numerical simulation and a data analysis. *Progress in Oceanography, 27*, 273–340.

Roquet, H., 1994. Projet OPERA, Rapport d'activité,, Météo-France, SCEM/PREVI/MAR, 42 Av. G. Coriolis, 31057 TOULOUSE Cedex, France, 21pp.

Roquet, H., Planton, S., & Gaspar, P. (1993). Determination of ocean surface heat fluxes by a variational method. *Journal of Geophysical Research*, *98*(C6), 10211–10221.

Servain, J, 1996. PIRATA, Pilote Research Moored Array in the Tropical Atlantic, Centre ORSTOM de Brest, BP 70, 29280 Plouzané, France, 58pp.

Servain, J., Lukas, S., 1990. Climatic atlas of the tropical Atlantic wind stress and sea surface temperature 1985–1989, Centre ORSTOM de Brest, BP 70, 29280 Plouzané, France, 154pp.

Simonot, J.Y., & Le Treut, H. (1987). A climatological field of mean optical properties of the world ocean. *Journal of Geophysical Research*, *91*(C5), 6642–6646.

Simpson, J.J., & Dickey, T.D. (1981). The relationship between downward irradiance and upper ocean structure. *Journal of Physical Oceanography*, *3*, 309–323.

Smith, W.H.F. (1993). On the accuracy of digital bathymetric data. *Journal of Geophysical Research*, *98*(B6), 9591–9603.

Tang, T.Y., & Weisberg, R.H. (1993). Seasonal variations in equatorial Atlantic ocean volume transport at 28°W. *Journal of Geophysical Research*, *98*(C6), 10145–10153.

Temam, R., 1989. Attractors for the Navier-Stokes equations: localization and approximation, Journal of Faculty of Sciences of the Univers, Sect. IA, Mathematics, 36 n°3, 629–647, Tokyo, Japan.

Pergamon Progress in Oceanography 41 (1998) 203–247

Progress in Oceanography

Twelve monthly experiments of 4D-variational assimilation in the tropical Atlantic during 1987: Part 2: Oceanographic interpretation

Eric Greiner[a], Sabine Arnault[b,*], Alain Morlière[c]

[a]*CERFACS, 42 avenue Coriolis, 31057 Toulouse cedex, France*
[b]*LODYC, T14-15 2eme boite 100, 4 place Jussieu, 75252 Paris cedex 05, France*
[c]*ORSTOM, IS BP 917, Abidjan 15, Ivory Coast*

Abstract

GEOSAT sea level anomalies, XBT temperature profiles and Levitus climatologies were assimilated monthly during 1987 into a non-linear primitive equation model of the tropical Atlantic ocean. Assimilating GEOSAT sea level anomalies increased the variability of the north equatorial currents when it was too weak without assimilation. The assimilated run simulates both the 1987 to 1988 sea level rise in the equatorial band and lowering in the tropics. The comparison with Reynolds satellite SST data is useful to identify the upwelling areas as the zones of highest error for the model SST. The SST warming of early 1988 is little changed by the assimilation. It confirms that this warming was determined more by the wind forcing than by the internal dynamics. As previously deduced from inverted echo sounders, we find that the North Equatorial Counter Current (NECC) increased its transport during 1987. The assimilation reveals in addition that the NECC formed a strong gyre with the North Equatorial Current (NEC). Consistently with previous analysis, this strengthening of the gyre was a result of the anomaly in ITCZ position and intensity. The heat gain by the Equatorial Under Current (EUC) was reduced because of this northward drift of the NECC. The South equatorial Current (SEC) was strong in spring and summer, moving warm surface water to the west. The eastward transport of the underlying EUC was thus reduced, leading to a deficit of warm water in the Gulf of Guinea in 1987. Comparisons of the assimilated northward heat transport (NHT) with climatological data estimates principally suggests that there was a heat gain of up to 1 petaWatt in the northern tropics (3°N–18°N) in 1987. The assimilated NHT was nil at 25°N and negative within 5°S–15°S. The 1987–88 warm events in the tropical Atlantic ocean presents a temporal

* Corresponding author. Tel.: + 33-1-44-27-49-72; Fax: + 33-1-44-27-38-05;
E-mail: arnault@lodyc.jussieu.fr

PII: S0079-6611(98)00017-2

progression from the north to the south. The assimilation presents an increased transport of warm water by the EUC after September 1987. It confirms the positive impact of the mass redistribution on the subsurface warming of the Gulf of Guinea. The other significant impact in 1988 is an increase of the gyre formed by the SEC and the South Equatorial Counter Current (SECC) and an inhibition of the coastal upwelling off Namibia.

Contents

1. Introduction 206
2. Data comparisons 208
    2.1. Comparison with reynolds satellite sst 208
        2.1.1. Basin maps 208
        2.1.2. Seasonal signal in 1987 210
    2.2. Hydrological comparisons 212
    2.3. Geosat comparisons 213
    2.4. Mass transport comparisons 219
3. Resulting fields 221
    3.1. Horizontal maps between 20°S–20°N and 60°W–20°E 221
    3.2. Meridional section at 25°W 226
    3.3. Analysis of the correction 228
        3.3.1. Description of the correction 229
        3.3.2. Mechanisms 235
    3.4. Mass redistribution between 1987 and 1988 237
    3.5. Northward heat transport during 1987 240
    3.6. Warm event of early 1988 241
4. Discussion and conclusions 244
5. Acknowledgements 247
6. References 247

1. Introduction

As stated in the first part of this paper, the last decade was characterized by the increase of oceanic observations, in particular from the improved satellite observations of Sea Surface Height (SSH) and Sea Surface Temperature (SST). Important progress has also been made in numerical simulations of the tropical ocean. Hence, it is now possible to compare numerical simulations and data.

One basic aim of data assimilation (Morlière et al., 1989) is the initialization of the models which is a critical point because of the many uncertainties in the forcing fields and ocean dynamics. Data assimilation can also provide a more realistic description of the ocean as well as an evaluation of the model validity. These two results are of major importance for oceanographers especially for short term climate studies.

Specific concerns of this study are the links between the rainfall in Brazil (Rao

et al., 1993) and Sahel (Lamb and Peppler, 1992), the SST and the oceanic heat transport towards northern Europe. Although the thermodynamics of the tropical Atlantic are now well documented (Merle, 1980; Arnault, 1987; Hénin and Hisard, 1987; Tang and Weisberg, 1993), there are still some gaps in the understanding of the oceanic circulation. In particular, the interannual warming of the SST in the Eastern equatorial Atlantic (1984, 1988) has not yet been fully linked with the subsurface thermodynamics. Important progress on this subject has been recently achieved by the concurrent analysis of the satellite SST and the outputs of a model forced by ECMWF windstress (Carton and Huang, 1994, hereinafter CH94). This paper revealed the analogies and differences between the two warm events of 1983–84 and 1987–88. Another recent paper (Enfield and Mayer, 1997, hereinafter EM97) has provided through a careful EOF analysis of SST and windstress time series, the "typical" evolution of an Atlantic warm event and its connexion with the ENSO. In this paper, we would like to study the dynamical mechanisms and evaluate to what extent they contribute to the warm event of early 1988. For this purpose, data assimilation is necessary in order to obtain a model–data combined synoptic description of the ocean. The variational method enabled us to take advantage of both in situ temperature data and satellite SSH in the tropics with a sophisticated general circulation model.

The principle of the variational assimilation is to minimize the model–data misfit relative to the initial conditions with the use of the adjoint model. Starting from given initial conditions, the forward model is run with the external forcings prescribed. The model values (SST, SSH, velocity, . . .) are then compared to the data. A user defined cost function measuring the model–data misfit is then minimized. The particularity of the variational method is to use the backward adjoint model to compute the gradient of the cost function (Courtier and Talagrand, 1990). From the physical point of view, the variational method respects the modeled physics and allows us to assimilate directly any data that could be simulated by the model. The limitations of this method concern the smoothness of the model physics (the cost function must be regular for an easy minimization) and the limited spatial/temporal resolution (the model states must be saved).

In Part 1 of this study (Greiner, Arnault and Morlière, 1998, further referred to as GAM98), we described this methodology and the statistical results that we obtained. The main points were the following. We made a monthly variational assimilation of GEOSAT sea level anomalies, XBT temperature profiles and Levitus climatologies (Levitus, 1982) during 1987 into a non-linear primitive equation model of the tropical Atlantic Ocean. The model has a resolution of 1° longitude × 1/3° latitude × 20 vertical levels extending from 50°S to 50°N. The physics include an imbedded 1D-mixed layer model, a 3D-Richardson's parameterization under the mixed layer, a solar penetrating flux and varying water types and river runoff. The model was forced monthly by observed ship winds and Oberhüber's climatologies of heat and fresh water fluxes (Oberhüber, 1988). A 2° longitude × 1° latitude gridded optimal interpolation analysis of GEOSAT sea level anomalies (Arnault et al., 1992) was assimilated between 20°S and 20°N at each node of the model during 1987.

Validated TOGA XBT profiles (Rebert, 1993) were assimilated at their exact location between 30°S and 30°N.

In GAM98, we found that the biggest impact of assimilation appears where the GEOSAT variability is the highest, e.g. around the North Equatorial Counter Current (NECC) and the North Equatorial Current (NEC) within 5°N–15°N. The temperatures simulated with assimilation agree on the large scale with the XBT profiles; on the other hand, the surface stratification and thermocline details are missing, and the equatorial upwelling is too strong. The main statistics of the assimilated run are the following. The root mean square (hereafter rms) difference between the simulated SSH and GEOSAT is below 2 cm. The rms difference between the simulated temperature and the XBTs are 1.8°C in the near surface, 2.7°C in the thermocline and 1.1°C below. This leads to an error in the depth of the 20°C isotherm < 10 m between 4°S and 4°N. The forecast over the first 7 months of 1988 compared to XBT profiles showed that the initialization of the model has a positive impact at or below the thermocline level.

In Section 2 of this paper, we make physical comparisons between the model fields and various datasets. In Section 3, we examine the corrections given by assimilation with a special interest to the mass redistribution from 1987 to 1988, and the warm event of early 1988. Discussion and conclusions are given in Section 4.

2. Data comparisons

One can distinguish among the corrections provided by assimilation three distinct features. These will be examined more thoroughly in Section 3 but a summary follows. One feature is the change in thermocline depth at about 10°N-25°W. Unfortunately, it is too far south to be checked by the XBT temperature profiles along the shipping lines, and its SST signature is not clear enough for a validation with satellite data. Its relation to an interannual signal forced by the wind change is examined later. The second change concerns the NEC and NECC circulations; it is partly validated in this section. The third change concerns the Equator where some propagation is visible near the center of the basin. However, the signal is weaker than in the northern tropics so that equatorial propagation speeds and reflections are not well defined. Hence, given the GEOSAT and simulation accuracies, we cannot identify any particular oceanic processes at the Equator.

2.1. Comparison with Reynolds satellite SST

2.1.1. Basin maps

We saw in GAM98 that data assimilation had rather a negative impact on the near surface temperature when statistically compared to XBT data. In this section, we will use the $1° \times 1°$ monthly Reynolds satellite SST (Reynolds and Smith, 1994) in order to provide an independant basinwide diagnostic, not limited to shipping tracks. We remind the reader that the Reynolds data were not included in the assimilation. However, we did use a heat flux correction to drag the model towards Levitus SST

(20W/m^2 per degree Celsius, see GAM98, section 2.3). Fig. 1 shows the rms difference over 1987 between the simulated SST[1] without assimilation (reference run) and the satellite data. As pointed out in GAM98, we must keep in mind that these statistics can reflect either a potential bias or a phasing problem. The mean rms (1°C) is clearly less than when compared to XBTs above 25°C (1.6°C). This is probably because of the time and spatial averaging included in the temperature satellite data processing, which produces smoother SST than the XBTs. As a comparison, the standard deviation between Reynolds satellite SST and TAO in situ temperature measurements in the Pacific is about 0.4°C (J. Boutin, personal communication, 1996). The accuracy of the AVHRR analysis is estimated to be around 0.6°C. Hence, the model error is not much larger than the uncertainty of the measure itself.

The reference run is satisfying except along the eastern coast. In particular, the model does not simulate well the Dakar (~ 15°W-10°N) and the Namibian (~ 10°E,15°S) coastal upwellings. However, satellite-SST uncertainty is known to be higher along the Congo coast (Reynolds and Smith, 1994, figures 5, 6 and 16); spatial averaging of the data may also be responsible for a smoothing of the sharp gradients of the upwellings. So the larger rms error could partly result from the data error. On the other hand, the central equatorial upwelling seems to be correctly simulated.

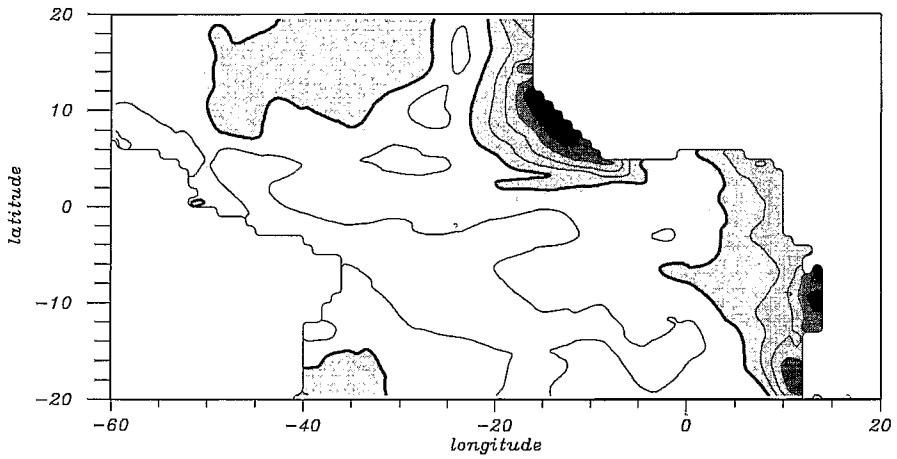

Fig. 1. Mean of the rms difference between the monthly mean of the reference run and the Reynolds SST for 1987. Contour interval is 0.5°C. The thick line is at 1°C. Darker shadings correspond to higher rms.

[1] The first two layers of the model correspond to 5 m and 15 m. A linear extrapolation provides the surface values. If the surface stratification is strong (heating), the temperature at the surface can be 2°C warmer than at 5 m.

Fig. 2 shows the rms difference between the simulated SST with assimilation and the satellite data. This run is very similar to the reference one except for the equatorial upwelling (~ 20°W-0°N). This signal seems to be less well reproduced with assimilation with a rms reaching 2°C (it becomes too cold).

The standard deviation[2] of the difference between the simulated SST without assimilation and the satellite data is smaller (0.7°C in mean) than the rms difference (1°C) and the only two remaining clear features are the coastal upwellings near Dakar and Angola. This statistic is very similar for the assimilated run (figures not shown). So, the rms emphasized the effect of the central upwelling in Fig. 2, but it was only the sign of an increased negative bias in the mean assimilated SST. Another impact of the assimilation is that it increased (up to + 0.5°C) the time variability in the eastern part of the basin so that the simulated variability is closer to the data. We examine in the next section two characteristic examples of time evolution in SST.

2.1.2. Seasonal signal in 1987

As previously noticed, the warm bias of the model is maximum in the region south of Dakar and west of Conakry. The examination of the SST evolution at 18°W-10°N (Fig. 3) confirms that the reference run produces some seasonal signal in rough agreement with data (0.62 in correlation) in spite of the bias. However, the 4°C cooling of February–March is missed whereas the 0.5°C cooling of July–October is emphasized. The assimilation (0.69 in correlation) improves the cooling of February–March but the cooling of July–September is rather degraded and the amplitude of the signal remains too weak.

We saw in GAM98 (section 6.3.3) that the thermodynamics of this region were mostly determined by the climatological forcings. It explains why the optimization

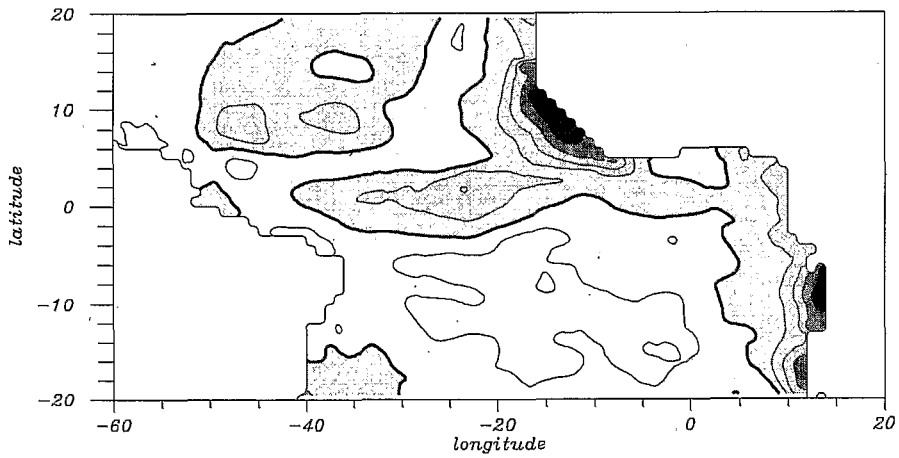

Fig. 2. Same as Fig. 1 for the assimilated run.

[2] (Standard deviation (y) = rms[y – mean(y)]: this statistic removes the mean and thus the bias.

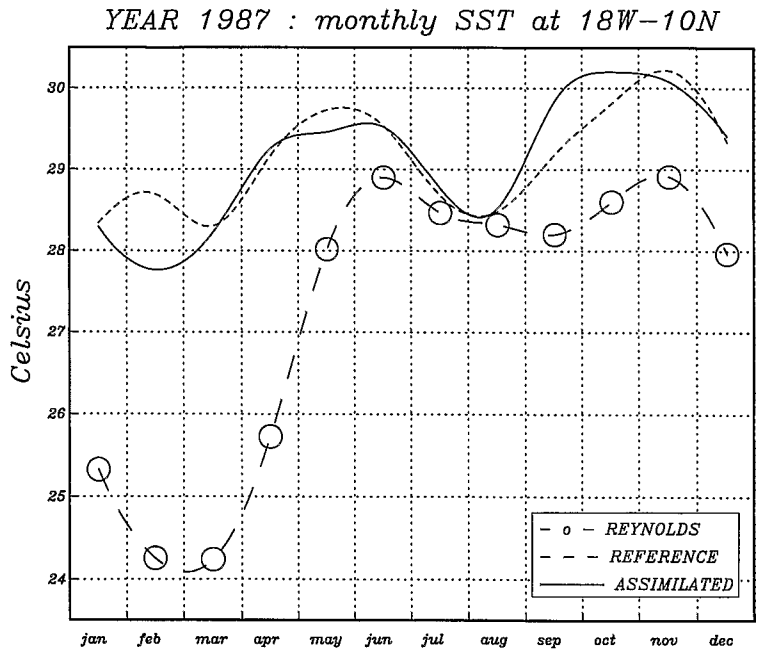

Fig. 3. Evolution throughout 1987 of the monthly mean of the reference (dashed line) and assimilated (solid line) SSTs and of Reynolds satellite data (long dashed line with circles) at 10°N-18°W.

of the initial conditions has a lesser impact than the forcing input. Moreover, GEOSAT revealed that the second half of 1987 was almost uncorrelated (0.11) with the climatology. The inconsistency between the thermodynamics and the forcings during the second part of 1987 explains why the assimilation performed worse then.

Now, let us consider the opposite case, i.e. the case of a cold bias. We selected a point in the core of the simulated upwelling at 20°W–0°N (Fig. 4). The correlation is about 0.91 with or without assimilation. The timing of the upwelling is simulated correctly with or without assimilation but the assimilation over-emphasizes this phenomenon (– 2°C compared to the reference, – 3°C compared to the data). In this case, the increased variability from the assimilation is not necessarily an improvement. The assimilation simply introduced a cold bias in the central area.

We saw in GAM98 that the modelled thermocline was generally too deep without assimilation. In order to fit the numerous XBTs below the surface, the assimilation raised the thermocline. This surface cooling generates a positive correction of the heat flux (20W/m^2 per °C) since our heat flux correction is proportional to the Levitus SST. Consequently, the increased heating leads to a shallower mixed layer. Thus, the coefficient of vertical viscosity becomes smaller near the surface and it gives faster horizontal velocity. The consequences at the Equator are an increased divergence and upwelling in the upper meters (see section 2 in GAM98).

From these first results, it appears that this variational assimilation is unable to

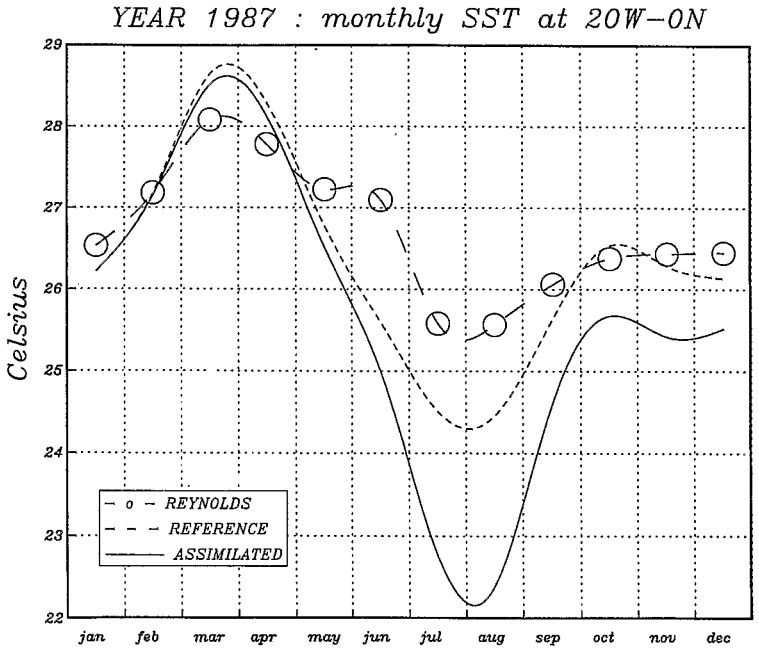

Fig. 4. Same as Fig. 3 at 20°W-0°N.

really improve the simulated SST. It points out that initial conditions are not an adequate control for the near surface water in the tropics in the case of surface heating.[3] In the case of surface cooling, the initial conditions have some importance and the assimilation had some impact. Unfortunately, the climatological flux correction and the diagnostic mixed layer model led sometimes to an even worse SST simulation. So the determination of the initial conditions near the surface is of little benefit in this configuration.

2.2. *Hydrological comparisons*

Unfortunately, the oceanic circulation simulated by the model cannot be checked with independant buoy measurements or moorings because there are no adequate data for this period. We have found only one trajectory near 20°S and close to Africa at the end of the year. Its 10° drift has little interest as a check, especially because in 1987 most of the current activity was located in the north. Although quantitative comparisons are impossible, some qualitative comparisons are made in the following.

[3] More exactly in the case of positive surface buoyancy flux.

In January 1987 (Fig. 5), the NECC in the assimilated run is weak except in the Gulf of Guinea where the coastal Guinea Current is still flowing to the East.

In April 1987 (Fig. 6), the NECC of the assimilated run has a strong retroflection along the Brazilian coast at 4°N but, near 33°W, it joins a branch of the South Equatorial Current (SEC) and flows to the north. At about 15°N-25°W, it turns westward into the NEC. Philander and Pacanowski (1986) suggest that most of the NECC lost is through downwelling into the thermocline, towards the Equatorial Under Current (EUC). Usually the NECC is weak or absent west of 20°W from January to May (Richardson and Reverdin, 1987). This unusual NECC could be anticipated straight from the GEOSAT comparison between March 1987 and March 1988 (Arnault et al., 1992, Figs. 14 and 17): the NECC is clearly tilted to the north east. Northward drift toward the NEC usually occurs closer to Africa. The strong northward drift is thus particularly anomalous at this location. A comparison with drifters from March, April and May 1983 (Richardson and Reverdin, 1987) documents this important point. In particular, in each of the above mentioned months, one of the buoys drifted unusually toward the north within 35–30°W at about 5°N. Other buoys trajectories reveal a surface circulation which is close to the assimilated one. For instance, buoys reveal a recirculation zone within 30–25°W at about 5°N.

In July 1987 (Fig. 7), the assimilation suggests the NECC is not purely zonal and eastward but oscillates in meanders within 6°N–10°N. These meanders were clearly marked on GEOSAT (Arnault et al., 1992, Fig. 15). This kind of circulation has already been observed in situ since a trajectory of a surface drifting buoy presented some oscillations from 47°W to 30°W within 5°N–8°N in July 1983 (Richardson and Reverdin, 1987, Figs. 4 and 7). The meanders have a strong signature in Sea Surface Salinity (SSS) (and less so in SST), with a front corresponding to the limit between the NEC and the NECC (Dessier and Donguy, 1994). Because precipition is weak in this area, the salinity can be used as a tracer of the oceanic circulation, although the density of observations was too low over 1986–89 to observe the interannual change. A qualitative comparison is still possible between the monthly climatology as deduced from the bucket SSS (Dessier and Donguy, 1994, Fig. 6) and the assimilated run. In particular, the shape of the 36 psu isosalinity at about 12°N compares well with the bucket data, especially in July and October (Fig. 7, Fig. 8). It is one or two degrees further north in the assimilated run than in the bucket climatology, but this shift is consistent with the northern position of the Intertropical Convergence Zone (ITCZ) in 1987. The three meanders are centered at the same longitudes (50°W, 30°W, 18°W). The seasonal Levitus climatology (figure not shown), which partly determined the freshwater flux of the model, presents a much smoother signature in SSS. Hence, the assimilation had a positive impact on the front.

In summary, these qualitative comparisons support the validity of the assimilated oceanic circulation and the unusual path of the NECC. It also indicates some resemblance between the 1983–84 and 1987–88 events. We will return later to this point.

2.3. *GEOSAT comparisons*

If the previous section suggests that the circulation pattern produced by assimilation is qualitatively acceptable, it is important to check more precisely that the

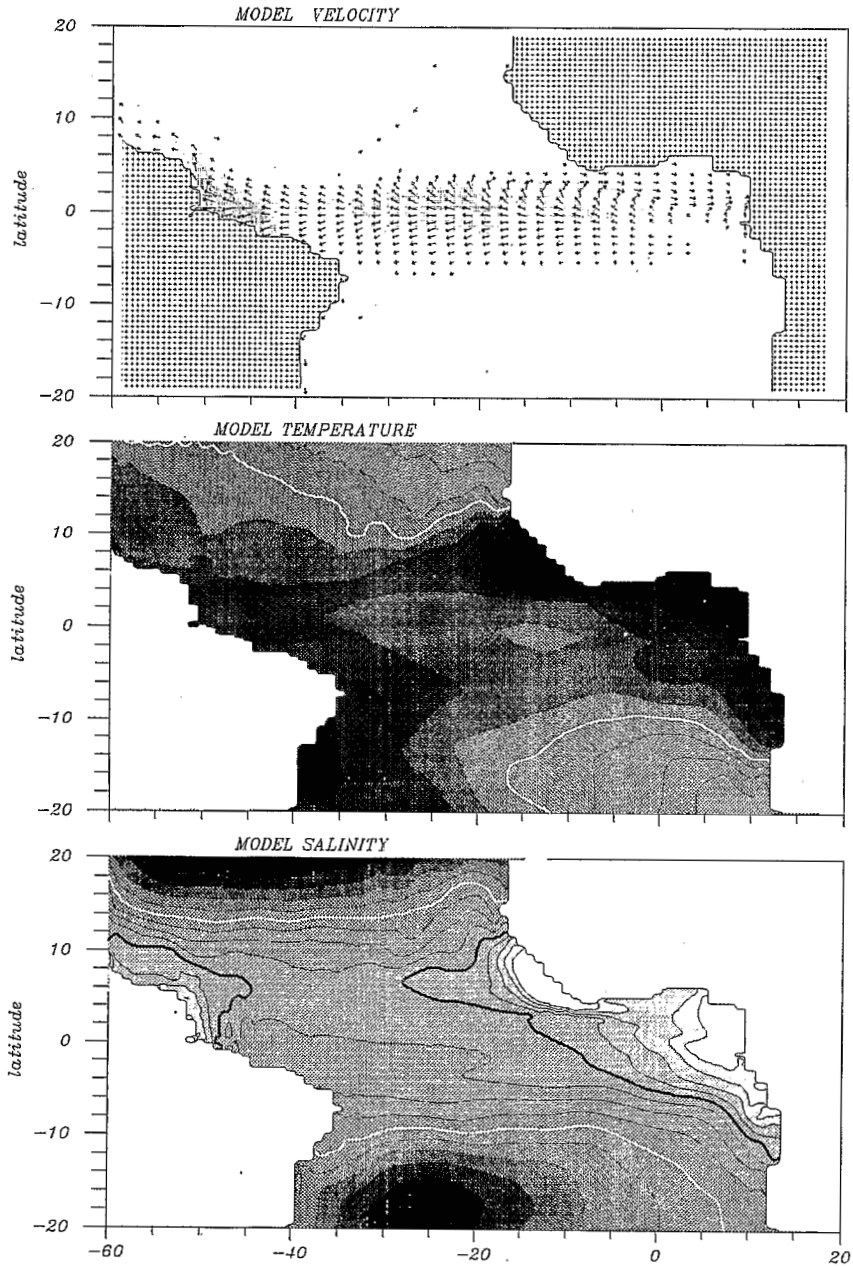

Fig. 5. Monthly mean values of the assimilated run during January 1987. Horizontal velocity, temperature and salinity are plotted at 5 m. Arrows are drawn at each second node of the model in longitude and latitude. The length of the arrows is proportional to the square root of the velocity. Arrows are not visible under 10 cm/s. Darker shading corresponds to higher velocity. Temperature contouring is from 15°C to 29°C; the contour interval is 1°C; the heavy black line corresponds to the 20°C isotherm and the heavy white line corresponds to the 25°C isotherm. Salinity contouring is from 34 psu to 37 psu; the contour interval is 0.25 psu; the heavy black line corresponds to the 35 psu isoline and the heavy white line corresponds to the 36 psu isoline.

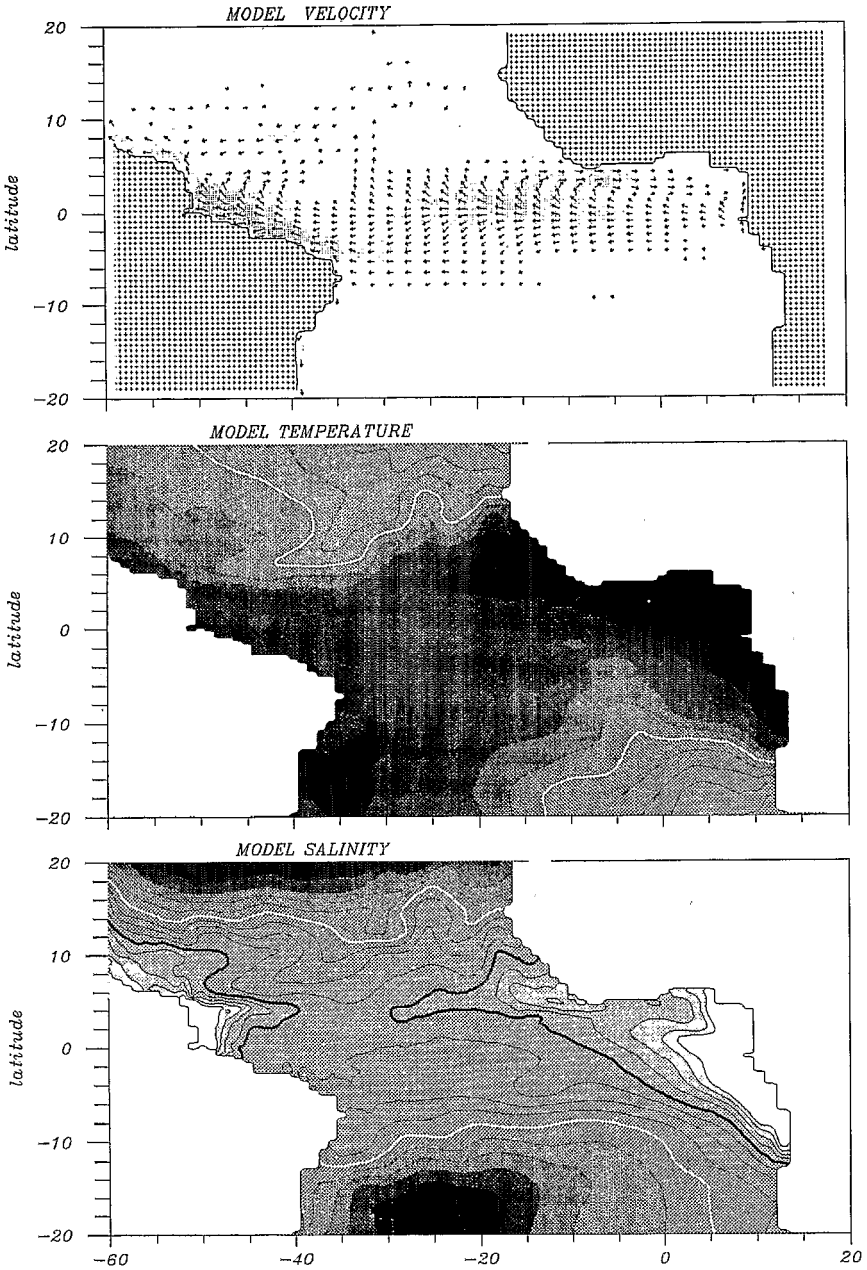

Fig. 6. Same as Fig. 5 for April 1987.

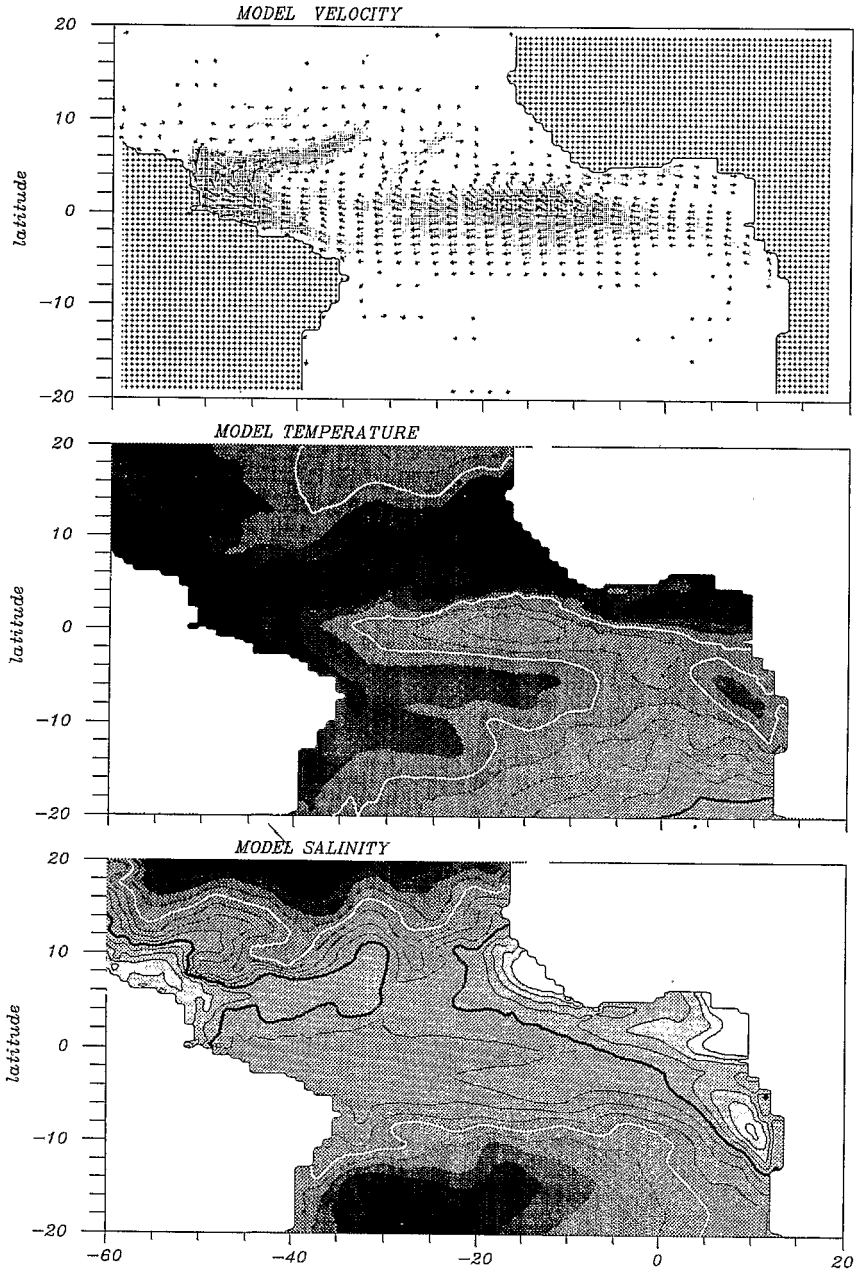

Fig. 7. Same as Fig. 5 for July 1987.

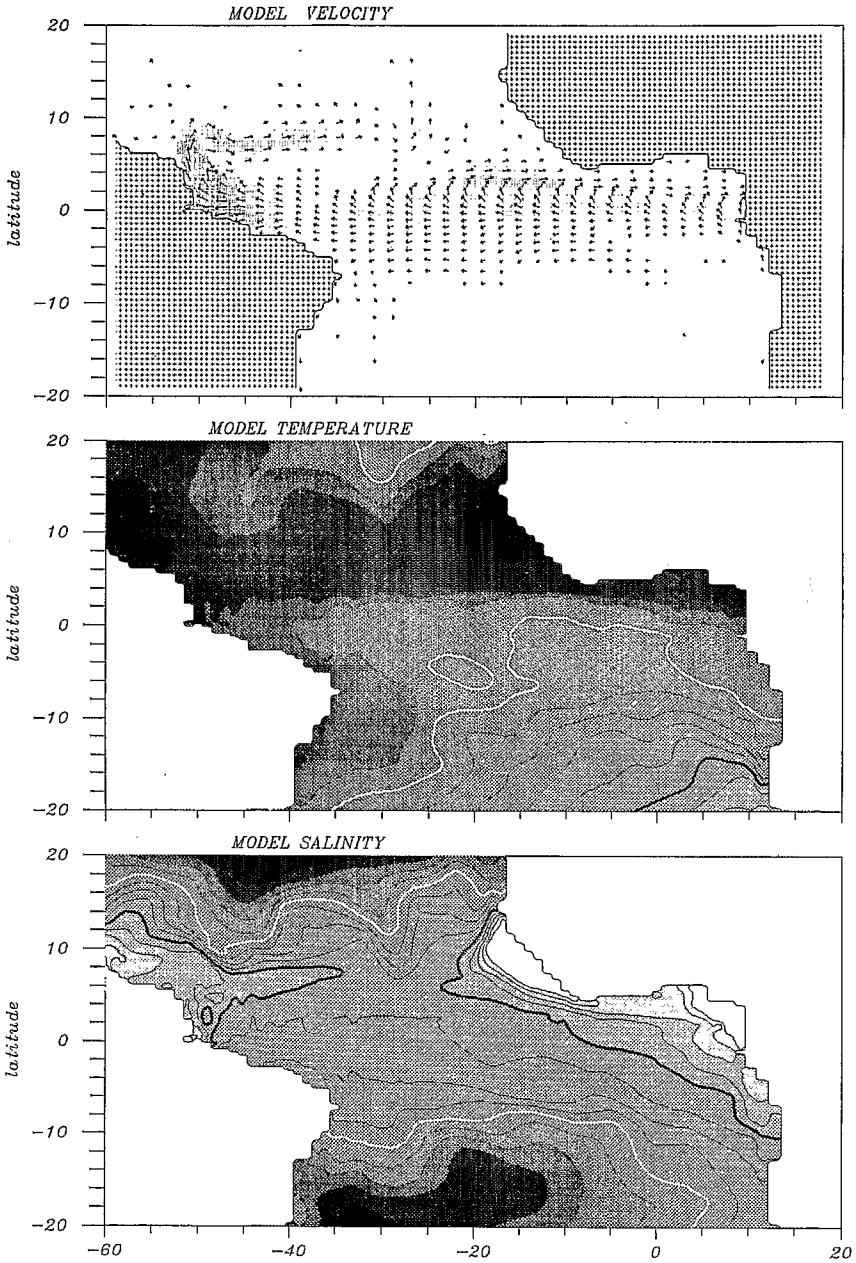

Fig. 8. Same as Fig. 5 for October 1987.

northern position of the modelled NEC-NECC (which follows the ITCZ) is consistent with GEOSAT. Indeed, even if GEOSAT anomalies were monthly assimilated with a good precision (2 cm in rms) into the modelled surface pressure, it does not imply that the model dynamics[4] and the absolute GEOSAT SSH are continuously consistent from one month to the next. This ambiguity between the sterical and dynamical effects is exposed in greater detail in GAM98, sections 4.3 and 6.3).

For this purpose, we consider the SSH as observed by GEOSAT at 40°W-10°N (Fig. 9). As expected, one can check that the SSH produced by the assimilated run is in quite good agreement with the GEOSAT data. It is also worth noting the 50 day oscillations at the begining of the year which match the observations (Richardson et al., 1994; Johns et al., 1990). More important, the figure presents the evolution of the meridional velocity component integrated between 0 and 400 m from the model. The correlation between GEOSAT and the meridional velocity at this position is 0.75. It suggests that the model reproduced the annual meridional migration of the NEC-NECC at the right time and at the right position.

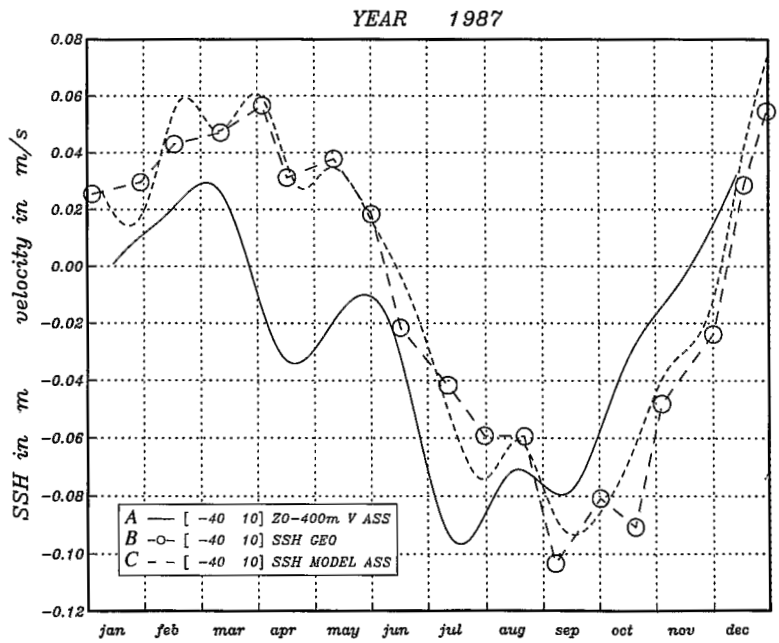

Fig. 9. Time plot of SSH anomalies during 1987 at 10°N-40°W observed by (B) GEOSAT (long dashed line with circle) and (C) simulated with assimilation (short dashed line). The meridional mean velocity between 0 and 400 m (A) simulated with assimilation is plotted in solid line. Units are m for the SSH and m/s for the velocity.

[4] One can imagine a data assimilation producing transitory corrections in temperature or salinity: these corrections could give a good resemblance with GEOSAT over a given month, but an unrealistic or unstable velocity field.

2.4. Mass transport comparisons

Although the terminology of the currents of the tropical Atlantic is well defined, the knowledge of their behavior has not yet been achieved. In situ velocity observations along ship sections are very limited. Ageostrophy and shearing are strong enough to limit the access to the vertical current structure using SSH alone. Hence, in order to estimate the mass and heat transports, so important for climatic studies, a promising way for the near future is to compute transports with a model after data assimilation.

Some partial indirect validation can be done for the NECC with inverted echo sounders. Two sounders were placed at 3°N–38°W and 9°N–38°W from 1983 to 1989. The traveltime of the sounders is converted into dynamic height relative to 500 m (Katz, 1993). The difference between the two sounders is then filtered and smoothed. A nonlinear regression[5] gives finally an estimate of the geostrophic transport of the NECC. Katz found that this current had an anomalously high transport in 1987. The transport exceeded 20 Sv from June 1987 to January 1988 (Fig. 10) whereas the climatological NECC hardly exceeded 20 Sv from August to November.

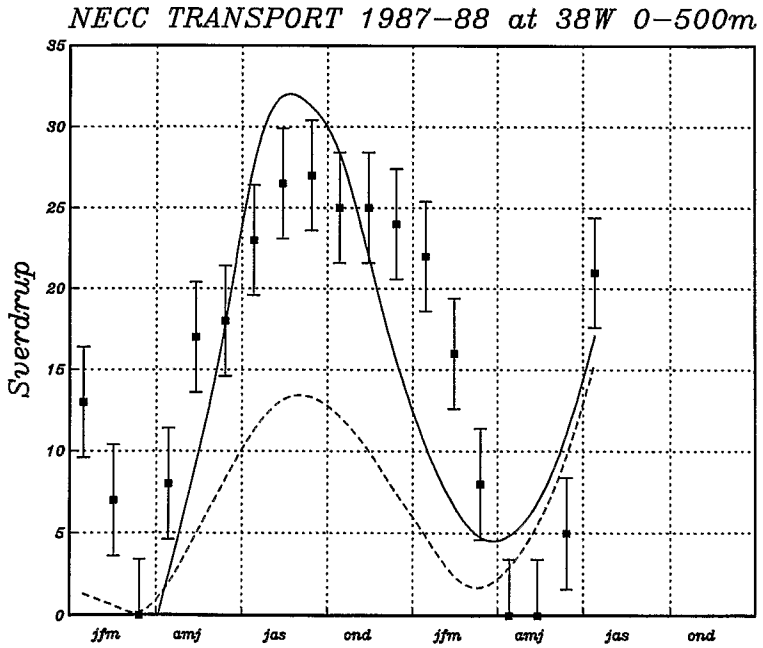

Fig. 10. Eastward transport of the NECC at 38°W from 0 to 500 m in Sverdrups. The dashed line is the reference run, the solid line is the assimilated run (1987) continued by the forecast run (1988). Katz's (1993) nonlinear estimate is displayed by black boxes and error bars.

[5] Geostrophic NECC transport [Sv] = 4.2 $\sqrt{}$(dynamic height difference [cm]) ± 3.4.

The total transport of the modelled flow (ageostrophic flow included) for the reference run and the assimilated runs was computed and smoothed between[6] 3°N and 10°N from 0 to 500 m (Fig. 10). The reference run simulates a NECC which is clearly below Katz's lowest estimate, whereas the summer transport appears to be overestimated by the assimilated run. The fall transport is still underestimated, even if there is an improvement compared to the reference run. Overall, the assimilated run simulates a NECC transport which is closer to Katz's nonlinear estimates.

Molinari (1982) has estimated the transport of the central SEC from 1978–80 in situ transects. It is highly variable between 7 and 26 Sv within 25–28°W from 0 to 1000 m. Fig. 11 shows the westward transport computed between 5°S and 3°N from 0 to 500 m (as in Fig. 10). The reference run simulates a rather steady transport, presenting a semi-annual signal similar to the climatological run in Philander and Pacanowski (1986), with maximum in June and November. The assimilated run is less regular with high values in spring and summer 1987, comparable with the NECC transport (Fig. 10). This suggests an accumulation of warm water in the west from the Gulf of Guinea in 1987, and a much weaker loss of eastern surface water in 1988.

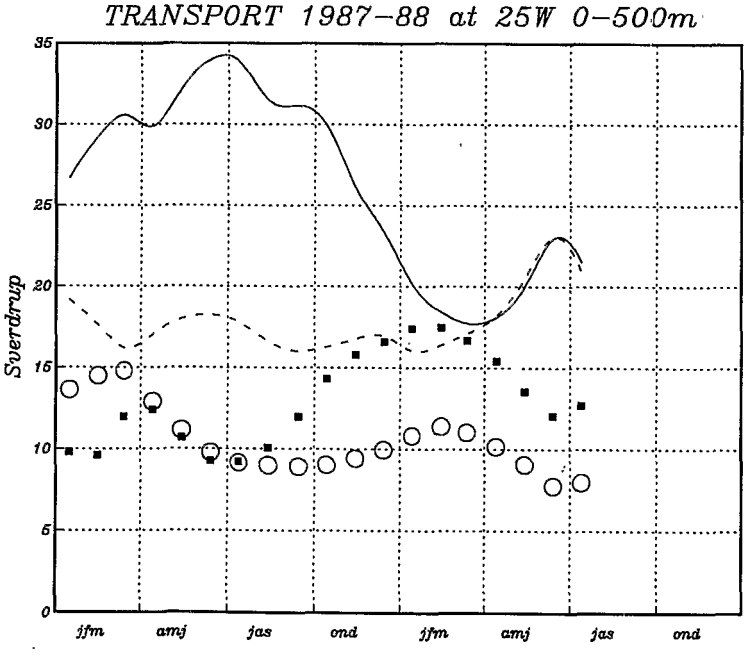

Fig. 11. Transport of the SEC for the reference run (dashed line), the SEC for the assimilated run continued by the forecast run (solid line), the EUC the reference run (circles), the EUC for the assimilated run continued by the forecast run (black boxes).

[6] As in Huang et al., 1995: the NECC extends up to 10°N in 1987 so it would be a truncation to limit it at 9°N.

Tang and Weisberg (1993) have estimated from three current meters that the transport of the EUC at 28°W from 10 to 150 m was within 20.3 ± 4.7 Sv in 1983–84. Hisard and Hénin (1987) have estimated from current meters the transport of the EUC at 23°W from 0 to 500 m flows eastward faster than 20 cm/s. The transport was within 10–25 Sv in the early eighties (16 Sv in mean), the highest estimate being 44 Sv in March 1980. The minimum was reached in July 1983 (6 Sv), thereafter a regular increase was noticed. The EUC transport (only eastward contributions faster than 20 cm/s are kept) simulated by the reference run is steady and somewhat balances the SEC transport; the reference run circulation is rather zonal, with a EUC balancing the zonal pressure gradient along the Equator which results from the accumulation of water in the west by the SEC. The assimilated run presents a EUC which does not balance the SEC. This is because of the stronger exchanges between the Equator and the northern tropics. The assimilated budget is positive (up to 25 Sv) for the west in 1987, is nil in spring 1988, and returns positive afterwards (up to 9 Sv). The reference budget is much weaker (up to 8 Sv) to the west in 1987, and increases (up to 14 Sv) in 1988. In summary, the reference run is steady, without a mark of equatorial mass redistribution. In contrast, the assimilated run presents an accumulation of surface water in the west up until fall 1987. The strong surface westward SEC resulted in a slowing of the subsurface EUC eastwards. By the end of 1987, there was a surge of western water into the Gulf of Guinea, which continued through into 1988. It is interesting to note that, according to GEOSAT (Arnault et al., 1992, Fig. 22), the downwelling Kelvin wave was restricted to the western half of the basin in early 1987, whereas it crossed the basin in 1988. According to the forecast run, the east–west exchanges reached a minimum in spring 1988, enhancing the vertical mixed layer processes.

3. Resulting fields

Before the examination of the model fields, we briefly summarize the context of 1987. April 1985 was the start of a long phase of wind reinforcement of the equatorial easterlies and the north equatorial trade winds. The increase reached its maximum in late 1987 but two brief wind relaxations occurred in March–May and August–September 1987 (Servain and Lukas, 1990). The NECC increased in 1987 but its impact on the SST was not direct. In November 1987 a strong wind relaxation occurred, returning to "normal values". Following the GEOSAT and XBT analysis, a mass redistribution between the tropics and the Equator occurred in 1987 (Arnault and Cheney, 1994). The heat content of the equatorial region (5°N–5°S) then increased whereas in the north equatorial (10°N–10°S) and south equatorial (10°S–25°S) regions it decreased.

3.1. Horizontal maps between 20°S–20°N and 60°W–20°E

The assimilated velocity, temperature and salinity fields are displayed horizontally at 5 m (Fig. 5) and 65 m[7] (Fig. 12) for January 1987. At the surface, the easterly

[7] This model layer corresponds to the mean position of the thermocline and the Equatorial Under Current.

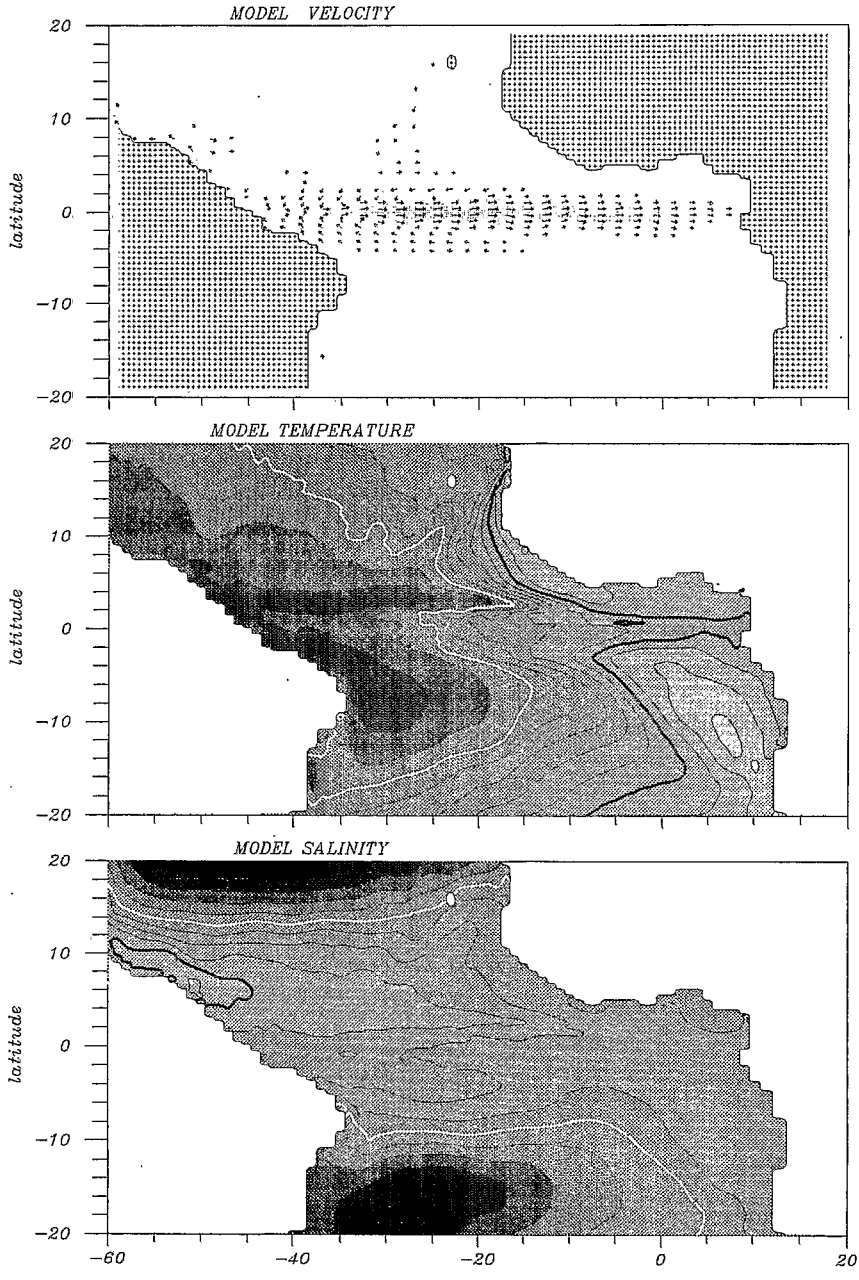

Fig. 12. Same as Fig. 5 at 65 m for January 1987.

equatorial winds create a broad SEC and a weak central upwelling. In the Gulf of Guinea, the Guinea Current (GC) follows the local westerly monsoon and accumulates hot water in the Gulf. The NECC is weak at the surface (arrows are not plotted under 10 cm/s). The Brazilian Current (BC) flows to the north along the American coast, carrying warmer surface waters towards the Carribean. The Niger and Congo rivers outflows and the Guinea rainfall (near 13°W–6°N) produce a strong signal in the SSS, developing a shallow mixed layer along the coast.

At 65 m (Fig. 12), the Angola dome is visible in the temperature field near 12°S–7°E. The Guinea dome near 20°W–8°N is less defined. Instead, another smaller dome appears near 28°W–12°N. Connected with this dome, a south-west current originates near the sea mount at 16°N–25°W and ends at about 6°N–35°W (visible at 5 m or 65 m). The NECC at 65 m is weak (< 20 cm/s) and only significant between 20°W and 30°W, along 5°N, and around 8°N–45°W along the American coast. In fact, the most noticeable feature of the model velocity at 65 m is the usual presence of a well defined eastward EUC, all along the Equator. This EUC is partly fed, in its western part, by two westward branches located respectively at 3°N and 3°S.

In April 1987 (Fig. 6 and Fig. 13), the solar heating and the weak equatorial winds produce the warmest SST of the year, in particular in the Gulf of Guinea (up to 30°C). SST and SSS fronts are linked to the surface currents between 0°N and 20°N. The surface currents present a somewhat complex gyre for the westward NEC and the NECC (between 50°W–7°N and 25°W–15°N).

At 65 m (Fig. 13), the western coastal BC is southward from 8°N to the Equator. The NEC provides dense (cold and salty) waters from the middle of the basin to the NECC and EUC. In replacement, the NECC provides light (warm and fresh) water at about 10°N–25°W. The SEC provides warm water from 10°S to the EUC. The EUC exports the mix to the east, as can be seen on the salinity field at about 10°W–0°N. In addition, from January 1987 the thermocline is domed in the centre of the basin.

In July (Fig. 7 and Fig. 14), the equatorial winds intensify and the central equatorial upwelling is maximum. It was particularly strong in 1987. This results in a sharp tongue of cold surface water developing along the Equator, and curving southeastward along the African coast. The fresh waters which flooded a large part of the equatorial African coast in April are now limited to the Guinea coast (near 6°N-13°W) and around the mouths of Congo and Niger rivers. The influence of the Amazon runoff, on the South American side, is perceptible on the SSS. The BC no longer flows to the north-west and totally feeds the NECC instead. All the surface currents deepen and strengthen (for instance, + 40 cm/s for the NECC in the west).

At 65 m (Fig. 14), the NECC is still strong but separates into branches near 33°W. In addition to the usual eastward flow, a branch flows to the north toward the NEC, and another branch flows to the south toward the SEC and then EUC after sinking below 80 m (Schott et al., 1993). The EUC disappears at 7°W (also in GAM98, figure 25). The coastal BC is southward along the American coast from 60°W. There are large undulations of the thermal structure along 10°N which split the Guinea dome into three centres at 40°W, 26°W and 18°W. Globally, the intrusion of warm waters from the NECC warmed the region of the Guinea Dome.

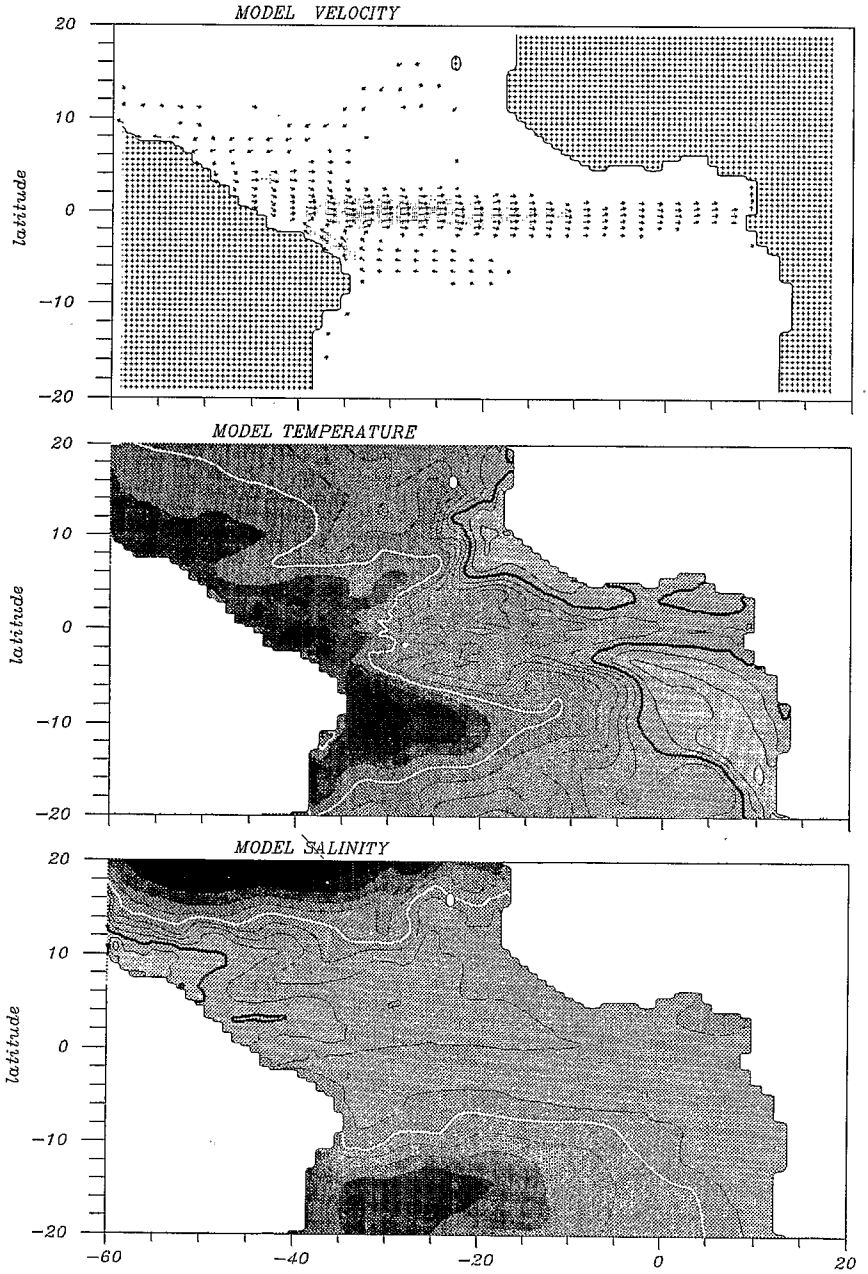

Fig. 13. Same as Fig. 5 at 65 m for April 1987.

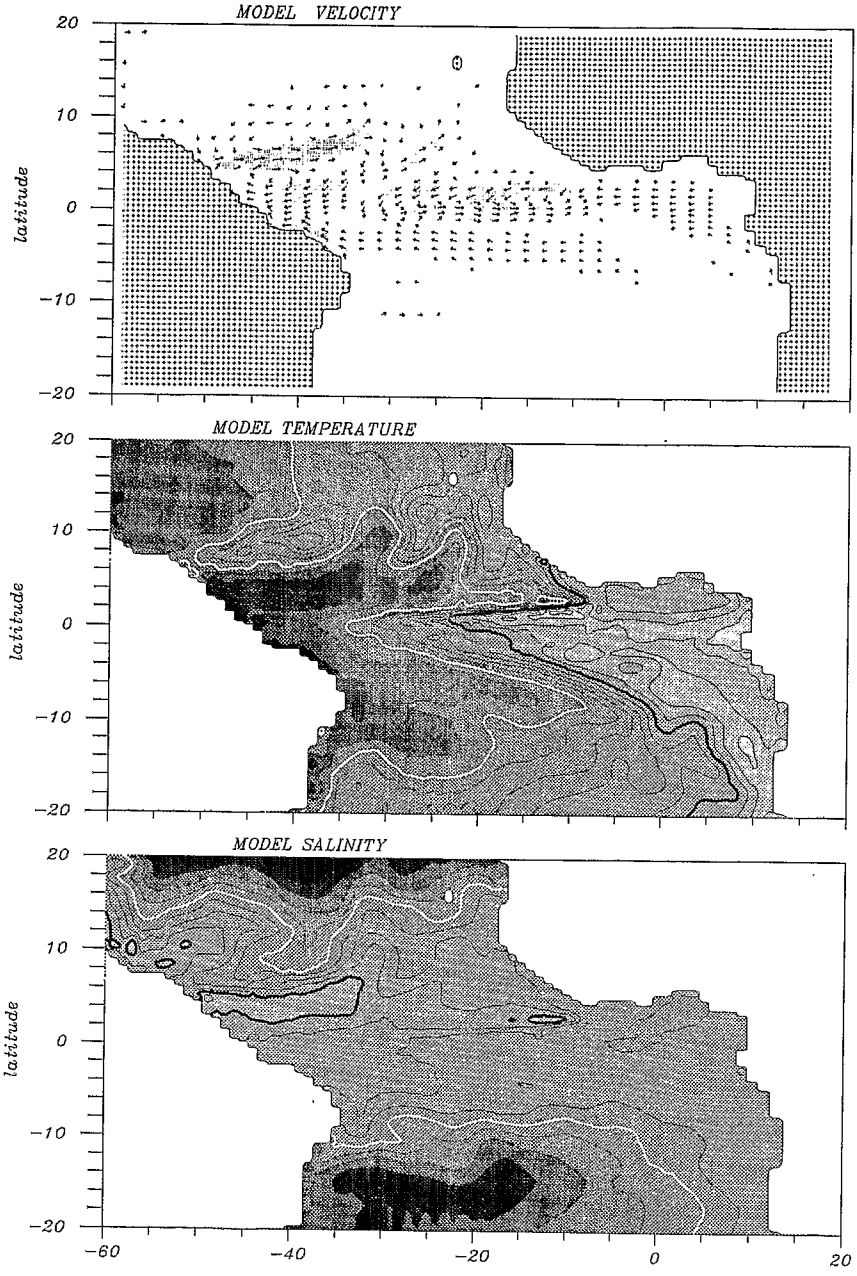

Fig. 14. Same as Fig. 5 at 65 m for July 1987.

In October 1987 the mass redistribution now affected the Gulf of Guinea more than the northern currents (Fig. 8 and Fig. 15). The NEC stopped providing cold waters to the NECC. The surface NECC is strong at 40°W and partly flows north at 25°W whereas normally it flows into the eastward coastal GC. The GC now appears like a retroflexion of the SEC at about 20–30°W.

The mass redistribution is very well marked on the temperature field at 65 m (Fig. 15). In particular, the assimilated run shows a flat east–west slope at 10°N: the Guinea Dome is stretched toward the south (18°W-6°N) and toward the west (45°W–10°N). The three domes at 10°N are well marked on GEOSAT (Arnault et al., 1992, Fig. 16). It is also worth noting that once again the NECC loses water equatorward into the EUC. It is the turning point of the mass redistribution which will then concern the east and the south east. The Gulf of Guinea is warming up at depth. This warming will continue over the next months (figures not shown, see Section 2.3). Note the development of a westward undercurrent along the Ivory Coast which has already been described in Lemasson and Rebert (1973).

3.2. Meridional section at 25°W

We saw that the main signal provided in 1987 by the assimilation concerns the band 15°N–5°N. The signal at the Equator is determined from slight perturbations of the thermocline and the strength of the EUC. In order to gain an insight on the mass redistribution from the tropics toward the Equator, we prefer to examine a meridional section at 25°W where the assimilation impact is strong.

In January 1987 (Fig. 16), the thermocline is well defined and sharp. The mixed layer is deeper at 20°N (80 m) than at 20°S (25 m). The zonal current clearly shows the EUC core at about 70 m is symmetrical about the Equator, and surrounded by the westward SEC. However, the SEC is more developed and shifted northward, like the ITCZ. Between 4°N and 10°N, the eastward NECC is weak, but usually it is absent at the beginning of the year.

In April 1987 (Fig. 17), the EUC weakens and shallows. The NECC looks like a deep extension of the EUC (it is then hard to distinguish between the transports of the two currents). The surface currents are very weak and mostly westward. The northern branch of the SEC is absent at 25°W (first wind relaxation). A slight rise in the 25°C isotherm (thick white line) at the Equator marks the onset of equatorial upwelling.

In July 1987 (Fig. 18), the upwelling is fully developed, as a result of the wind forcing. Everywhere the mixed layer has deepened and the thickness of the homogeneous layer is about 70 m within 10°N-10°S. The SEC, EUC and NECC strengthen and deepen. As already noticed elsewhere (Philander and Pacanowski, 1986), as a result of Coriolis force, the increase of the SEC–NECC shearing produces a strong downwelling of warm waters between 4°N–12°N. The SEC is shifted northward because of the northern position of the ITCZ. The ITCZ shift leads to weaker easterly winds south of the Equator. Weak easterlies and southern SEC allowed the development of the South Equatorial Counter Current (SECC) between 14°S and 9°S, with a maximal intensity below 40 m. This intermittent current has been observed between

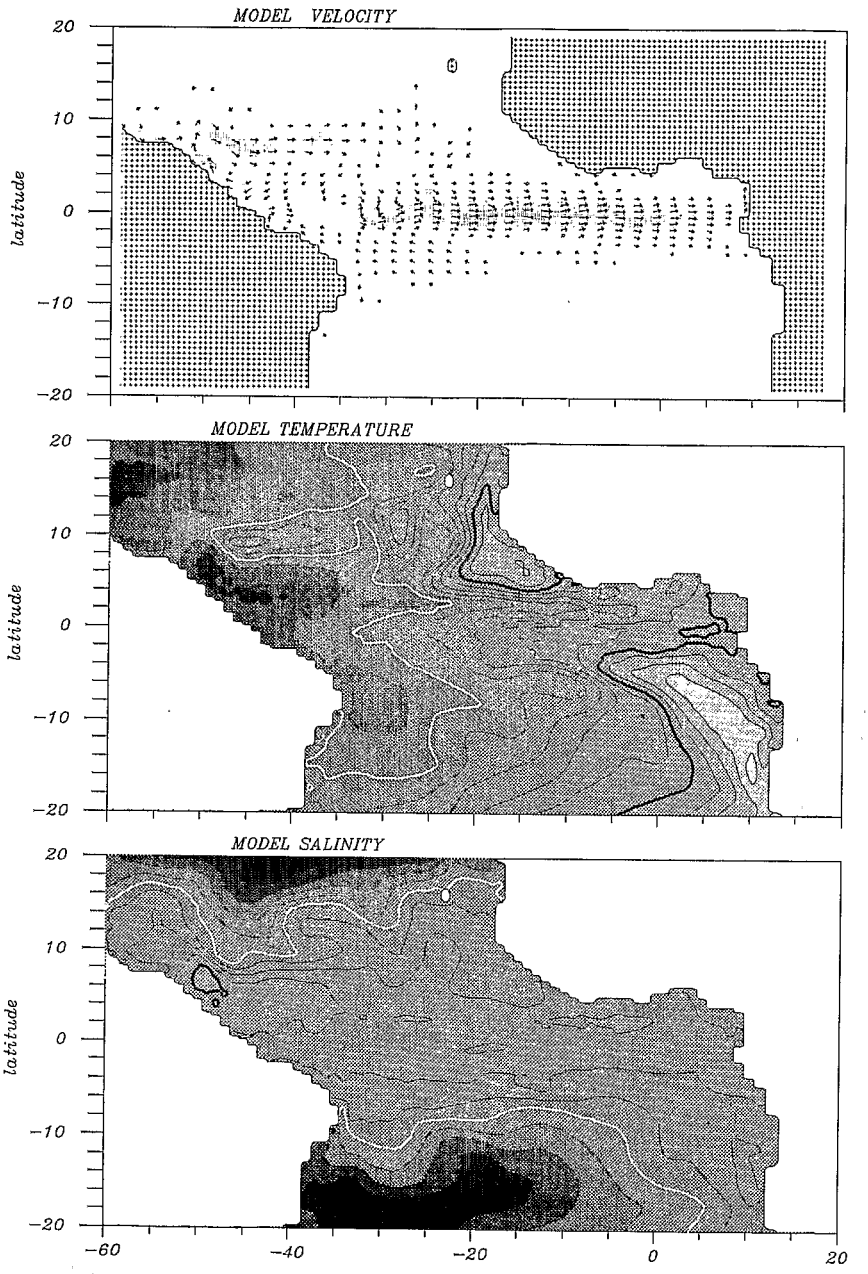

Fig. 15. Same as Fig. 5 at 65 m for October 1987.

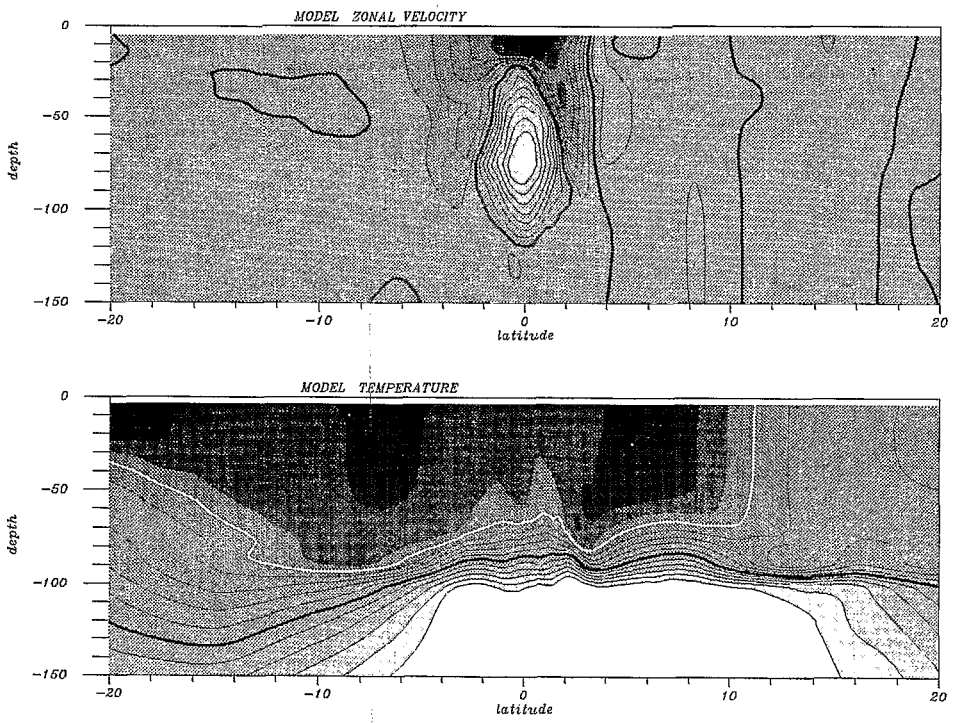

Fig. 16. Monthly mean values of the assimilated run during January 1987. Meridional sections of velocity and temperature are plotted at 25°W. Darker shading corresponds to westward velocity; the contour interval is 10 cm/s; the heavy black line corresponds to the 0 cm/s isoline. Same conventions as Fig. 12 for temperature.

6°S and 9°S (Molinari, 1982). The definition of this weak current remains ambiguous, but a maximum at about 275 m was generally ruled out. The southern position suggested by the simulation could be another effect of the ITCZ shift.

In October 1987 (Fig. 19), the seasonal contrast between the warm Northern and cooler Southern Hemisphere is clear in the mixed layer. At the Equator the rise in the depth of the thermocline is as marked as its deepening at about 10°N. The SEC is uniform across the Equator, whereas the EUC core is directly linked to a surface branch of the NECC between 2°N and 4°N: the NECC starts to export warm surface waters toward the Gulf of Guinea via the EUC.

3.3. Analysis of the correction

The previous sections showed the thermodynamical interpretation of the 1987 mass redistribution as given by the assimilation. In particular, the role of the north equatorial currents was pointed out. The present section aims to identify which physical processes were either emphasized by assimilation or were missed in its absence. For instance, if we neglect forcing errors (perfect model), and assume that the evol-

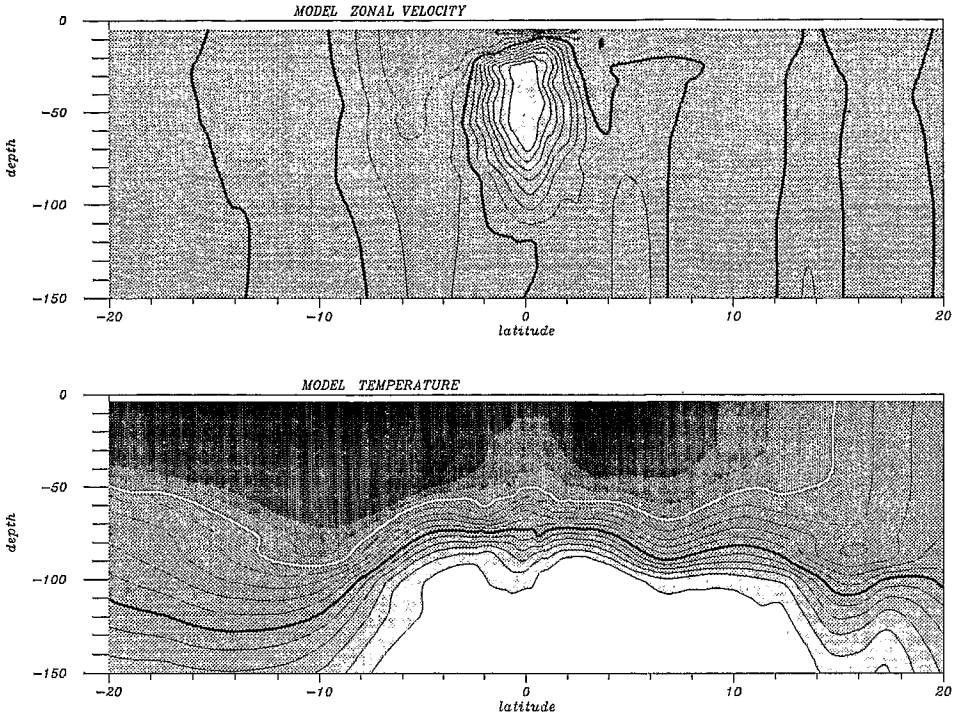

Fig. 17. Same as Fig. 16 for April 1987.

ution of the difference between the assimilated run and the reference run, ϵ, is given at the first order by:

$$\frac{\partial}{\partial t}\epsilon = \boldsymbol{L}(t)\epsilon.$$

The objective is then to identify in the linearised operator $L(t)$ some leading mechanisms (wave, advection, diffusion, . . .), and which data provided the information. To this end, we analyse the main corrections provided by the assimilation to the horizontal velocity, temperature and salinity between 20°N and 20°S during 1987.

3.3.1. Description of the correction

We computed the monthly differences between the assimilated run (presented at 5 m and 65 m in Section 3.1) and the reference one. The signal is weaker at 5 m than at 65 m. In particular, the corrections in SST are not strong enough ($\approx$ 0.5°C) for a validation with satellite data. Moreover, if the SST anomalies are increased by the assimilation, their evolution is not really modified (see Section 2). So we choose to discuss the impact of the assimilation at 65 m.

In January 1987, the corrections are weak after only one month of assimilation (less than 4 cm/s and 0.2°C at 65 m, figure not shown) because of the weight of

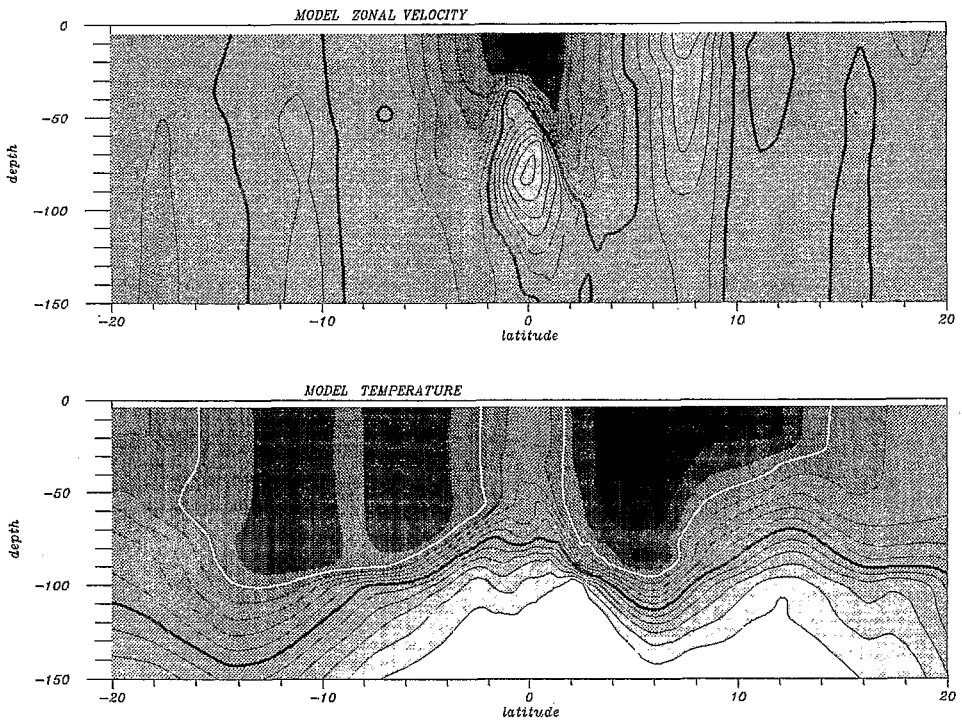

Fig. 18. Same as Fig. 16 for July 1987.

the first guess data (see GAM98, section 4.4). The strongest correction in temperature provided by assimilation (2°C at 88 m) is a flattening of the Guinea dome near 20°W–8°N. Also, the assimilation raised the thermocline between 4°S and 12°N at 25°W by more than 10 m.

In April 1987 (Fig. 20), after 4 months of assimilation, the corrections are clearly marked. There is a succession of corrections of the current in the opposite direction within 13°S–11°N from the Brazilian coast to 20°W. In particular, there is an increase in velocity within the gyre NEC–NECC, extending from the Brazilian coast up to 16°N–25°W, which became clear after 2 months of assimilation.[8] There is a strong pattern of positive and negative anomalies in the temperature field centered around 25°W. The impact of the assimilation at 25°W is principally a deepening (– 10 m, corresponding to a warming) of the thermocline between 6°N and 16°N and a rising (corresponding to a cooling) between 6°S–4°N. Similarly, there is a weaker series of anomalies symmetrical around the Equator between 0°W and 30°W. This is a snapshot of eastward and westward propagations visible from February to September (figures not shown). The EUC is also increased (by more than 10 cm/s) by the assimilation, and the correction presents oscillations around the Equator.

[8] Around the same position.

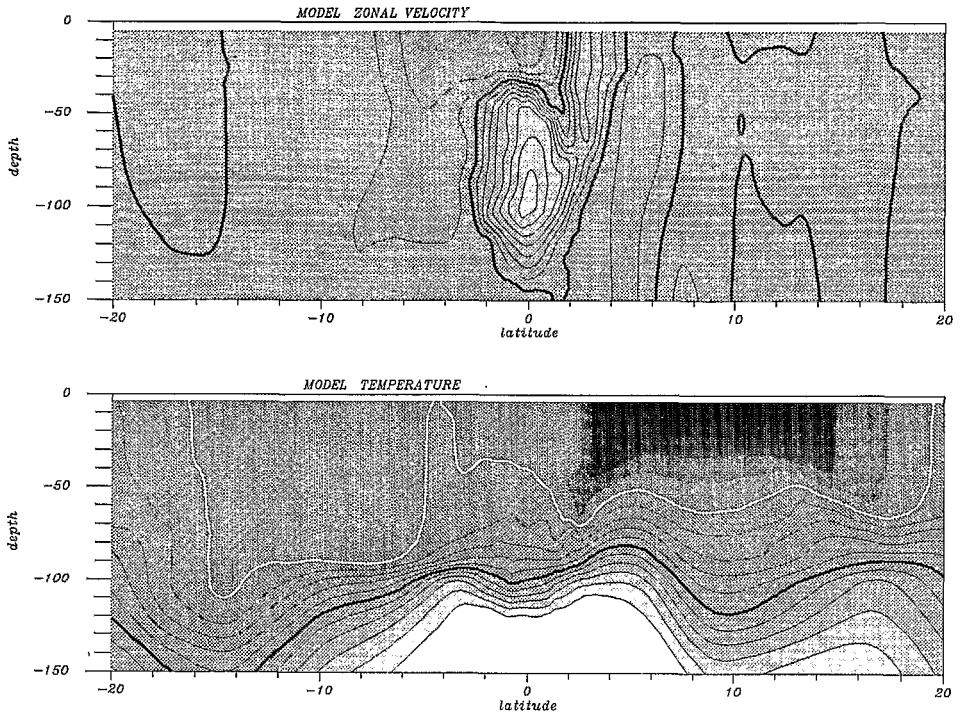

Fig. 19. Same as Fig. 16 for October 1987.

In July 1987 (Fig. 21), the succession of ridges and troughs of the velocity correction (from 60°W to 20°W) intensifies. The gyre NEC–NECC oscillated in its position after April but did not migrate. The western half of the basin is cooler between 8°S and 12°N. Corrections in temperature mainly follow the gyre NEC–NECC: they go to the north between 20°W and 25°W and turn to the south-west beyond 15°N. This is clear when one compares the path of the positive correction placed at 8°N–24°W in April and the assimilated velocity field (Fig. 6 and Fig. 13). We have checked[9] that advection migrates the temperature corrections between 6°N and 14°N with local recirculation, dispersion and convergence. Variations in salinity have now developed in clear patches that migrate to the west at about 15°N. The maximum signal in salinity is located further north because the salinity is rather homogeneous between 8°S and 10°N (Figs. 5 and 8).

In October 1987 (Fig. 22), the current corrections are orientated more zonally and the southern corrections disappear. In the west, the NECC is strengthened and shifted northward by about 2°. It corresponds to the northward shift of the ITCZ. Corrections in temperature migrate to the west. The apparent mass transfer from 6°N–16°N (thermocline 40 m deeper) to 6°S–4°N is very clear. Salinity corrections are propa-

[9] By advecting particles in the assimilated velocity fields.

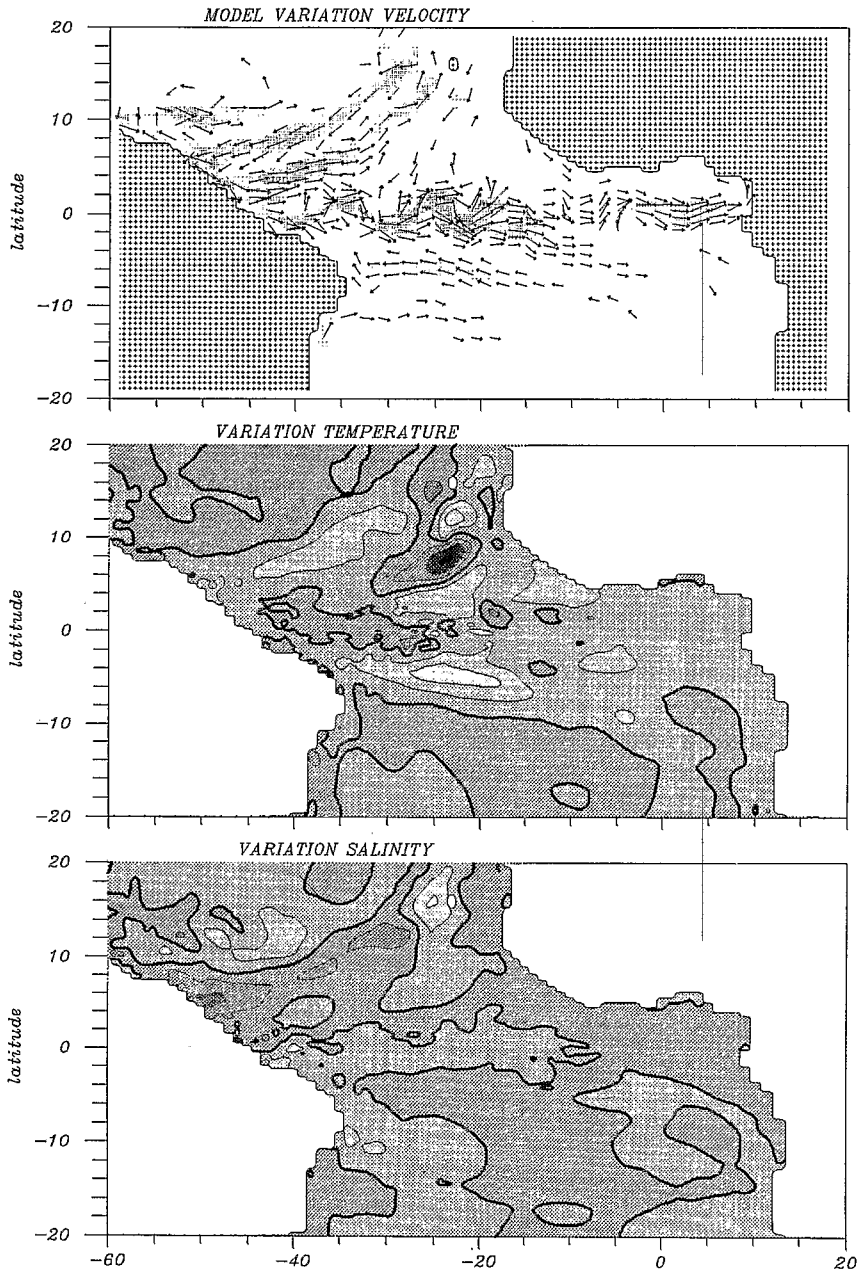

Fig. 20. Monthly mean values of the difference between the assimilated run and the reference run during April 1987. This difference is plotted for the horizontal velocity, temperature and salinity at 65 m. Arrows are drawn at each second node of the model in longitude and latitude. The length of the arrows is proportional to the square root of the velocity. Arrows are not visible under 5 cm/s. Darker shading corresponds to higher velocity. Temperature contouring starts from –3°C and ends at + 3°C; the contour interval is 1°C; the heavy black line corresponds to the 0°C isotherm. Salinity contouring starts from – 0.75 psu and ends at + 0.75 psu; the contour interval is 0.25 psu; the heavy black line corresponds to the 0 psu isoline.

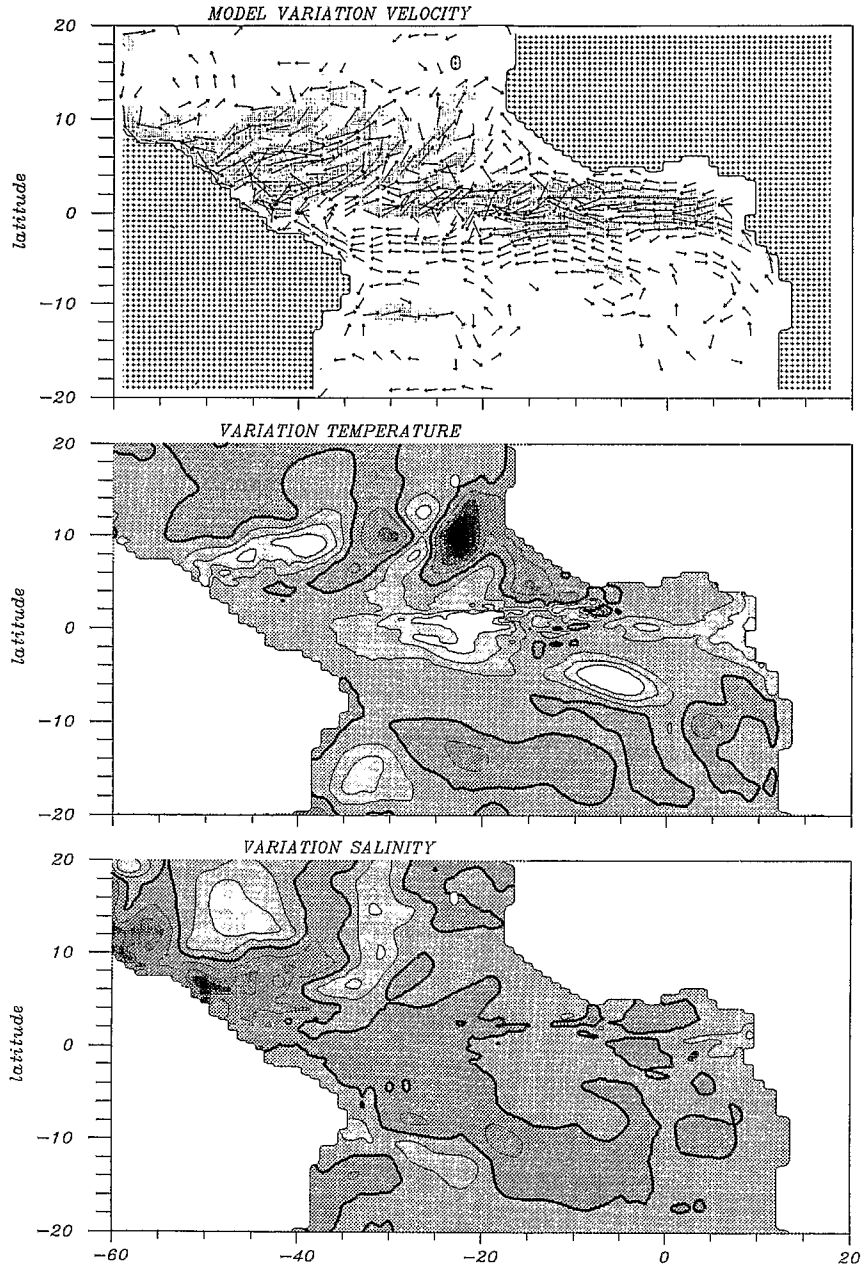

Fig. 21. Same as Fig. 20 for July 1987.

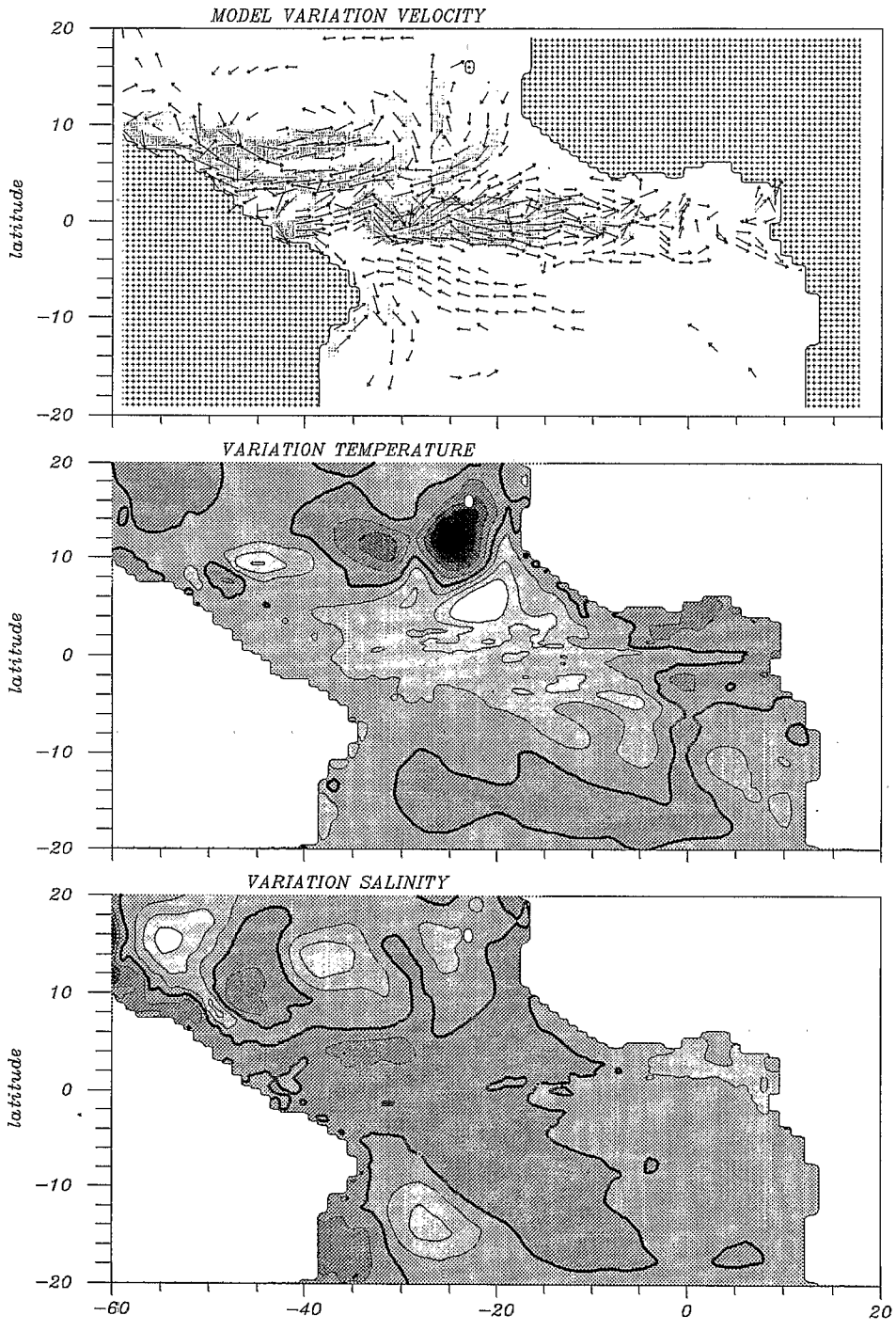

Fig. 22. Same as Fig. 20 for October 1987.

gated to the west up to the Brazilian coast and then deflect toward the north. Salty waters are also being advected at the surface by the GC as in 1983 (Hénin and Hisard, 1987).

In summary, a warm correction migrates north-eastward in association with the NECC, whereas cold corrections migrate in association with the NEC. Weaker corrections propagate at the Equator. Concerning the origin of the northern warm corrections, we have checked that the XBT casts did not account principally for their origin (the XBT lines did not sample this region in early 1987). On the other hand, GEOSAT is directly responsible for the increase of the NECC (see GAM98, section 6.3). This increase implies warming through downwelling resulting from the Coriolis force.

3.3.2. Mechanisms

Possible Rossby waves were observed in GEOSAT near 14°N (Arnault et al., 1992). The propagation speed at 14°N deduced from the model[10] is 9 cm/s (± 3 cm/s). This value is in agreement not only with the theoretical[11] Rossby wave propagation speed of 9 cm/s for this latitude, but also with the mean westward NEC value at 14°N. Within the accuracy of GEOSAT and those of the model simulations, we cannot conclude here whether wave or advection played a prominent role in the displacement of the corrections.

The latitudinal shifting of the NEC–NECC system occurs along the northern coast of Brazil. The NECC is located at about 4°N in boreal spring, and at about 10°N in fall. The previous section revealed that the correction provided by assimilation migrates northwestward along this axis. The mean north-west velocity (from 0 to 400 m) computed from the assimilated run is 3 cm/s in April and 24 cm/s in October near 10°N-50°W (further from the coast than the BC). The mean value for 1987 is 8.8 cm/s. This corresponds well with the speed of the eddies (9 cm/s) as deduced from drifters and RAFOS floats from 1989 to 1992 (Richardson et al., 1994). The increase of the speed during the second half of the year is in phase with the seasonal variation of the coastal currents in that area: Johns et al. (1990) observed, from three moorings located here, a stronger upper layer mean flow during September–January 1987–88 compared to the February–June situation. Didden and Schott (1990), observed a similar spring to fall increase in the WOCE Community Modelling Effort model results in the western tropical Atlantic and in GEOSAT altimetry. Thus, these results suggest that in our assimilated run, the correction was partly advected by the mean flow. Recently, McClean and Klinck (1995) analyzed the WOCE model results in the NECC retroflection region and show Rossby waves of the first and second orders are generated neither by wind forcing nor by barotropic instability. Thus a lot of work still needs to be done to understand the complex dynamics of this region.

In the introduction to this section, we assumed that the model is perfect. However,

[10] Anomalies in dynamic height relative to 400 m.

[11] $c \approx \beta R^2$ (R Rossby radius, β planetary vorticity gradient) gives 8.6 cm/s and 4.0 cm/s for the two first baroclinic modes.

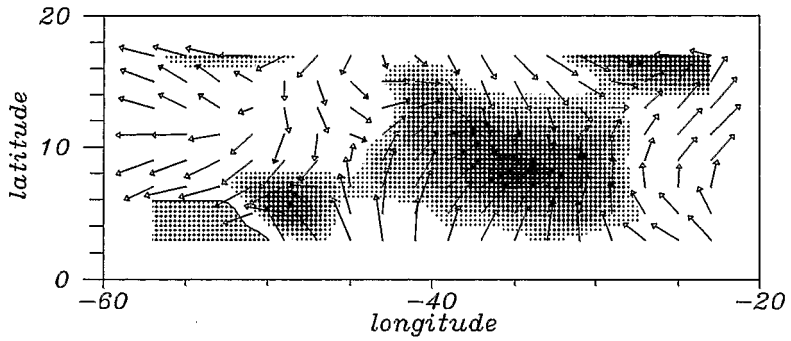

Fig. 23. Ship windstress change from March 1987 to April 1987. The length of the arrows is proportional to the square root of the velocity. Dark shading indicates the convergence intensity (negative divergence).

we can imagine that the model error could be linked to the windstress. For example, in the case of an inadequate transmission coefficient (too weak viscosity at the surface, for example), then the time evolution of the model will be forced by a function (the viscosity error) of the windstress evolution. Assimilation revealed that the NEC–NECC gyre was strongly active in spring 1987. GAM98 illustrated this by the fairly high unusual springtime sea level variability as shown by GEOSAT. We still have to identify both the physical origin of this anomaly, and which effect the assimilation has corrected. In order to get rid of the long trend of increase in windstress from 1985 to late 1987, we have computed the change in windstress from March to April 1987 (Fig. 23). The most striking feature is a north-west axis of convergence in the region of the NEC–NECC gyre. For comparison, we present the difference in the change from March to April 1987 for the surface velocity field between the assimilated and the reference runs (Fig. 24). In this figure, the change in the NEC–NECC gyre is located about the same north-west axis. This increase in the gyre appears to be the geostrophic response of the ocean to the increase in atmospheric convection.

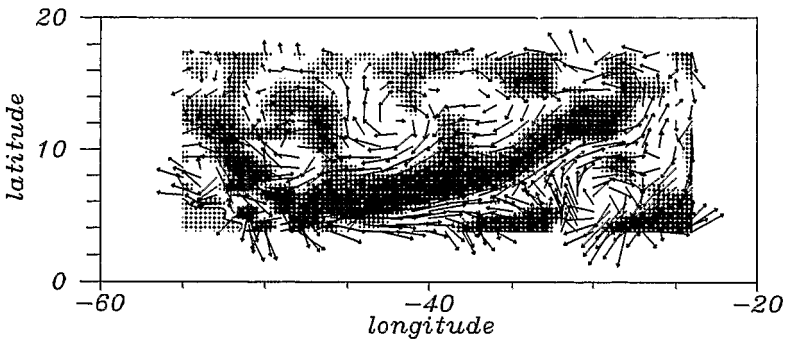

Fig. 24. Change in 5 m current corrections (assimilated-reference) from March 1987 to April 1987. Arrows are drawn at each node of the model. The length of the arrows is proportional to the square root of the velocity. Dark shading indicates the anticyclonic intensity (negative curl).

The assimilation has reinforced the effect of this convection. Amongst the possible reasons of the need of such a reinforcement, one can mention an underestimation of the convection by the ship winds, or a too weak coefficient of transmission in the model (the wind input of energy depends on the mixed layer model).

3.4. Mass redistribution between 1987 and 1988

We have already noticed that there was a mass redistribution between the tropics and the Equator in 1987–88. This phenomena is consistent with GEOSAT, XBT and wind analysis (Arnault and Cheney, 1994). The heat content of the equatorial region (5°N–5°S) increased whereas in the north equatorial (10°N–20°N) and south equatorial (10°S–25°S) regions it decreased. Moreover, it was shown that the biggest change occurred between spring 1987 and spring 1988. The change was also maximum in SST between these periods (next section). In July, the change between the two years was mainly limited to the equatorial upwelling area. The weakening of the NEC–NECC gyre in October 1987 suggests that the mass redistribution had reached a maximum earlier. This is confirmed by a peak inversion in November 1987 in the EOF analysis of the interannual change (Arnault and Cheney, 1994). In the following, we will present differences between spring (Jan–May) 1988 and spring 1987.

The anomaly in GEOSAT SSH (Fig. 25) presents a south equatorial lowering (≈ 6°S–10°S), a rise in the Gulf of Guinea and a lowering off Senegal, consistent with the mass redistribution. These signals were observed by altimetry thanks to the sterical effect which revealed the change in heat content. However, the prominent signal around 4°N-40°W is more the result of a dynamic effect. The water is rather homogeneous in this area (deep mixed layer) and so the highs and lows result more from

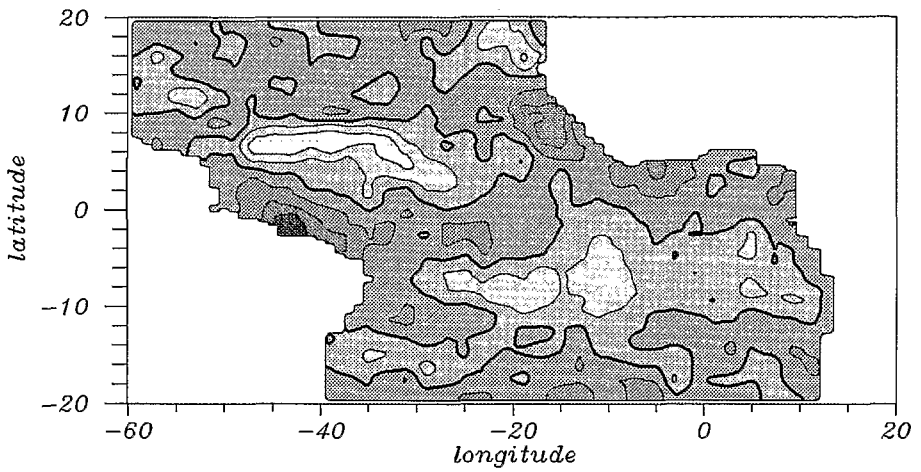

Fig. 25. GEOSAT sea level anomaly between spring (January-May) 1988 and spring 1987. Contour interval is 2 cm. The thick black contour is the zero level. Dark shading indicates a positive anomaly (rising).

the surface currents. The dipole marks the NEC–NECC gyre and the coastal BC, and can be compared to a distortion of the seasonal signal, the meridional tilting caused by the ITCZ migration. The meridional gradient at 4°N provides evidence of the strong change in NECC. We saw in previous sections that the assimilated run was more effective in simulating the strong NECC of 1987, so now we concentrate on the subsurface thermodynamics (SSTs are examined later). The anomaly at 200 m between the two springs for the reference run is displayed (Fig. 26). The main signals are the weakening of the EUC and some cooling in the west at 15°N. Globally, the year-to-year change is very weak and it is difficult to find a resemblance

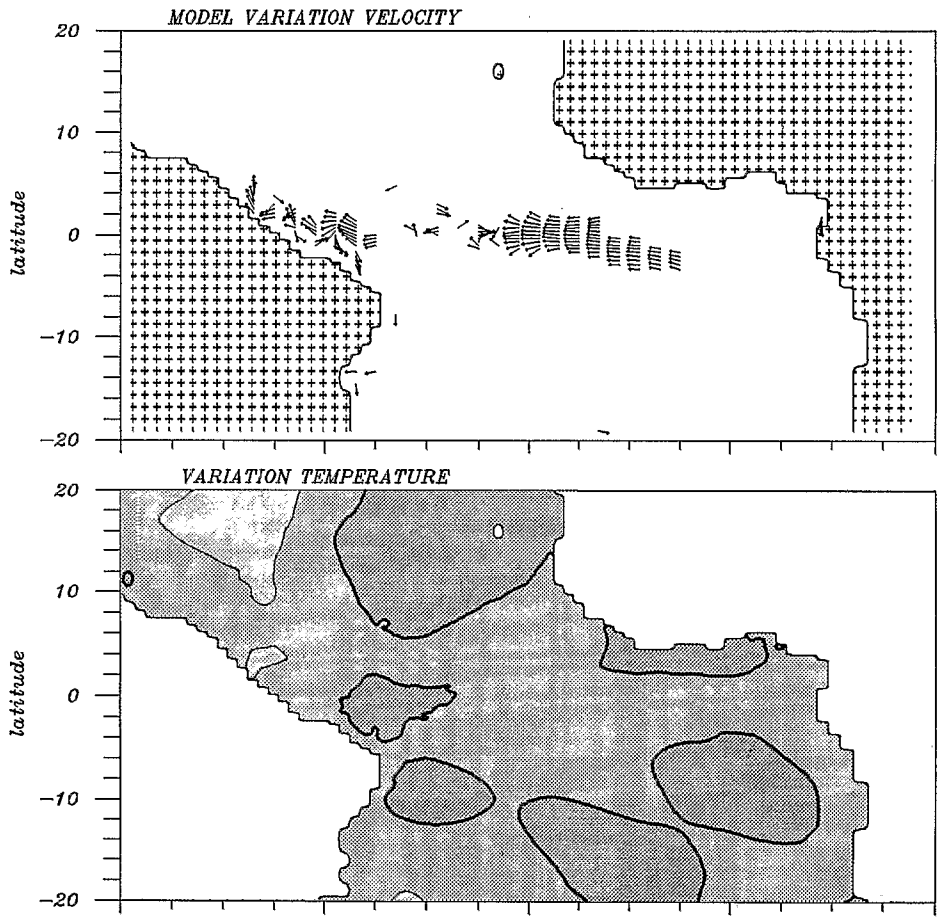

Fig. 26. Model anomaly between spring (January-May) 1988 and spring 1987 for the reference run at 200 m. Arrows are drawn at each second node of the model in longitude and at each node in latitude. The length of the arrows is proportional to the square root of the velocity. Arrows are not visible under 1 cm/s. Temperature contour interval is 0.5°C; the heavy black line corresponds to the 0°C isotherm. Darker shading corresponds to warmer anomalies.

with GEOSAT. The anomaly for the assimilated run at 200 m is shown in Fig. 27. The assimilated velocity illustrates the dynamical interpretation of the mass change. Globally, it shows a complex northern gyre at about 6°N and a southern gyre at about 8°S, as well as a strong equatorial eastward transport, deflected to the south along the African coast. The two anticyclonic gyres and their subsequent lowering are well captured by GEOSAT. The piling up of the warm water along the African coast in the Gulf of Guinea is also well marked in GEOSAT, with a maximum rise along the coast. The rise at 5°N–20°W is explained in the model by a convergence (downwelling). Interestingly, the meanders (thick line on the figure) of the front between the weakened NECC and increased EUC are somewhat similar to GEOSAT (2°N–32°W, 12°N–55°W, 6°N–25°W, for example). The westward jet at 10°N and

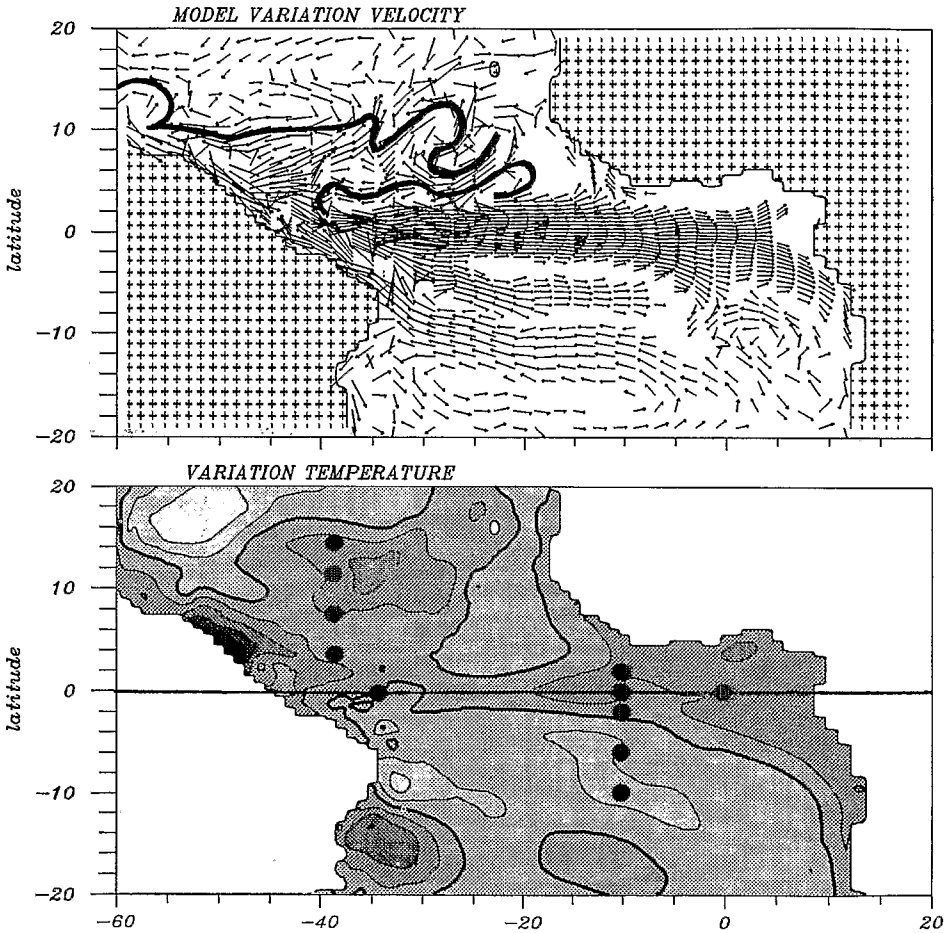

Fig. 27. Same as Fig. 26 between the forecasted spring (January–May) 1988 and the assimilated spring 1987.

the eastward jet at 5°N within 50°W–40°W are strong features both in the model and in GEOSAT.

In summary, the reference run produces a weak mass redistribution, mainly limited to the central equatorial subsurface. The assimilated run simulates a stronger signal, which affects also the northern and southern equatorial currents, as well as the EUC at depth. This suggests a circulation scheme for the mass redistribution. At the surface or at the thermocline level, the NEC–NECC gyre weakened from spring 1987 to spring 1988, whereas the southern SEC–SECC gyre strengthened. This latter gyre is in geostrophic balance with the south equatorial cooling. Deeper (150–200 m), the EUC strengthened from spring 1987 to spring 1988, increasing the heat content of the Gulf of Guinea.

3.5. Northward heat transport during 1987

One important benefit of the variational assimilation (Greiner and Périgaud, 1996) is to derive transport estimations that agree both with the data and all the physical processes resolved by the model (not only geostrophy). The Northward Heat Transport (NHT) in the tropical Atlantic ocean is particularly important for the climate of Brazil, Sahel, and northern Europe (Rao et al., 1993; Lamb and Peppler, 1992). So, we have computed the NHT[12] and its error estimate[13] during 1987. The value of the simulated NHT must be regarded with caution since its error is of the same order as the transport itself. The assimilated NHT at the Equator in January, April, July and October 1987 are respectively 0.49, 0.65, 0.58 and 0 petawatts. The associated errors are 0.47, 0.66, 2.11 and 0.65 petawatts, respectively, the maximum uncertainty being reached in July as a result of the equatorial upwelling (and divergence). However, up until now, this uncertainty has been common to most of the transports discussed in the literature. Hence, this must be taken as an assimilation attempt to evaluate the NHT.

A recent constrained estimate of the NHT (da Silva and Levitus, 1996) is represented by a thick line in Fig. 28 (uncertainty is not given). It corresponds to a mean "climatological" NHT. In comparison, the NHT deduced from a climatological ocean model (Philander and Pacanowski, 1986) is represented by a dashed line. It is higher than the data estimation, but the equatorial increase is consistent with the data. The reference run (dotted line) presents a 1987 NHT which is weaker than the climatologies, but a meridional variation that is consistent with the data estimate. The assimilated run exhibits a quite different meridional variation. All estimates are

[12] As the integral of the product of the meridional velocity by the temperature from the surface to the bottom.

[13] We have estimated the error on the NHT at the equator by computing

$$\underset{|\delta T| \leq 1°C}{\mathrm{SUP}} \iint u\, \delta T \, \mathrm{d}x \, \mathrm{d}z.$$

This corresponds to the error produced by an uncertainty δT of 1°C on the temperature. The velocity u is simulated by the model (we checked that an uncertainty of 20 cm/s produces a weaker error).

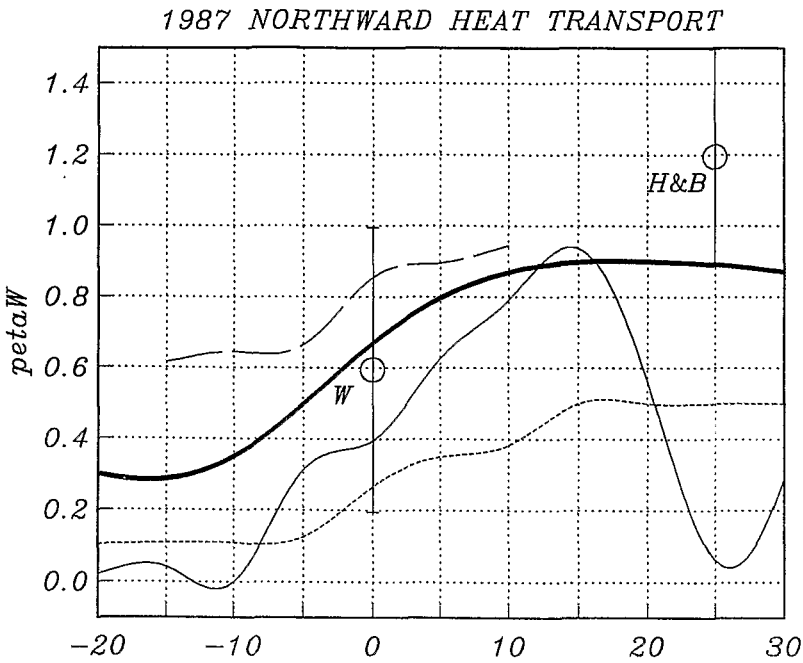

Fig. 28. Northward heat transport during 1987 for the reference run (dotted line) and the assimilated run (solid line). Climatological data estimate of da Silva and Levitus (1996) is represented by a thick line, the Wunsch (1984) one is indicated by a "W" and the Hall and Bryden (1982) one is indicated by a "H&B". Climatological model estimate of Philander and Pacanowski (1986) is represented by a dashed line.

within error bars of the estimate of Wunsch (1984), but the assimilated NHT is significantly lower than the Hall and Bryden (1982) estimate at 25°N.

The seemingly weak 1987 transport of the reference run is not unlikely. The ITCZ reached its most northerly position since 1984, and changed less from 1986 to 1987 than from 1984 to 1985, or 1985 to 1986. Compared to all estimates, the assimilated run suggests a very weak NHT beyond 20°N. Compared to the reference run, the assimilation suggests a stronger NHT within 3°N–18°N. Changes in NHT south of the Equator are weaker. In summary, the assimilation suggests a weaker than normal NHT in 1987, with a heat gain of the northern subtropics (3°N–18°N) from the northern tropics (beyond 22°N). Given the levels of uncertainty, the heat gain south of 8°S may not be as significant, but it is consistent with a pure data analysis (Arnault and Cheney, 1994).

3.6. Warm event of early 1988

The most remarkable event of 1985–1989 in the tropical Atlantic was the warming of the eastern equatorial Atlantic in early 1988. This interannual signal was first detected by SST observations, notably in the Gulf of Guinea. In fact, as confirmed

by the Reynolds SST, the whole of the basin east of 20°W and between approximately 6°N and 12°S was affected. In terms of the anomaly between 1987 and 1988, the warming was rather consistent (0.5°C to 1°C) east of 20°W in February, whereas in April, the warming was principally restricted between 20°W and 10°W at the equator, and at the African coast there was cooling. On the whole, the entire cold tongue was affected by the warming, from Namibia to the Equator. In June, the warming along the equator reached 1.5°C between 5°W and 0°W but decreased elsewhere. Along the coasts of Cameroun and Gabon, the warming was over by June.

The differences in SST between spring (Jan–May) 1988 and spring (Jan–May) 1987 are shown for the data in (Fig. 29). SSTs are in agreement with GEOSAT anomalies (Fig. 25) for the south Equator but less so for the Gulf of Guinea. It supports the weak coupling between the SST warming and the underlying dynamics. As already mentioned, SSTs do not exhibit the strong dipole seen in SSH, representing the NECC change. This is because the mixed layer is deep ($\approx$ 100 m) in this region so that the SST signature is weak. One can also note that the cooling off Guinea at about 20°W–10°N corresponds to a rising in GEOSAT. However, we saw (Section 3.4) that this appearent mismatch is explained by the assimilation by a clear warming at the thermocline depth. The reference run (Fig. 30) agrees rather well with the data on the large scale. It is worth noting that the anomalous central equatorial warming is simulated in spite of the climatological heat flux correction. A previous analysis (Servain et al., 1994) already showed a strong correlation between the in situ SST anomalies and the wind stress we used in this study. The reference runs prove in addition that the windstress is the leading term, compared to the thermohaline fluxes, regarding the development of the warm event. The cooling west of Guinea is less convincing because it is too close to the coast and too cold. Fig. 31 shows the difference between the forecast of April 1988 and the assimilated run of April 1987. Off Guinea the cooling has an amplitude and a position which is closer

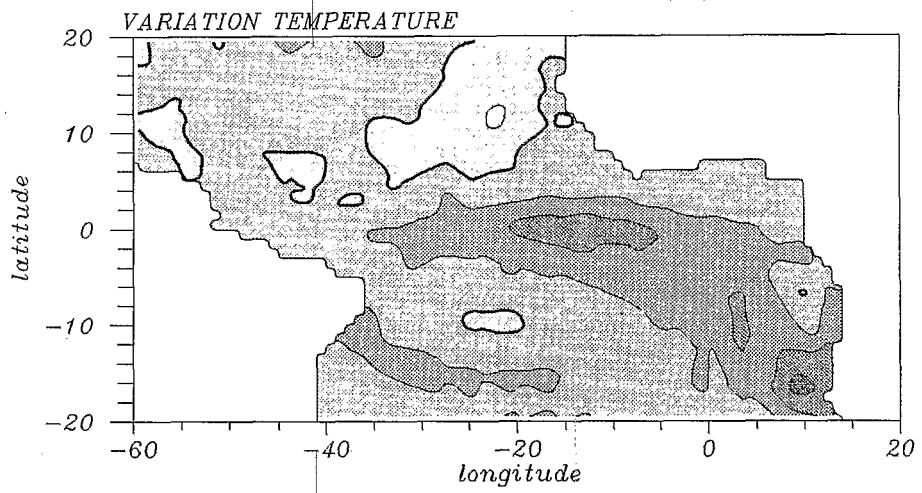

Fig. 29. Anomaly between spring (January–May) 1988 and spring 1987 for Reynolds SST.

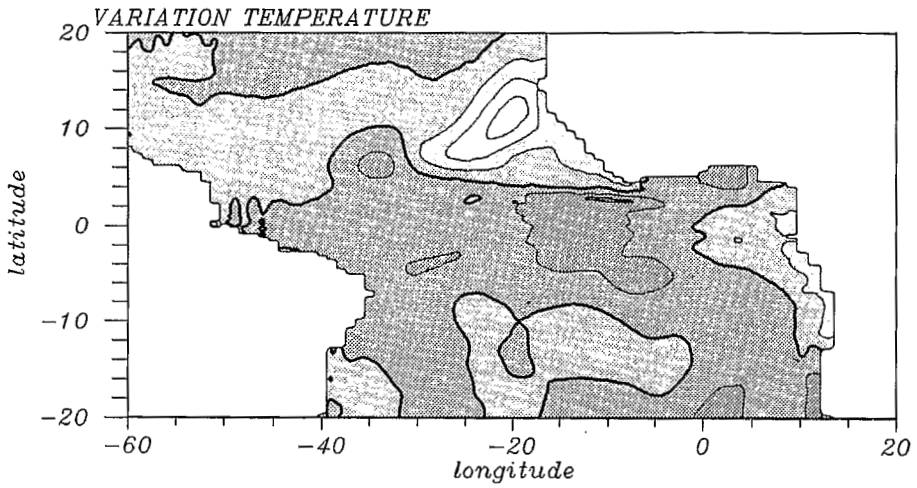

Fig. 30. Same as Fig. 29 for the reference run.

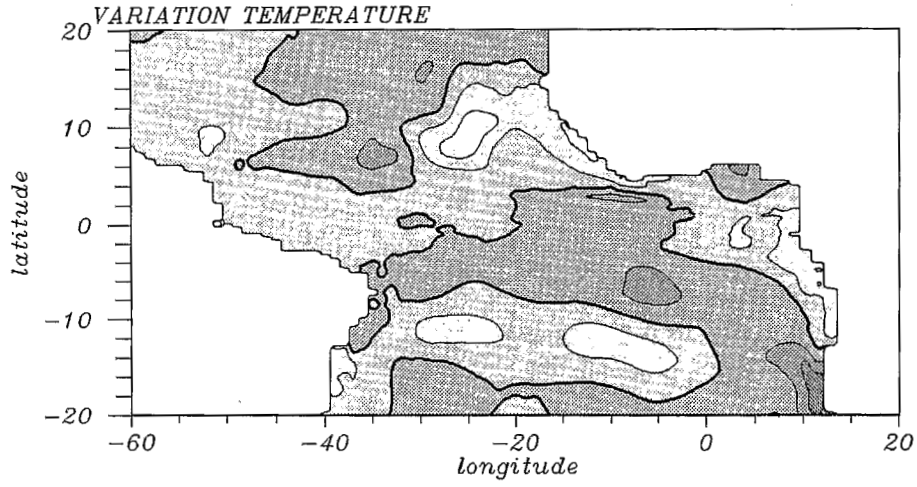

Fig. 31. Same as Fig. 29 for the assimilated run (1987) followed by the forecast run (1988).

to the observed. The warming off Angola is also better represented. On the large scale, the opposition between the 10°N and 10°S cooling and the warming of the cold tongue is clearer and looks like the Reynolds data. The most noticeable change concerns the cooling at about 10°S. In summary, this assimilation had little impact on the eastern equatorial warming, although the impact was clear in the south east cooling.

4. Discussion and conclusions

The simulated variability between 5°N–15°N is associated with a succession of ridges and troughs in the north equatorial currents. Assimilating GEOSAT sea level anomalies increased the variability of these currents when this variability was too weak to assess without assimilation. Regarding the resulting change in SSH, the assimilation provides corrections in temperature and salinity that can be of the same order in the tropics. This can be expected theoretically since temperature and salinity have a different impact on seawater density and dynamics. It could indicate that the assimilation of the SSH gives us the possibility to have separate insights into the thermal and haline structure. Moreover, the strong impact of the assimilation on the SSS front between the NEC and the NECC, can be analysed more thoroughly in the future thanks to the increasing dataset of bucket SSS.

The assimilated run simulates both the 1987 to 1988 sea level rise in the equatorial band and its lowering in the tropics. It confirms (Greiner and Périgaud, 1994; Greiner and Périgaud, 1996) that the variational assimilation transferred the altimetric signal into large scale tropical ocean dynamics. This was not obvious for two reasons. First, the lack of an altimetric reference level (equivalent to the mean circulation) is a handicap. Secondly, the sea level information ambiguously contains sterical (heat content) and dynamical (currents) effects. These experiments encourage further developments.

The comparison with Reynolds satellite SST data is useful to diagnose some of the model deficiencies. Upwelling areas are identified as being the zones of highest error for the model SST. The coastal upwellings off Dakar and off Angola are underestimated by the model. The central equatorial upwelling is overestimated, in particular with assimilation. Apart from the equatorial upwelling, the impact of the assimilation is better in the case of cooling. This is because subsurface dynamics play a more important role in such a situation. In the case of heating, the SST is mostly driven by the heat flux loss resulting from evaporation, so that the initialization has a lesser impact. More specifically, it was recently demonstrated that a reduced cooling from the fluxes affected by the wind (principally evaporation and entrainment) was the leading term for the SST in the Atlantic within 5°N–10°S in spring or early summer (EM97). Apart from the equatorial upwelling, the signature of this assimilation on the model SST is of the order of the error in satellite SST data. In any case, rather than improving the initialization, a better use of satellite SST for the modelization may lie in the determination of the heat flux by surface relaxation, or by assimilation (Roquet et al., 1993) with a prognostic mixed layer model (Blanke and Delecluse, 1993).

As a side consequence, even if the assimilation reproduces the mass redistribution of 1987 and the reference run does it less well, the SST warming of early 1988 is little changed by the assimilation. Thus, this warming is more determined by the wind forcing than by the internal dynamics. This is consistent with the initialization tests of sensitivity from CH94 (Fig. 9): the authors estimated that three quarters of the 1984 warming was the result of wind stress after June 1983. In addition, they

showed that the 1988 warming was even more dependant on the equatorial windstress of spring 1988.

As previously deduced from inverted echo sounders (Katz, 1993), we find that the NECC increased its transport during 1987. The assimilation reveals in addition that the NECC not only flowed into either Guinea Current or the EUC, but also formed a strong gyre with the NEC. The build up of the warm event in 1987 is thus not the straight result of meridional transfers as can be thought from satellite SSH and SST snapshots. Zonal currents like NEC and NECC also participated in the meridional redistribution. The analysis of the correction provided by assimilation suggests the following scenario for the 1987 redistribution. The increase in the NECC caused a downwelling south west off the coast of Guinea (Ekman convergence). This warm anomaly was then advected by the gyre and replaced the Guinea Dome, which was pushed westwards. The heat gain by the EUC was reduced as a result of the northward drift of the NECC. The SEC was strong in spring and summer, transferring warm surface water westwards, and slowing the EUC underneath it. The transport of the EUC was thus reduced, leading to a deficit of warm water in the Gulf of Guinea.

Amongst the sources of model error, one can mention the climatological thermohaline fluxes. As shown in GAM98 for the region of the Guinea Dome (section 6.3.3), the wind anomaly must be associated to thermohaline flux anomaly. About the physical mechanisms, it was evidenced (CH94) that wind anomalies were significantly linked to SST anomalies in the Gulf of Guinea. One could extrapolate that some of the observed propagations in 1987–88 may be partly wind-forced. This coupling is consistent with CH94 and EM97 about the atmospheric retroaction on the ocean to SST anomalies.

The comparison between the wind stress change and the corrections provided by assimilation reveals a direct link within the NEC–NECC gyre. The effect of the atmospheric convection was underestimated by the reference run and corrected by assimilation. This could result from an underestimation of the ship windstress or from an error in the transmission coefficient given by the mixed layer model. The gyre increase was a consequence of the anomaly in ITCZ position and intensity. This relation between the 1987 redistribution and the ITCZ is consistent with ship winds and GEOSAT information. This is also consistent with EM97 analysis (section 4.3). Moreover, they showed that February–April anomalous convergence is correlated with ENSO.

Comparisons of the assimilated NHT with climatological data estimates suggest principally a heat gain up to 1 petaWatt of the northern tropics (3°N–18°N) in 1987. The assimilated NHT was nil at 25°N and negative within 5°S–15°S. According to Philander and Pacanowski (1986), the most heat lost from the NECC is equatorward into the EUC. But, in 1987, the ITCZ northern position led to an Ekman north eastward drift of the NECC into the NEC. Hence, there was a heat loss of the Equator and a heat gain of the northern tropics in 1987. It contributates to the first interannual EOF of GEOSAT (Arnault and Cheney, 1994) which describes the shoaling of the equatorial thermocline and the tropical deepening from 1987 to 1988. This is a prom-

ising issue because it means that assimilation will allow us to have a quantitative insight into the climatical changes in low latitudes.[14]

A remarkable warm event occurred in 1984 in the tropical Atlantic, with warm waters in the Gulf of Guinea (Hisard and Hénin, 1987). A strong increase of the transport of warm waters by the NECC was observed from late 1983 which persisted until at least July 1984 (Hénin and Hisard, 1987). Drifters in 1983 provided a pattern in the surface circulation which is close to that observed in 1987. In particular, northward drifts of the NECC were observed in spring. A very weak EUC was also observed in July 1983, followed by a regular increase over 1984 (Hénin and Hisard, 1987). These points support the analogy of the dynamics between 1983–84 and 1987–88.

EM97 showed (section 6.2) that ENSO related events in the tropical Atlantic ocean present a temporal progression from the north to the south, and this is verified by this study. The assimilation shows an increased transport of warm water by the EUC after September 1987, rising to a maximum in February 1988. It confirms the positive impact of the mass redistribution on the subsurface warming of the Gulf of Guinea (CH94, EM97). CH94 also noticed that the anomalous thermocline deepening peaked in February whereas the warming was maximum in early summer. The other significant impact in 1988 was an increase in the SEC–SECC gyre. The cooling in SST is the visible signature of the downwelling resulting from the southern gyre. Following EM97 data analysis (sections 4.3, 5.4 and 6.2), the northward shift of the ITCZ leads to a reinforcement of the south east trades at low latitudes. It precedes by several months the appearence of weak surface cooling off Angola. This is a result of the southward shift of the ITCZ which creates an anticyclonic barotropic gyre anomaly, as a response to an altered Sverdrup balance. The ITCZ reverted to its normal position in 1988. According to EM97, it strengthened the impact of the mass redistribution on the SEC–SECC gyre and the cooling off Angola. CH94 remarked that in 1984 the subsurface warm water advected into Angolan waters by the EUC both perturbed the SECC and inhibited the coastal upwelling off Namibia (as verified locally by in situ measurements). Such a mechanism is also predicted in the 1988 forecast.

Even if the period 1987–88 is dynamically original, it suffers from a lack of in situ data compared to 1983–84. More precisely, there are very few XBTs with which to test the impact of the mass redistribution on 1988. We have superimposed the PIRATA network (Servain, 1996) on the temperature anomaly between spring 1988 and spring 1987 as given by the assimilated and the forecast runs (Fig. 27). This network, similar to the TAO network in the Pacific, could have helped in understanding the 1987–1988 phenomenon even if the mooring location is not optimal. But satellite data and current measurements are still essential to the knowledge of the tropical Atlantic interannual variability. Finally, if correlations between coastal Nam-

[14] This is a specific problem because SSH is not precisely linked through geostrophy at the Equator to the complex vertical distribution of the velocity field.

ibian and Angolan SSTs were further demonstrated, it suggests a possible role for satellite and in situ monitoring more than a year in advance in this region.

5. Acknowledgements

The authors thank J. P. Rebert (ORSTOM) who provided the XBT data and the staff at the TOGA Center of Brest who validated the data; J. Servain (ORSTOM) for the good wind data; and R. Morrow for her fruitful comments on the manuscript. They also thank LODYC (Paris), GRGS (Toulouse) and CERFACS (Toulouse) for this collaboration. E. Greiner's research was funded by CNES, La Société de Secours des Amis des Sciences and CERFACS. S. Arnault and A. Morlière were supported by ORSTOM, PNTS and PNEDC. CPU time on C98 was provided by IDRIS. Additional computations were made at the LODYC, GRGS and CERFACS.

6. References

Arnault, S. (1987). Tropical Atlantic geostrophic currents and ship drifts. *Journal of Geophysical Research, 92*(C5), 5076–5088.

Arnault, S., & Cheney, R.E. (1994). Tropical Atlantic sea level variability from Geosat (1985–1989). *Journal of Geophysical Research, 99*(C9), 18207–18223.

Arnault, S., Morlière, A., Merle, J., & Ménard, Y. (1992). Low-frequency variability of the tropical Atlantic surface topography: altimetry and model comparison. *Journal of Geophysical Research, 97*(C9), 14259–14288.

Blanke, B., & Delecluse, P. (1993). Variability of the tropical Atlantic ocean simulated by a general circulation model with two mixed layer physics. *Journal of Physical Oceanography, 23*, 1363–1388.

Carton, J.A., & Huang, B. (1994). Warm events in the tropical Atlantic. *Journal of Physical Oceanography, 24*, 888–903.

Courtier, P., & Talagrand, O. (1990). Variational assimilation of meteorological observations with the direct and adjoint shallow-water equations. *Tellus, 42A*, 531–549.

da Silva, A. and Levitus, S., 1996. Revised surface marine fluxes over the global oceans: the UVM/COADS data set. WRCP-95 WMO-TD 762, 13–18.

Didden, N., & Schott, F.A. (1990). Seasonal variations in the western tropical Atlantic: surface circulation from GEOSAT altimetry and WOCE model results. *Journal of Geophysical Research, 97*(C3), 3529–3541.

Dessier, A., & Donguy, J.R. (1994). The sea surface salinity in the tropical Atlantic between 10°S and 30°N—seasonal and interannual variations (1977–1989). *Deep-Sea Research, I, 41*, 81–100.

Enfield, D.B., & Mayer, D.A. (1997). Tropical Atlantic variability and its relation to El Niño Southern Oscillation. *Journal of Geophysical Research, 102*(C1), 929–945.

Greiner, E., Arnault, S., & Morlière, A. (1998). Twelve monthly experiments of 4D-variational assimilation in the tropical Atlantic during 1987: Part 1: method and statistical results. *Progress in Oceanography, 41*, 141–203.

Greiner, E., & Périgaud, C. (1994). Assimilation of Geosat altimetric data in a nonlinear reduced-gravity model of the Indian Ocean by adjoint approach, Part 1: Methods and statistical results. *Journal of Physical Oceanography, 24*(8), 1783–1804.

Greiner, E., & Périgaud, C. (1996). Assimilation of Geosat altimetric data in a nonlinear reduced-gravity model of the Indian Ocean by adjoint approach, Part 2: Physical results. *Journal of Physical Oceanography, 26*, 1735–1746.

Hall, M.M., & Bryden, H.L. (1982). Direct estimates and mechanisms of ocean heat transport. *Deep Sea Research A, 29*(3), 339–359.

Hénin, C., & Hisard, P. (1987). The North Equatorial Countercurrent observed during the Programme Français Océan Climat dans l'Atlantique, equatorial experiment in the Atlantic ocean July 1982 to August 1984. *Journal of Geophysical Research, 92*(C4), 3751–3758.

Hisard, P., & Hénin, C. (1987). Response of the Equatorial Atlantic ocean to the 1983–1984 wind, from the Programme Français Océan Climat dans l'Atlantique equatorial cruise data set July 1982 to August 1984. *Journal of Geophysical Research, 92*(C4), 3759–3768.

Huang, B., Carton, J.A., & Shukla, J.S. (1995). A numerical simulation of the variability in the tropical Atlantic Ocean, 1980–88. *Journal of Physical Oceanography, 25*, 835–854.

Johns, W.E., Lee, T.N., Schott, F.A., & Zantopp, R.J. (1990). The North Brazil Current retroflection seasonal structure and eddy variability. *Journal of Geophysical Research, 95*(C12), 22103–22120.

Katz, E.J. (1993). An interannual study of the Atlantic north Equatorial Countercurrent. *Journal of Physical Oceanography, 23*, 116–123.

Lamb, P.J., & Peppler, R.A. (1992). Further case studies of tropical Atlantic surface atmospheric and oceanic patterns associated with sub-saharan drought. *Journal of Climate, 5*, 476–488.

Lemasson, L., & Rebert, J.P. (1973). Circulation dans la partie orientale de l'Atlantique Sud. *Doc. Scient. CRO Abidjan IV, 1*, 91–124.

Levitus, S., 1982. Climatological atlas of the world ocean. NOAA professional paper, 13. US Department of Commerce, Rockville, MD, 174 pp.

McClean, J.L., & Klinck, J.M. (1995). Description and vorticity analysis of 50-day oscillations in the western tropical region of the CME model. *Journal of Physical Oceanography, 25*, 2498–2517.

Merle, J. (1980). Seasonal heat budget in the equatorial Atlantic Ocean. *Journal of Physical Oceanography, 10*, 464–469.

Molinari, R.L. (1982). Observations of eastward currents in the tropical South Atlantic Ocean: 1978–1979. *Journal of Geophysical Research, 87*, 9707–9714.

Morlière, A., Reverdin, G., & Merle, J. (1989). Assimilation of temperature profiles in a general circulation model of tropical Atlantic. *Journal of Physical Oceanography, 19*(12), 1892–1899.

Oberhüber, J.M., 1988. An atlas based on the "coads" data set: the budgets of heat, buoyancy and turbulent kinetic energy at the surface of the global ocean, Max Planck Institut für Meteorologie, Germany, 15, 202 pp.

Philander, S.G.H., & Pacanowski, R.C. (1986). The mass and heat budget in a model of the tropical Atlantic ocean. *Journal of Geophysical Research, 91*(C12), 14212–14220.

Rao, V.B., De Lima, M.C., & Franchito, S.H. (1993). Seasonal and interannual variations of rainfall over eastern northeast Brazil. *Journal of Climate, 6*, 1754–1763.

Rebert, J.P., 1993. Data quality control at the TOGA subsurface data Centre, Manual of quality control procedures for validation of Oceanographic data, Manual and Guides, 26, UNESCO, 13 pp.

Reynolds, R.W., & Smith, T. (1994). Improved global sea surface temperature analysis using optimum interpolation. *Journal of Climate, 7*, 929–948.

Richardson, P.L., & Reverdin, G. (1987). Seasonal cycle of velocity in the Atlantic north Equatorial Counter Current as measured by surface drifters, current meters and ship drifts. *Journal of Geophysical Research, 92*, 3691–3708.

Richardson, P.L., Hufford, G.E., Limeburner, R., & Brown, W.S. (1994). North Brazil current retroflection. *Journal of Geophysical Research, 99*(C3), 5081–5093.

Roquet, H., Planton, S., & Gaspar, P. (1993). Determination of ocean surface heat fluxes by a variational method. *Journal of Geophysical Research, 98*(C6), 10211–10221.

Schott, F., Fisher, J., Reppin, J., & Send, U. (1993). On mean and seasonal currents and transports at the western boundary of the equatorial Atlantic. *Journal of Geophysical Research, 98*(C8), 14353–14368.

Servain, J., 1996. PIRATA, Pilot Reseach Moored Array in the Tropical Atlantic. Centre ORSTOM de Brest, BP 70, 2980 Plouzané, France, 58 pp.

Servain, J. and Lukas, S., 1990. Climatic atlas of the tropical Atlantic wind stress and sea surface temperature 1985–1989. Centre ORSTOM de Brest, BP 70, 2980 Plouzané, France, 154 pp.

Servain, J., Morlière, A., & Pereira, C.S. (1994). Simulated versus observed sea surface temperature in the tropical Atlantic Ocean. *The Global Atmosphere and Ocean System, 2*, 1–20.

Tang, T.Y., & Weisberg, R.H. (1993). Seasonal variations in equatorial Atlantic ocean volume transport at 28°W. *Journal of Geophysical Research*, *98*(C6), 10145–10153.

Wunsch, C. (1984). An eclectic Atlantic ocean circulation model, Part 1: The meridional flux of heat. *Journal of Physical Oceanography*, *14*, 1712–1733.